PROPAGATION OF ELECTROMAGNETIC WAVES IN STRUCTURED METAMATERIALS AND SYSTEM OF TWO-LEVEL ATOMS

By

Abdurahman Ahmed

SUBMITTED AS A REQUIREMENT FOR THE
DEGREE OF DOCTOR OF PHILOSOPHY
AT
ADDIS ABABA UNIVERSITY

ADDIS ABABA, ETHIOPIA
MAY 2017

ADDIS ABABA UNIVERSITY
DEPARTMENT OF PHYSICS

The undersigned hereby certify that they have read and recommend to the College of Natural Sciences for acceptance a dissertation entitled "**Propagation of Electromagnetic Waves in Structured Metamaterials and System of Two-Level Atoms**" by **Abdurahman Ahmed** as a requirement for the degree of **Doctor of Philosophy**.

Dated: May 2017

External Examiner: _____
Prof. Lee Sing

Internal Examiner: _____
Prof. Ashok V. Gholap

Research Supervisors: _____
Prof. V. N. Mal'nev/Dr. Belayneh Mesfin

Chairman: _____
Dr. Teshome Senbeta

DECLARATION

I, the undersigned, declare that this Ph.D. dissertation is my original work and has not been presented for a degree in any other university, and that all sources of materials used for the dissertation have been duly acknowledged.

Author: _____

Abdurahman Ahmed

This Ph.D. dissertation has been submitted for examination with my approval as university research supervisor.

Research Supervisor: _____

Prof. V. N. Mal'nev/Dr. Belayneh Mesfin

Place: **Department of Physics, Addis Ababa University**

Date: **May, 2017**

The dissertation is dedicated to

my wife Amira,

my son Akrem,

and

the late Professor Vadim N. Mal'nev

Table of Contents

List of Tables

List of Figures

Abstract

Metamaterials are artificially engineered composites that exhibit superior properties not observed in nature or in the constituent materials. Because of the sub-wavelength periodicity of their constituent materials, metamaterials appear as homogeneous entity to an incident wave and can be described by effective parameters, such as electric and magnetic material properties, that are controlled by the unit cells geometry and the type of its constituent parts. These controllable material properties, in turn, makes structured metamaterials (SMMs) more interesting for diverse potential device applications. Consequently, it is of vital importance to investigate the responses of SMMs to electromagnetic waves (EMWs).

In this dissertation, the dispersion properties of SMMs consisting of strips of a copper wire (electron subsystem) and square copper split-ring-resonators (magnetic subsystem) with different and coinciding resonant frequencies are studied. In a narrow frequency band above the resonant frequency of the electron subsystem, the structured metamaterial is described by a negative refractive index. In addition to this, there are some peculiar properties observed in these metamaterials. Among these properties is the nonanalytic behavior of the real part of the refractive index as a function of the frequency with a discontinuity of its derivative in the metamaterial with two resonances. It is also shown that the superluminal, slow, and backward microwaves can exist in the structured metamaterials. However, in the absence of gain components, only the slow microwaves can propagate considerably.

In addition, we investigated the propagation of narrow packets of EMWs in frequency dispersive medium with the consideration of the complex refractive index. It

is shown that taking into account of the dispersion of the complex refractive index within the context of the conventional expression of the group velocity of narrow wave packets of EMWs propagating in a dispersive medium results in the appearance of additional constraints on the group velocity, which dictates that the physically acceptable group velocity can only be realized in the case of a negligible imaginary part of the group index. The conditions that allow one to realize the physically acceptable group velocity are formulated and analyzed numerically for the relevant model of the refractive index of a system of two-level atoms in the optical frequency range. It is shown that in the frequency band where superluminal light propagation is expected, there is a strong dispersion of the refractive index that is accompanied with strong absorption, resulting in a strongly attenuated superluminal light.

Acknowledgements

First, I would like to express my deepest gratitude and respect to my supervisor Professor Vadim N. Mal'nev, for his invaluable guidance, helpful suggestions and endless support. My special thanks goes to Dr. Belayneh Mesfin who took the full responsibility of advisement after the passage of Professor Vadim Mal'nev.

A PhD study cannot be completed without help and support from various sources. Here I would like to thank those people who have helped me in one way or another to get to this stage. In particular:

- All academic and administrative staff members of the Department of Physics of the Addis Ababa University (AAU), specially, Dr. Fesseha Kassahun, Dr. Teshome Senbeta, Dr. Lemmi Demeyu, Dr. Deribe Hirpo, and the Department's secretary W/o Tsilat Adinew.
- Kotebe Metropolitan University (KMU) and the Addis Ababa City Adminstration (via KMU) for sponsoring my study.
- The management staff members of KMU and staff members of the Department of Physics of KMU.
- My wife Amira and my son Akrem, who always created conducive environment and unlimited support at home.
- My brother Nejib Ahmed who supported me with materials when needed.
- Finally, my thoughts and appreciations go to my friends, especially; Dr. Mesfin Tadesse, Dr. Mekbib Alemu, Dr. Sebsibe Teferi, and Derese Terfa for their sensible advises and optimism.

Abdurahman Ahmed
Addis Ababa, Ethiopia
May 2017

Introduction

Materials that are artificially fabricated to have the desired material properties that do not exist in nature are referred to as metamaterials. The word was first introduced by R.M. Walser [1] in which he defined metamaterials as "macroscopic composites having a man-made, three dimensional, periodic cellular architecture designed to produce an optimized combination, not available in nature, of two or more responses to a specific excitation." Nowadays, the term metamaterial refers to macroscopic as well as microscopic engineered composite "that exhibits superior properties not observed in nature or in the constituent materials. The superior properties of a metamaterial are a result of their engineered constructs" [2].

Structured metamaterials with negative refractive index

The fundamental quantities that are often employed to determine the response of a medium to electromagnetic fields are the electric permittivity ϵ and the magnetic permeability μ. In 1968, Veselago considered the electrodynamics of materials having simultaneous negative values of permittivity and permeability, and hence negative refractive index [3]. He predicted such types of materials possess some peculiar features, such as reversed Doppler shift, anomalous refraction, and backward Cerenkov radiation, and introduced the idea of superlens. He called these media left-handed

media (LHM). Since then, these media are known by several names, such as Veselago media, negative-refractive-index media, backward wave media, and double-negative media.

Even though negative refraction received great attention recently, its possibility has been suggested in some other ways a long time ago. The existence of backward waves in mechanical systems was suggested by Lamb [4] who identified that for these waves the phase moves in the direction opposite to the energy flow (group velocity). Backward waves in electromagnetic systems were first investigated by Schuster [5] who also predicted on the possibility of having negative refraction. In connection, Pocklington [6] illustrated that in a specific backward wave medium, a source produces a wave whose group velocity is directed away from the source, while its phase velocity moves toward the source.

Despite these, Veselago's work was largely overlooked over 30 years, mainly, due to the absence of naturally existing materials with the LHM properties. The diverse and rapidly growing field of metamaterials research that exists today was born in 1999, when John Pendry et al. [7] suggested the use of split-ring-resonators to create artificial media with a possibly negative magnetic response. In 2000, Smith et al. [8] demonstrated metamaterial made of array of metallic wires and split-ring-resonators which possesses simultaneous negative values of permittivity and permeability. Shelby et al. [9] constructed a structured metamaterials (SMMs) from square copper split-ring-resonators and copper wire and verified experimentally the existence of negative refractive index. Their work was also consolidated by Parazzoli et al. [10] who reported the results of a Snell's law experiment on a negative index material in free space in the frequency range between 12.6 and 13.2 GHz, confirming the possibility

of fabricating materials having negative refractive index.

Motivated by the works of Shelby et al. [8], several researchers made experimental and theoretical studies and constructed various new LHM samples which show left-handed material properties [11-18]. Markos et al. [19] have analyzed numerically the transmission properties of a periodic arrangements of thin metallic wires and showed that the medium's effective permittivity depends on the wire radius and on the conductance of the wires. Other structures proposed to attain negative effective permittivity include metamaterials made of arrays of metallic wires with square cross-sections embedded in a dielectric host medium [20] and a canonical structure of the wire medium [21]. Similarly, the electromagnetic resonances in different structures of split-ring-resonators (SRRs) as a possible structure possessing negative effective permeability has been investigated. Gay-Balmaz et al. [22] studied the behavior of an individual SRR, as well as the coupling and showed that for an individual SRR both electric and magnetic fields can induce resonances, the magnetic one being the strongest between several SRRs. Markos et al. [23] have studied transmission properties of LHMs and SRRs. They found that the LHM transmission peak depends on the imaginary part of the metallic permittivity ε_m, the length of the system, and the size of the unit cell.

Furthermore, Zhou et al. [24] investigated wire-pair structures built from H-shaped wires as alternatives to conventional SRR-based negative index materials (NIMs). In the wire-pair arrangement, the conventional SRR is replaced with a pair of short parallel wires, which provide both negative magnetic and electric response; avoiding the conventional continuous wires structure. They measured experimentally

both the transmittance and the reflectance properties and found that a negative refractive index with $n_1 < 0$ and $n_2 > 0$, where n_1 and n_2 are real and imaginary parts of the refractive index, respectively.

After the initial groundbreaking work on negative index metamaterials, it was soon realized that the potential applications of metamaterials is much broader. Because of the opportunity to precisely control electric and magnetic material properties, the new research area of transformation optics emerged. Its most notable application is the design of invisibility cloaks, which guide electromagnetic waves around a hidden object and have already been demonstrated in the microwave and optical parts of the spectrum. On the other hand, the study of 3D-chiral metamaterials has led to the observation of giant optical activity and the discovery of a new class of negative index metamaterials [25].

Because of the sub-wavelength periodicity of their constituent materials, metamaterials do not diffract [25]. Consequently, they appear as homogeneous entity to an incident wave and can be described by effective parameters that are controlled by the unit cell's geometry and the type of its constituent parts. In particular, negative index metamaterials provide the opportunity to precisely control the electric and magnetic material properties which makes these materials interesting for diverse potential device applications. Hence, it is of vital importance studying in detail the responses of these materials to EMWs.

Superluminal, backward, and slow propagation

The study of superluminal, backward, and slow narrow packets of light waves propagating in different media in the frequency range of strong dispersion of the refractive

index have had a long history [26]. It is well known that Einstein's 1905 special theory of relativity is based on the assumption that "the speed of a material object cannot exceed the speed of light c in vacuum". Shortly afterwards, Sommerfeld [26] criticized Einstein's assertion by arguing that the phase and group velocities of EMWs can become superluminal, as that is observed inside a dielectric medium. Sommerfeld pointed out that while it is true that both the phase and the group velocities in media can exceed c, the front velocity, defined as the velocity of a discontinuous jump in the initial wave amplitude from zero to a definite value, cannot exceed c. In subsequent work, Sommerfeld and Brillouin [26] showed that the "front" is accompanied by two kinds of "precursors", namely, the "high-frequency" and "low-frequency" precursors. These precursors are weak ringing waveforms that follow the abrupt onset of the front, but they precede the gradual onset of the strong main signal.

Currently, the question on the existence, physical meanings, and potential consequences of such waves has become a hot research topic and sometimes controversial. In this respect, there are two groups of researchers: those who support the existence of superluminal electromagnetic waves [27] and those who reject such reports [28]. In 1970 it was reported in Ref. [29] that Gaussian packets of electromagnetic waves can travel in dispersive media with group velocity exceeding the velocity of light in vacuum with no restrictions what so ever. Recently, the topic has been discussed theoretically in many papers again and even some have reported on the experimental realization of such waves in strongly dispersive media [27-37]. Garret and McCumber [29] examined the propagation of Gaussian light pulse in a medium having a positive or negative absorption line and showed that pulse remained substantially Gaussian unchanged in

width for many exponential absorption depths, and that the locus of instants of maximum amplitude follows classical expression for the group velocity which is greater than the velocity of light, or negative. The predictions of Garret and McCumber were tested experimentally by Chu and Wong [33]. The next theoretical advance in the theory of superluminal propagation was made by Chiao [38], who studied theoretically the propagation of limited-bandwidth signals in an inverted two-level atomic medium and predicted that the velocity of the signals can be superluminal, without violating the causality principle. Later, his predictions were tested experimentally using various experimental techniques, such as electromagnetically induced transparency for gain media [27, 34, 39] and coherent population oscillations [35, 39, 40, 41] demonstrating slow as well as fast propagations, with no violation of the principle of relativity.

Despite the many theoretical and experimental reports on superluminal wave propagation, others doubt the credibility of such reports on grounds that it contradicts the special theory of relativity and consequently the so-called superluminal light has no physical meaning [28]. Chen et al. [42] considered Gaussian pulse propagation constructed from many monochromatic modes with different phase velocities and obtained a group velocity that becomes superluminal and even negative. However, he argued that the observed 'superluminal' effect is due to a coherent optical wave superposition effect, so that whatever the velocity of the 'pick', the whole pulse cannot travel with a speed greater than the fastest phase velocity of its component modes. Thus, concluded that "the maximum speed for information transfer, which involves the sending of finite pulse, cannot be greater than the maximum phase velocity in the medium". Zhang [43] using the contour integral techniques proved that relativity forbids superluminal wave propagation. Tanka et al. [44] experimentally obtained

negative group velocity as well as pulse velocity (group velocity) that can exceed the speed of light in vacuum in Rb vapor. Moreover, they showed that at the frequency band where this velocity is attained the intensity of the transmitted pulse is reduced by strong dispersion and consequently concluded that the observed velocity is not the velocity of energy flow, i.e., group velocity.

Similarly, it is reported that electromagnetic wave packet may travel at a superluminal velocity as well as negative group velocity. However, the information carried by them is not superluminally transmitted and the information velocity carried by the wave front is still positive [45]. In a recent study, Dexin et al. observed strongly distorted discrete half-sine packets with a non-superluminal wave front [46]. This finding agrees with Brillouin's assertion that "the severe distortion of seemingly superluminal wave packets makes the definition of group velocity physically meaningless in the anomalously dispersive region".

The interesting topic that needs further investigation concerns the superluminal light with group velocity V_g exceeding the speed of light in vacuum. Such a value of V_g is commonly obtained with the help of the conventional formula that does not take into account the dispersion of the imaginary part of the refractive index.

Structure of the dissertation

In this dissertation, we take into account [9] the dispersion of the refractive index and the group velocity of microwaves in left handed metamaterial fabricated for the verification of negative refraction to investigate the frequency range in which this material supports slow, backward and superluminal propagation. We also investigate the propagation of light in an assembly of two level atoms. Accordingly, it is organized

in six chapters:

In Chapter 1, a theoretical review of wave propagation in a medium is presented. Maxwell's equations, the electromagnetic constitutive relations, the permittivity, the permeability, the dispersion relation for isotropic media, the Poynting vector, the group and phase velocities are introduced. In addition, wave propagation in dispersive and nondispersive media, the concepts of superluminal, slow and backward waves as well as the conditions under which these wave are realized are discussed.

Chapter 2 focuses on the theory and various material parameters of structured metamaterials and their potential applications as LHM is explored. In particular, employing Maxwell's equation the propagation of electromagnetic waves in left-handed media, the consequences of having negative refractive index, and the dispersive and dissipative nature of LHM media are explored. Moreover, the effective permittivity and permeability of a structured metamaterial that consists of array of long metallic strips and split-ring-resonators is introduced.

The interaction of a classical monochromatic light field with a two-level atom is reviewed in Chapter 3. Using semiclassical approach, the density matrix for a model of two-level atom and its time evolution are derived. Furthermore, the steady state solutions of the density matrix equation is applied to calculate the electric susceptibility of a system of closed two-level atom.

In Chapter 4, we studied the propagation of electromagnetic waves in a structured metamaterial (SMM) that consists of square split ring resonators and array of long metallic wires (ALMWs) made of copper. Using the effective permittivity and permeability proposed by Pendry et al. the refractive index is analyzed and the frequency domain where the SMM behaves as negative refractive index medium is identified.

Further, the analysis of group velocity, group index, superluminal, slow, and backward waves propagating in the structured metamaterial is carried out. Moreover, it is shown that by appropriately tuning the parameters of the electric (ALMWs) and magnetic subsystems (SRRs), the propagation of EMWs in the SMM with coinciding frequencies of the electron and magnetic subsystems are discussed.

In Chapter 5, we presented the evolutions of narrow Gaussian packets of electromagnetic waves in a frequency dispersive media taking in to account the dispersion of the imaginary part of the refractive index and the conditions under which the physically consistent group velocity can be realized are obtained. Moreover, the frequency bands where the physically acceptable group velocity of light is realized is determined by introducing the relevant refractive index of an assembly of two-level atoms.

Chapter 6, summarizes the results of our findings in this dissertation.

Chapter 1

Electromagnetic Waves in a Medium

1.1 Introduction

Electromagnetic waves can propagate in most material media and vacuum. Material media include both natural and artificial materials. The propagation of electromagnetic waves (EMWs) is governed by Maxwell's equations and the constitutive relations. Practically, all material media are dissipative and possess the most diverse values of permittivity (ε) and permeability (μ) [47]. To describe the interaction of electromagnetic waves with many natural and artificial materials, it is sufficient to assign a complex permittivity and permeability [26, 47]. These parameters characterize the macroscopic polarization and magnetization responses in a material.

In this chapter we consider concepts related to the propagation of electromagnetic waves in media. In section 1.2, Maxwell's equations in matter in their differential forms along with the constitutive relations are introduced. In Section 1.3, the permittivity and permeability, and their relations with electric and magnetic susceptibilities respectively are explained. The wave equation for the electric and magnetic fields and

the dispersion relation for linear, isotropic materials is discussed in Section 1.4. The phase velocity, group velocity, and the complex group refractive index are defined in Section 1.5. In Section 1.6, a detailed analysis of the propagation electromagnetic wave packets in dispersive as well as nondispersive media is presented. Section 1.7 discusses the relation ship between Poynting vector and intensity, and using this relationship the coefficient of absorption is derived. In Section 1.8, we introduce the concepts of superluminal, backward, and slow EMWs observed in various systems and discuss the conditions under which these waves are realized. Finally the results of the chapter are summarized in Section 1.9.

1.2 Maxwell's equations in matter

The properties of electromagnetic waves in a material medium can be described by Maxwell's equations. These are

$$\vec{\nabla} \cdot \vec{D} = 4\pi\rho_f, \tag{1.2.1}$$

$$\vec{\nabla} \cdot \vec{B} = 0, \tag{1.2.2}$$

$$\vec{\nabla} \times \vec{E} = -\frac{1}{c}\frac{\partial \vec{B}}{\partial t}, \tag{1.2.3}$$

and

$$\vec{\nabla} \times \vec{H} = \frac{4\pi}{c}\vec{j}_f + \frac{1}{c}\frac{\partial \vec{D}}{\partial t}, \tag{1.2.4}$$

where $\vec{D}$, $\vec{B}$, $\vec{E}$, and $\vec{H}$ are the electric displacement, magnetic induction, electric field, and magnetic field vectors, whereas ρ_f and $\vec{j}_f$ are the free charge and free current densities, respectively.

In order to allow calculation of electromagnetic processes in the presence of a material medium, Maxwell's equations must be supplemented by the electromagnetic constitutive relations defined by

$$\vec{D} = \varepsilon \vec{E}, \tag{1.2.5}$$

and

$$\vec{B} = \mu \vec{H}, \tag{1.2.6}$$

where ε and μ are the permittivity and permeability of the medium. The constitutive relations describe the electromagnetic properties of the medium and have a definite form for a specific medium. The set of field equations (1.2.1-1.2.4) and the constitutive relations (1.2.5) and (1.2.6) forms the complete system of equations, for the description of any properties of EM wave propagation in matter.

1.3 Polarization and Magnetization

When electromagnetic waves propagate through a material system, as opposed to free-space, there is an interaction that occurs at the atomic or molecular level which uniquely modifies the wave propagation. The electric and magnetic fields of the waves cause a deformation of the microscopic electric charge distribution of the system's atoms or molecules. This deformation of the charge distribution causes the constituent particles of the system to behave as microscopic dipoles, which tend to align themselves with the propagating electric and magnetic fields. These dipoles are driven to oscillate at the frequency of the incident electromagnetic waves, which then radiate their own wave fronts at this frequency. Thus the resulting macroscopic wave

observed in the material is a linear superposition of the primary incident electromagnetic waves and the secondary dipole radiated waves, that oscillates at the incident frequency.

Quantitatively, the interaction of the electromagnetic wave's electromagnetic fields with the material that induces and aligns dipoles is described by the polarizing effect in the medium. The collective behavior of the particles is macroscopically described by the (electric) polarization, $\vec{P}$, and magnetization, $\vec{M}$, which are the electric and magnetic dipole moments per unit volume of the bulk material. Below, we derive equations for the permittivity and permeability of materials.

1.3.1 Permittivity

When an insulator is placed in an electric field, the bound charges in it rearrange themselves in such a way that there is a slight separation between the average positions of the positive and the negative charges. This separation is known as the polarization of the charge distribution and the materials that acquire polarization are referred as dielectrics. The effect of the applied electric field on a dielectric material is mainly to produce dipoles [48, 49].

Consider a dielectric material that is placed in an external electric field and that the average dipole moment of an atom is $\vec{p}$, directed along the field. Then, the dipole moment per unit volume $\vec{P}$, also known as the polarization, is defined as $\vec{P} = n\vec{p}$, where n is the number of atoms per unit volume. The total charge density ρ in the dielectrics can be expressed in terms of the free and the bound charge density as $\rho = \rho_f + \rho_p = \rho_f - \nabla \cdot \vec{P}$, where ρ_f is the free charge density and $\rho_p = -\nabla \cdot \vec{P}$ is the bound charge density. Also, the electric field inside the medium satisfies Gauss' law

given by

$$\nabla \cdot \vec{E} = 4\pi(\rho_f + \rho_p) = 4\pi(\rho_f - \nabla \cdot \vec{P}). \tag{1.3.1}$$

Further, rewriting Eq. (1.3.1), we obtain

$$\nabla \cdot \vec{D} = 4\pi\rho_f, \tag{1.3.2}$$

where the field term in (1.3.2) is referred as the electric displacement $\vec{D}$, defined by

$$\vec{D} = \vec{E} + 4\pi\vec{P}. \tag{1.3.3}$$

For linear and isotropic dielectrics, the polarization is related to the electric field by

$$\vec{P} = \chi\vec{E}, \tag{1.3.4}$$

where the constant χ is called the electric susceptibility. Substituting (1.3.4) into (1.3.3), we find that

$$\vec{D} = \varepsilon\vec{E}, \tag{1.3.5}$$

where

$$\varepsilon = 1 + 4\pi\chi. \tag{1.3.6}$$

Here, ε is called the dielectric constant of the material. Both χ and ε are determined by the atomic properties of the dielectric.

In an isotropic medium the induced polarization is always parallel to the electric field, that is independent of the direction along which the field is applied [50]. This is no longer true in anisotropic media. Since crystals are periodic arrays of atoms with certain symmetry, the induced polarization depends, both in its magnitude and direction, on the direction of applied field. In this case the polarization is given by

$$P_i = \sum_j \chi_{ij} E_j, \tag{1.3.7}$$

where χ_{ij} with $i,\ j = x,\ y,\ z$ is known as the electric susceptibility tensor. We can also describe the dielectric response of crystals by means of the electric permittivity tensor, ε_{ij}, defined by

$$D_i = \sum_j (1 + 4\pi\chi_{ij})E_j = \sum_j \varepsilon_{ij}E_j, \tag{1.3.8}$$

from which we get the expression to the permittivity tensor to be

$$\hat{\varepsilon} = \varepsilon_{ij} = 1 + 4\pi\chi_{ij}. \tag{1.3.9}$$

In general, the nine components that appear in ε_{ij} are constants of the medium and constitute the electric permittivity tensor, given by

$$\varepsilon_{ij} = \begin{pmatrix} \varepsilon_{xx} & \varepsilon_{xy} & \varepsilon_{xz} \\ \varepsilon_{yx} & \varepsilon_{yy} & \varepsilon_{yz} \\ \varepsilon_{zx} & \varepsilon_{zy} & \varepsilon_{zz} \end{pmatrix}. \tag{1.3.10}$$

1.3.2 Permeability

In any material medium, all the electrons within the atoms of the material are always in motion that involves both orbital and spin motion. These circulating charges constitute currents, which give the atom a magnetic moment generating a magnetic field surrounding the atom [49]. When the material is placed in a region where an external magnetic field is present, the atomic magnetic moments realign themselves, so that the magnetic fields of these moments change the original external magnetic field.

Suppose an external magnetic field is applied in a material so that the average magnetic dipole moment of the individual atoms is $\vec{m}$. Due to the applied field, these dipole moments will align along the direction of the magnetic field. The effect of

the field can be described by the magnetization vector $\vec{M}$, i.e., the magnetic dipole moment per unit volume, of the medium which is defined by $\vec{M} = n\vec{m}$, where n is the number of atoms per unit volume.

Conveniently, Ampere's law for the vector $\vec{B}$ can be written in terms of the free current $\vec{j}_f$ and the magnetization current $\vec{j}_m$ as

$$\nabla \times \vec{B} = \frac{4\pi}{c}(\vec{j}_f + \vec{j}_m) = \frac{4\pi}{c}(\vec{j}_f) + \nabla \times \vec{M}. \tag{1.3.11}$$

where the magnetization current is defined by $\vec{j}_m = c\nabla \times \vec{M}$. Rearranging (1.3.11), we get

$$\nabla \times \vec{H} = \frac{4\pi}{c}\vec{j}_f, \tag{1.3.12}$$

where

$$\vec{H} = \vec{B} - 4\pi\vec{M}, \tag{1.3.13}$$

Here, $\vec{H}$ is known as the magnetic field and $\vec{B}$ is called the magnetic induction vector.

In linear, isotropic magnetic materials, the magnetization is directly proportional to the $\vec{H}$ field,

$$\vec{M} = \chi\vec{H}. \tag{1.3.14}$$

The constant of proportionality χ is called the magnetic susceptibility. Substituting (1.3.14) into (1.3.13), and rearranging, we get

$$\vec{B} = \mu\vec{H}, \tag{1.3.15}$$

where

$$\mu = 1 + 4\pi\chi, \tag{1.3.16}$$

where the constant μ is called the magnetic permittivity.

For paramagnetic and diamagnetic materials, Eq. (1.3.14) is a good approximation. Paramagnetic materials have $\chi > 0$ and $\mu > 1$ so that the magnetic field in it is increased compared with the original field, whereas diamagnetic materials have $\chi < 0$ and $\mu < 1$, so the magnetic field in the material is decreased. In the case of ferromagnetic materials, the linear relation (1.3.14) is not valid. In these materials, $\vec{B}$ and $\vec{M}$ are complicated nonlinear functions of $\vec{H}$ in which the function $B = B(H)$ is nonlinear and multiple-valued.

In addition, if the magnetic material is anisotropic, the magnetization $\vec{M}$ is not parallel to the applied field $\vec{H}$. The magnetic susceptibility in those types of materials is a second rank tensor, and the corresponding magnetization is given by

$$M_i = \sum_j \chi_{ij} H_j, \tag{1.3.17}$$

where $i,\ j = x,\ y,\ z$. Thus, the magnetic response of these materials can be expressed by

$$B_i = \sum_j (1 + 4\pi\chi_{ij}) H_j = \sum_j \mu_{ij} H_j. \tag{1.3.18}$$

where the permeability tensor μ_{ij} is defined by

$$\hat{\mu} = \mu_{ij} = 1 + 4\pi\chi_{ij}. \tag{1.3.19}$$

In matrix representation, (1.3.19) takes the form:

$$\mu_{ij} = \begin{pmatrix} \mu_{xx} & \mu_{xy} & \mu_{xz} \\ \mu_{yx} & \mu_{yy} & \mu_{yz} \\ \mu_{zx} & \mu_{zy} & \mu_{zz} \end{pmatrix}. \tag{1.3.20}$$

1.4 The wave equation and dispersion relation

The electromagnetic wave equations can be obtained from the set of equations (1.2.1-1.2.4). For simplicity, let us consider a linear, homogeneous, and isotropic dielectric medium under source free condition. For such media Eqs. (1.2.1-1.2.4) reduce to

$$\vec{\nabla} \cdot \vec{D} = 0, \tag{1.4.1}$$

$$\vec{\nabla} \cdot \vec{B} = 0, \tag{1.4.2}$$

$$\vec{\nabla} \times \vec{E} = -\frac{1}{c}\frac{\partial \vec{B}}{\partial t}, \tag{1.4.3}$$

and

$$\vec{\nabla} \times \vec{H} = \frac{1}{c}\frac{\partial \vec{D}}{\partial t}. \tag{1.4.4}$$

Taking the curl of Eqs. (1.4.3) and (1.4.4) and manipulating by using the constitutive relations (1.2.5) and (1.2.6), and the vector identity

$$\vec{\nabla} \times (\vec{\nabla} \times \vec{a}) = \vec{\nabla}(\vec{\nabla} \cdot \vec{a}) - \nabla^2 \vec{a}, \tag{1.4.5}$$

where $\vec{a}$ can be either $\vec{E}$ or $\vec{H}$, we arrive

$$\nabla^2 \vec{E} = -\frac{1}{v^2}\frac{\partial^2 \vec{E}}{\partial t^2}, \tag{1.4.6}$$

$$\nabla^2 \vec{H} = -\frac{1}{v^2}\frac{\partial^2 \vec{H}}{\partial t^2}. \tag{1.4.7}$$

Here, $v = c/\sqrt{\varepsilon\mu} = c/n$ is the speed of the wave in the medium. Equations (1.4.6) and (1.4.7) are the electromagnetic wave equations for the electric and magnetic fields, respectively. The plane wave solutions for these equations are given by

$$\vec{E}(\vec{r}, t) = \vec{E}_0 e^{i(\vec{k}\cdot\vec{r} - \omega t)}, \tag{1.4.8}$$

and

$$\vec{H}(\vec{r},t) = \vec{H}_0 e^{i(\vec{k}\cdot\vec{r}-\omega t)}, \tag{1.4.9}$$

where $\vec{E}_0$ and $\vec{H}_0$ are constant vectors giving the direction and amplitudes of the fields, $\vec{k}$ is the wave vector, and ω is the angular frequency of the EM field.

Now, if we insert plane waves for each of the fields in (1.4.1-1.4.7) and perform the vector operations, we obtain

$$\vec{k}\cdot\vec{D} = 0, \tag{1.4.10}$$

$$\vec{k}\cdot\vec{B} = 0, \tag{1.4.11}$$

$$\vec{k}\times\vec{E} = \frac{\omega}{c}\vec{B}, \tag{1.4.12}$$

and

$$\vec{k}\times\vec{H} = -\frac{\omega}{c}\vec{D}. \tag{1.4.13}$$

From Eqs. (1.4.10) and (1.4.13), we observe that (i) $\vec{k}$ is perpendicular to both $\vec{D}$ and $\vec{B}$, (ii) $\vec{B}$ is perpendicular to $\vec{E}$, and (iii) $\vec{H}$ is perpendicular to $\vec{D}$.

Dispersion relation in isotropic media

Moreover, substituting the pane wave solution (1.4.8) into the wave equation for the electric field, i.e., Eq. (1.4.6), we find that

$$k^2 = n^2\frac{\omega^2}{c^2}, \tag{1.4.14}$$

or

$$k(\omega) = \frac{\omega}{c}n(\omega), \tag{1.4.15}$$

where $n(\omega) = \sqrt{\varepsilon(\omega)\mu(\omega)}$ is the refractive index of the medium. Equation (1.4.15) is known as the dispersion relation for a linear and isotropic medium.

1.5 Phase and group velocities

Among the important parameters that are used to characterize the propagation of electromagnetic wave in a medium are the phase and group velocities. The phase velocity is defined by

$$\vec{v}_p = \frac{\omega}{k}\hat{k} = \frac{c}{|n|}\hat{k}, \tag{1.5.1}$$

where $\hat{k} = \vec{k}/k$ is the unit vector in the direction of the wave vector $\vec{k}$ and the dispersion relation $\vec{k} = (\omega/c)|n|\hat{k}$ is used.

The group velocity is defined

$$\vec{v}_g = \nabla_k \omega = \frac{d\omega}{dk}\hat{k} \tag{1.5.2}$$

Using the dispersion relation, Eq. (1.5.2) becomes

$$\vec{v}_g = \frac{c}{n + \omega\frac{dn}{d\omega}}\hat{k}. \tag{1.5.3}$$

From (1.5.3) we can observe that the group velocity is positive even if n is negative, as it is the case for LHM, since $\hat{k}$ is also negative.

The group velocity can also be written in terms of the phase velocity as

$$\vec{v}_g = \frac{\vec{v}_p}{1 + \frac{\omega}{n}\frac{dn}{d\omega}}. \tag{1.5.4}$$

It is worth noting that in linear, isotropic, and nondispersive media, the group velocity is equal to the phase velocity.

Group refractive index

The modern way of studying complex group velocity is achieved by using the group refractive index, which is defined in terms of refractive index and its derivative with

respect to frequency as

$$n_g = n + \omega \frac{dn}{d\omega}, \tag{1.5.5}$$

where $n = n_1 + in_2$ is a complex refractive index and ω is the frequency. Accordingly n_g is also a complex quantity having real n_{g1} and imaginary n_{g2} parts given by

$$n_{g1} = n_1 + \omega \frac{dn_1}{d\omega}, \tag{1.5.6}$$

and

$$n_{g2} = n_2 + \omega \frac{dn_2}{d\omega}. \tag{1.5.7}$$

Group velocity in lossy periodic systems and its relation to pulse propagation have been discussed several decades ago [26]. In loss-less periodic media, group velocity is unambiguously related to the time domain pulse velocity [51]. In lossy media, additional pulse propagation phenomena are observed, including pulse attenuation and peak reshaping. In general, $v_g(\omega)$ has both real and imaginary parts, as a result of the change in ω due to an infinitesimal change in k along the dispersion relation $\omega(k)$, requiring interpretation in terms of the aforementioned pulse propagation effects.

Brillouin [26] and Louden [52] have suggested that in the presence of significant loss, the connection between group velocity and pulse propagation collapses. In highly lossy and dispersive media [27, 33] or more recently in metamaterials [53, 54], $d\omega/dk$ (where k is real) often predicts a superluminal pulse, leading to the apparent violation of relativity and causality.

However, the complex quantity $d\omega/dk$ remains related to pulse propagation. Garrett and McCumber [29] have shown that $d\omega/dk$ still gives the velocity of the time domain peak of a Gaussian pulse, even when $d\omega/dk$, with real k, is superluminal [55]. These findings have been experimentally confirmed [29, 34]. Others have identified

the imaginary part of $d\omega/dk$ as a measure of the shift in the carrier frequency of a Gaussian pulse [56]. If $d\omega/dk$ is known over a broad frequency range, then the real and imaginary parts of $d\omega/dk$ correspond to propagation velocity and pulse reshaping respectively [57].

1.6 Propagation of wave packets

So far we have been discussing propagation of plane waves with single frequency. In reality except vacuum, media are dispersive, that is, no wave is truly monochromatic, although some waves, such as those produced by lasers, are exceedingly close to being so. In the case of linear media, the equations of motion for electromagnetic waves are completely linear and so any sum of harmonic solutions is also a solution. By making use of this superposition principle a wave packet can be constructed from plane waves. In dispersive media, the phase velocity depends on the frequency. As a result, different frequency components of the wave propagate with different speeds, accompanied by a phase change with respect to one another. This usually leads to a spreading of the wave packet as it propagates in dispersive medium [50].

Consider the propagation of wave packets which results from the superposition of a continuous spectrum of plane waves having wave numbers k. A wave packet that propagates along the z-axis can be represented by

$$\psi(z,t) = \frac{1}{\sqrt{2\pi}} \int_{-\infty}^{\infty} A(k) e^{i(kz-\omega t)} dk, \tag{1.6.1}$$

where ω is the angular frequency and $A(k)$ is the amplitude which describes the properties of the linear superposition of the different waves. It is worth noting that the amplitude factor $A(k)$ for each plane wave of wave number k is negligible except

when k lies within a small interval Δk.

In general, the angular frequency $\omega(k)$ is a function of k, so that the angular frequencies in the wave packet represented by $\psi(z,t)$ as well as the wave numbers vary from one plane wave to another. If $\omega(k)$ is a slowly varying function of k and the values of k are confined to a small range Δk, then $\omega(k)$ may be expanded in a Taylor series in k about some point k_0 within the interval Δk. That is,

$$\omega(k) = \omega_0 + \frac{d\omega}{dk}\Big|_{k_0}(k-k_0) + \frac{1}{2}\frac{d^2\omega}{dk^2}\Big|_{k_0}(k-k_0)^2 + ... \tag{1.6.2}$$

where ω_0 is the value of $\omega(k)$ at k_0. The quadratic and higher-order terms in the Taylor expansion (1.6.2) may be neglected because the interval Δk and, consequently, $k-k_0$ are small. Substitution of equation (1.6.2) into the phase for each plane wave in (1.6.1) then gives

$$\begin{aligned} kz - \omega t &\approx (k + k_0 - k_0)z - \omega_0 t - \frac{d\omega}{dk}\Big|_{k_0}(k-k_0)t \\ &= k_0 z - \omega_0 t + [z - \frac{d\omega}{dk}\Big|_{k_0} t](k-k_0), \end{aligned}$$

so that equation (1.6.1) becomes

$$\psi(z,t) = B(z,t)e^{i(k_0 z - \omega_0 t)}, \tag{1.6.3}$$

where

$$B(z,t) = \frac{1}{\sqrt{2\pi}}\int_{-\infty}^{\infty} A(k)e^{i[z-(d\omega/dk)|_{k_0}t](k-k_0)}dk. \tag{1.6.4}$$

Thus, the wave packet $\psi(z,t)$ represents a plane wave of wave number k_0 and angular frequency ω_0 with its amplitude modulated by the factor $B(z,t)$. This modulating function $B(z,t)$ depends on z and t through the relationship $[z - t(d\omega/dk)|_{k_0}]$, and it moves in the positive z-direction with group velocity v_g given by

$$v_g = \frac{d\omega}{dk}\Big|_{k_0}. \tag{1.6.5}$$

1.6.1 Propagation of a wave packet without dispersion

Next, we investigate the change in shape of a wave packet as it propagates with time, in a nondispersive medium. The general expression for a wave packet $\psi(z,t)$ is given by equation (1.6.1). The amplitude factor $A(k)$ is equal to the inverse Fourier transform of $\psi(z,t)$ at $t=0$ and thus given by

$$A(k) = \frac{1}{\sqrt{2\pi}} \int_{-\infty}^{\infty} \psi(z',0) e^{-ikz'} dz'. \tag{1.6.6}$$

Substitution of equation (1.6.6) into (1.6.1) yields

$$\psi(z,t) = \frac{1}{2\pi} \int_{-\infty}^{\infty} \int_{-\infty}^{\infty} \psi(z',0) e^{i[k(z-z')-\omega t]} dk dz'. \tag{1.6.7}$$

Equation (1.6.7) relates the wave packet $\psi(z,t)$ at time t to the wave packet $\psi(z,0)$ at time $t=0$. However, the angular frequency $\omega(k)$ is dependent on k and the functional form must be known before evaluating the integral over k.

If the dependence of the angular frequency on k is assumed to be linear, i.e., $\omega(k) = v_p k$ with $k = |k|$, then (1.6.7) gives

$$\psi(z,t) = \frac{1}{2\pi} \int_{-\infty}^{\infty} \int_{-\infty}^{\infty} \psi(z',0) e^{ik[z-v_p t-z']} dk dz' \tag{1.6.8}$$

The integral over k may be expressed by applying the Dirac delta function

$$\delta(y-y') = \frac{1}{2\pi} \int_{-\infty}^{\infty} e^{ik(y-y')} dk,$$

so that

$$\psi(z,t) = \int_{-\infty}^{\infty} \psi(z',0)\delta(z-v_p t-z') dz' = \psi(z-v_p t, 0). \tag{1.6.9}$$

Thus, the wave packet $\psi(z,t)$ has the same value at point z and time t that it had at point $(z-v_p t)$ at time $t=0$. The wave packet has traveled with velocity v_p

without a change in its shape, i.e., it has traveled without dispersion. Since the phase velocity v_p is defined by $v_p = \omega/k$ and the group velocity defined by $v_g = d\omega/(dk)$ is found to be $[d\omega/(dk)]|_{k_0} = v_p$ when evaluated at $k = k_0$, the two velocities are the same in a nondispersive media.

1.6.2 Propagation of a wave packet with dispersion

Next consider the more general situation where the angular frequency $\omega(k)$ is not proportional to $|k|$, but is instead expanded in the Taylor series (1.6.2) about $(k-k_0)$. Now, however, we retain the quadratic term, but still neglect the terms higher than the quadratic terms, so that

$$\omega(k) \approx \omega_0 + v_g(k - k_0) + \beta(k - k_0)^2, \tag{1.6.10}$$

where equation (1.6.5) has been substituted for the first-order derivative and the second-order derivative is denoted by $\beta = \{[d^2\omega/(dk^2)]/2\}|_{k_0}$.

The phase in equation (1.6.7) then becomes

$$\begin{aligned} k(z - z') - \omega t &= (k - k_0)(z - z') + k_0(z - z') - \omega_0 t - v_g t(k - k_0) - \beta t(k - k_0)^2 \\ &= k_0 z - \omega_0 t - k_0 z' + (z - v_g t - z')(k - k_0) - \beta t(k - k_0)^2, \end{aligned}$$

so that the wave packet (1.6.9) takes the form

$$\psi(z,t) = \frac{e^{i(k_0 z - \omega_0 t)}}{2\pi} \int_{-\infty}^{\infty} \int_{-\infty}^{\infty} \psi(z',0) e^{-ik_0 z'} e^{i[(z - v_g t - z')(k - k_0) - \beta t(k - k_0)^2]} dk dz'. \tag{1.6.11}$$

The integral over k may be evaluated using Poisson integral, giving the result

$$\psi(z,t) = \frac{e^{i(k_0 z - \omega_0 t)}}{2\sqrt{i\beta\pi t}} \int_{-\infty}^{\infty} \psi(z',0) e^{-ik_0 z'} e^{-(z - v_g t - z')^2/(4i\beta t)} dz'. \tag{1.6.12}$$

Equation (1.6.12) relates the wave packet at time t to the wave packet at time $t = 0$ if the k-dependence of the angular frequency includes terms up to k^2. The profile of the wave packet $\psi(z,t)$ changes as time progresses because of the factor $t^{-1/2}$ before the integral and the t in the exponent within the integral. The nature of time dependence in Eq. (1.6.12) becomes more evident, if we select a specific form for the wave packet at time $t = 0$ [58]. For this purpose let us choose a gaussian wave packet, and supposing $\psi(z,0)$ has a gaussian distribution

$$B(z,t) = \frac{1}{\sqrt{2\pi}} e^{-\alpha^2[z-v_g t]^2/2}$$

with as its profile, so that equation (1.6.3) at time $t = 0$ is

$$\psi(z',0) = e^{ik_0 z'} B(z',0) = \frac{1}{\sqrt{2\pi}} e^{ik_0 z'} e^{-\alpha^2 v_g^2/2}. \tag{1.6.13}$$

Substitution of Eq. (1.6.13) in Eq. (1.6.12) gives

$$\psi(z,t) = \frac{1}{\sqrt{2\pi}} \frac{e^{i(k_0 z - \omega_0 t)}}{2\sqrt{i\beta\pi t}} \int_{-\infty}^{\infty} e^{-\alpha^2 v_g^2/2} e^{-(z-v_g t-z')^2/(4i\beta t)} dz'. \tag{1.6.14}$$

The integral of Eq. (1.6.14) can be evaluated using the Poisson integral formula,

$$\int_{-\infty}^{\infty} e^{(-ax^2+bx)} dx = \frac{\sqrt{\pi}}{a} e^{b^2/4a^2},$$

resulting

$$\psi(z,t) = \frac{e^{i(k_0 z - \omega_0 t)}}{\sqrt{2\pi(1+2i\alpha^2\beta t)}} e^{-\alpha^2 (z-v_g t)^2/2(1+2i\alpha^2\beta t)}. \tag{1.6.15}$$

The wave packet, then, consists of the plane wave $expi[k_0 z - \omega_0 t]$ with its amplitude modulated by

$$\psi(z,t) = \frac{1}{\sqrt{2\pi(1+2i\alpha^2\beta t)}} e^{-\alpha^2 (z-v_g t)^2/2(1+2i\alpha^2\beta t)}, \tag{1.6.16}$$

which is a complex function that depends on the time t.

1.7 Poynting vector and intensity

The quantity that describes the energy flux carried by electromagnetic waves is known as the Poynting vector. It is defined by

$$\vec{S} = \frac{c}{4\pi}(\vec{E} \times \vec{H}), \tag{1.7.1}$$

where $\vec{E}$ and $\vec{H}$ are the electric and magnetic field, respectively, which in general are complex parameters.

Consider the propagation of plane electromagnetic wave in an absorbing medium, with the wave propagating along the z-axis and the electric field polarized along the x-axis. The spacial and time dependence electric field can be given by [49]

$$\vec{E}(z,t) = \vec{E}_0 e^{i(kz-\omega t)} = \hat{x} E_0 e^{i(kz-\omega t)}, \tag{1.7.2}$$

or in terms of complex refractive index $n = n_1 + in_2$, we have

$$\vec{E}(z,t) = \hat{x} E_0 e^{-\omega n_2 z/c} e^{i\omega(n_1 z/c - t)}. \tag{1.7.3}$$

Using the constitutive relations (1.2.5) and (1.2.6) and (1.2.3), the magnetic field associated with this electric field becomes

$$ik(\hat{z} \times \vec{E}) = i\frac{\omega\mu}{c}\vec{H}, \tag{1.7.4}$$

or

$$\vec{H} = \hat{y}\frac{kc}{\mu\omega} E_0 e^{i(kz-\omega t)} = \hat{y} H_0 e^{i(kz-\omega t)}, \tag{1.7.5}$$

where $H_0 = [ck/(\mu\omega)]E_0$ is the amplitude of the magnetic field.

The time-averaged value of the Poynting vector, $\langle\vec{S}\rangle$, can be shown to be [59]

$$\langle\vec{S}\rangle = \frac{c}{8\pi}\Re e(\vec{E} \times \vec{H}^*). \tag{1.7.6}$$

The parameter $\vec{S}$ describes the flux of energy through the medium. Substituting (1.7.2) and (1.7.5) into (1.7.6), noting that μ and n are complex, and simplifying, we find

$$\langle \vec{S} \rangle = \hat{z} \frac{c}{8\pi} \frac{(n_1\mu_1 + n_2\mu_2)}{(\mu_1^2 + \mu_2^2)} |\vec{E}_0|^2 e^{-2\omega n_2 z/c}. \tag{1.7.7}$$

The time-average value of $\langle \vec{S} \rangle$ is related to the wave intensity I, i.e., the energy flux per unit area via the following equation:

$$I = I_0 e^{-2\omega n_2 z/c} = I_0 e^{-\alpha z}, \tag{1.7.8}$$

where I_0 is the intensity in the xy-plane at $z = 0$, and

$$\alpha = 2\frac{\omega}{c} n_2, \tag{1.7.9}$$

is the absorption coefficient of the material whose dimension is in cm^{-1} in cgs. Equation (1.7.8) is known as the Beer-Lambert law. It relates the attenuation of electromagnetic wave to the properties of the material through which the wave is traveling.

1.8 Superluminal, slow, and backward waves

The terms superluminal, slow, and backward propagation of light are related to the group velocity v_g. When waves propagate in dispersive media, the phase velocity assumes different value due to the dependence of the refractive index on the frequency; and the wave motion is described by the group velocity. According to the definition of group velocity, it has an additional term $\omega(dn)/d\omega$ in its denominator compared to the phase velocity. This additional term characterizes what type of propagation is taking place in the medium. For normal dispersion, where the refractive index increases with the increase in frequency, $dn/d\omega > 0$ and $\omega(dn)/d\omega > 1$ slow light

propagates in the medium [30]. Slow light has been observed in a different systems, including room temperature solids [39, 40] and atomic vapors [60, 61, 62].

In regions of anomalous dispersion $dn/d\omega < 0$, which can lead to "fast light" effects. If the medium is only weakly dispersive, v_g may exceed c, and the pulse will appear to propagate faster than the speed of light. In regions of strong anomalous dispersion, the second term may actually become larger in magnitude than n and force the group velocity to become negative. Negative group velocity propagation has been predicted by Brillouin and others [26, 29, 38, 57, 63], and observed experimentally in different materials [33, 34, 39, 64]. However, for negative or anomalous dispersion, $dn/d\omega < 0$, and v_g exhibits a singularity at $\omega(dn/d\omega) \approx n$.

An infinite group velocity means that the peak of the pulse emerging from the medium occurs at the same time as the peak of the pulse entering the medium, i.e., the peak appears to cross the medium instantaneously. A negative group velocity means that the peak of the emerging pulse occurs at an earlier time than the peak of the incident pulse [29]. The special theory of relativity demands that a signal cannot propagate with a velocity exceeding c. Furthermore, information cannot be transmitted at a negative velocity because it would conflict with the principle of causality, since it implies that a signal would be received before having been emitted. This apparent paradox was resolved by Sommerfeld and Brillouin by distinguishing between the information or signal velocity and the group velocity, and requiring that the signal velocity should not exceed c. To study slow or superluminal light propagation we need media which show deep dispersion; which include normal dispersion and anomalous dispersion. One such media currently investigated are atomic vapors or a dilute gas of atoms with strong absorption resonance [65].

1.9 Summary

In this chapter, starting from the microscopic response of atoms to electromagnetic fields, we have explained the macroscopic permittivity and permeability through polarization and magnetization vectors. Starting from Maxwell's material equations by developing the wave equation for electric and magnetic fields, the dispersion relation for linear, homogeneous, and isotropic dielectric medium is derived. The difference between phase velocity and group velocity; the relation between these quantities is discussed.

From the basic definitions of the Poynting vector, we have derived an expression for the average value of the Poynting vector in its general form for isotropic medium without preferring whether the medium is magnetic or nonmagnetic. The expression can be used for both regular and left handed materials. In addition, we also derived Beer's equation of absorption coefficient.

Moreover, the propagation of wave packets in dispersive and non dispersive media is discussed. It is shown that, the packet retains its shape when propagating in non dispersive media, whereas it suffers in its shape as it propagates in dispersive media. The conditions when superluminal, slow, and back ward propagation in dispersive media are explained.

Chapter 2

Negative Refractive Index in Structured Metamaterials

2.1 Introduction

In the 1950s and 1960s, artificial dielectrics were intensively investigated theoretically and experimentally for the manufacture of light-weight microwave antenna lenses to simulate plasma to have refractive indices less than unity in order to replace the parabolic receivers [66, 67]. In 1968, V.G. Veselago [3] boldly come up with the theory of fabricating artificial materials, also known as structured metamaterials, having simultaneous negative values of the permittivity (ε) and permeability (μ) with a corresponding negative refractive index. Veselago referred those media where both ($\varepsilon < 0$) and ($\mu < 0$) as left-handed media (LHM).

However, his work was largely overlooked, mainly, due to the absence of naturally existing materials with the LHM properties, until 1996 J.B Pendry, et al. [68] proposed various types of metallic wire structures to realize effective negative permittivity medium. Motivated with this progress they extended their theoretical investigations to attain materials with effective negative permeability by exploiting the

strong magnetic activities observed in nonmagnetic conductors [7]. The investigation of Pendry, et al. was not limited on finding materials with negative permittivity and permeability, separately, but also on combining those material properties including realization of negative refractive index in a single, homogeneous entity; which opened up a completely new research area, nowadays known as metamaterials [7, 68].

In this chapter first in Section 2.2, we discuss the peculiar characteristics that arise from the propagation of EMW in the so-called left-handed media. In Section 2.3 the dispersive and dissipative nature of left handed media will be described. The consequences of negative refraction, namely, anomalous refraction (reversal of Snell's law), Doppler effect, and Cherenkov effect will be discussed in Section 2.4. In Section 2.5, the achievements of negative refractive index materials in the microwave frequency region in one dimension and two dimensions, and the difficulties to achieve magnetic activity at optical frequency will be briefly presented . In Section 2.6, the effective medium theory is described briefly. In Section 2.7, we will consider SMMs proposed by Pendry. SMM systems have two components that result in negative permittivity and permeability, namely array of thin wire strips and split ring resonators, respectively. Section 2.8 summarizes the results of the Chapter.

2.2 Maxwell's equations and left handed media

When plane electromagnetic waves having the form $\exp\left[i(\vec{k}\cdot\vec{r}-\omega t)\right]$ propagate in a medium, the Maxwell's curl equations in the absence of sources, Eqs. (1.4.3) and (1.4.4), together with the constitutive relations (1.2.5) and (1.2.6) give

$$\vec{k}\times\vec{E}=\frac{\omega}{c}\mu\vec{H}, \tag{2.2.1}$$

$$\vec{k} \times \vec{H} = -\frac{\omega}{c}\epsilon\vec{E}. \tag{2.2.2}$$

Equations (2.2.1) and (2.2.2) shows that if ϵ and μ are simultaneously positive, then the wave vector $\vec{k}$, the electric field $\vec{E}$, and the magnetic field $\vec{H}$ form a right-handed triplet. Media in which the three vectors form a right-handed triplet are known as ordinary or right-handed media (RHM). On the other hand, if ϵ and μ are simultaneously negative, then the vectors $\vec{k}$, $\vec{E}$, and $\vec{H}$ form a left-handed triplet. Consequently, such types of media are known as left-handed media (LHM) [3].

2.2.1 The Poynting vector

Recall that the Poynting vector is defined by

$$\vec{S} = \frac{c}{4\pi}(\vec{E} \times \vec{H}). \tag{2.2.3}$$

For a plane electromagnetic waves, using (2.2.1), (2.2.2), the vector identity

$$\vec{a} \times (\vec{b} \times \vec{c}) = \vec{b}(\vec{a} \cdot \vec{c}) - \vec{c}(\vec{a} \cdot \vec{b}),$$

and $\vec{k} \cdot \vec{E}$, Eq. (2.2.1) takes the form

$$\vec{S} = \frac{c^2}{4\pi\omega\mu}|\vec{E}|^2\vec{k}, \tag{2.2.4}$$

or,

$$\vec{S} = \frac{c^2}{4\pi\omega\epsilon}|\vec{H}|^2\vec{k}. \tag{2.2.5}$$

Note that from Eq. (2.2.3), the quantity $(\vec{E} \times \vec{H})$ gives the direction of the energy flow. For a RHM, the vectors $\vec{S}$, $\vec{E}$, and $\vec{H}$ form a right-handed triplets. Also, from (2.2.4) and (2.2.5) the direction of the energy flow is in the direction of the wave vector $\vec{k}$. In the case where ϵ and μ are simultaneously negative, i.e., LH medium, the

quantity $(\vec{E} \times \vec{H})$ still gives the direction of the energy flow but the wave vector $\vec{k}$ lies in opposite direction to that of the Poynting vector, in contrast to what is observed in ordinary medium (RHM). In addition, with $\epsilon < 0$ and $\mu < 0$ simultaneously, the vectors $\vec{k}$, $\vec{E}$, and $\vec{H}$ form a left-handed triplet of vectors and hence the name left-handed medium (LHM).

Figure 2.1 depicts the relative orientations of the vector $\vec{k}$, $\vec{E}$, $\vec{H}$, and $\vec{S}$ for both right-handed and left-handed media. Notice that (i) for RHM, $\vec{E}$, $\vec{H}$, and $\vec{k}$ form right-handed triplet, whereas $\vec{S}$ and $\vec{k}$ are directed parallel to each other (left hand side of Fig. 2.1). (Right hand side) For LHM, $\vec{E}$, $\vec{H}$, and $\vec{k}$, form left-handed triplet, while $\vec{S}$, and $\vec{k}$, are oppositely directed (right hand side of Fig. 2.1).

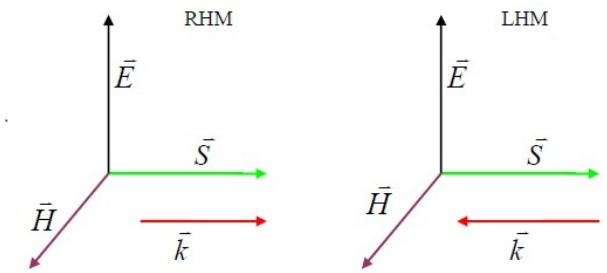

Figure 2.1: (Relative orientations of $\vec{E}$, $\vec{H}$, $\vec{k}$, and $\vec{S}$ in RHM (left hand side) and LHM (right hand side).

2.2.2 Dispersion relation in LHM

Recall that from (1.4.14), the dispersion relation for isotropic media is found to be

$$k^2 - \frac{\omega^2}{c^2}\epsilon\mu = 0, \tag{2.2.6}$$

or,

$$n^2 = \epsilon\mu = \frac{c^2k^2}{\omega^2}. \tag{2.2.7}$$

Further, Eq. (2.2.6) may be rewritten as

$$n_{\pm} = \pm\sqrt{\epsilon\mu}.$$

Electromagnetic waves propagate in a medium if and only if n^2 is positive. This can happen in two cases:

1. For regular medium, where both ϵ and μ are simultaneously positive, the positive root $n_+ = +\sqrt{(+\epsilon)(+\mu)} = +\sqrt{\epsilon\mu}$ must be taken to satisfy the requirement. This refractive index corresponds to RHM.

2. For the case where both ϵ and μ are simultaneously negative, Maxwell's equations remains valid provided that the negative root $n_- = -\sqrt{(-\epsilon)(-\mu)} = -\sqrt{\epsilon\mu}$ is taken, so that EMWs propagation in the medium is possible. This refractive index corresponds to LHM.

These are justified by considering the Poynting vector expressions given in Eqs. (2.2.4), and (2.2.5); that is when μ becomes negative then $\vec{k}$ has to be reversed, in Eq.(2.2.4), or when ε becomes negative then $\vec{k}$ has to be reversed, so that the Poynting vector to retain its direction.

2.2.3 Materials parameter space

The electromagnetic properties of materials can easily be described by means of material parameter space with ϵ as an abscissa and μ as an ordinate, as shown in Fig. 2.2. In this representation, materials are categorized based on their permittivity and permeability values. In Fig. 2.2, region I consists of materials with simultaneous positive values of ϵ and μ, which includes most of the dielectric materials. Region II

embraces materials with $\epsilon < 0$ and $\mu > 0$ such as metals, ferroelectric materials, and doped semiconductors that could exhibit negative permittivity at certain frequencies (below the plasma frequency). Region IV consists of materials with $\epsilon > 0$ and $\mu < 0$. Some of the ferrites for which the magnetic responses happens to quickly fade away above microwave frequencies belongs to this region. The most interesting region is region III, in which both ϵ and μ are simultaneously negative. Until now, no naturally existing materials possess such negative values of ϵ and μ, simultaneously.

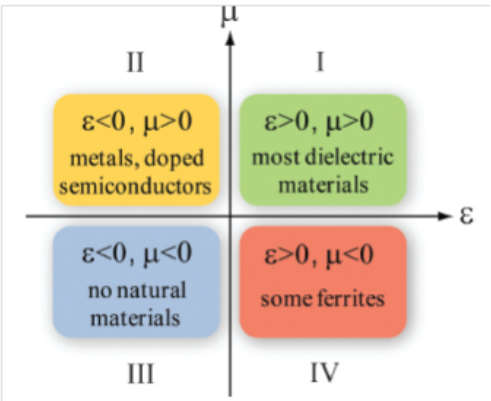

Figure 2.2: Material parameter space characterized by electric permittivity (ε) and magnetic permeability (μ) [69].

Moreover, the material parameter space also shows regions (materials) where the propagation of electromagnetic waves is enhanced, that is, in quadrant I both permittivity ε and permeability μ are positive making the square of the refractive index positive, and in region III, both permittivity ε and permeability μ are positive making the square of the refractive index positive, therefore in these quadrants, electromagnetic waves can propagate. In quadrants II and IV the waves are decaying and there is no propagation since parameters ε and μ have opposite signs.

2.3 Dispersive and dissipative nature of LHMs

In general, the permittivity and permeability, and the corresponding refractive index of materials are frequency dependent. In cases where these parameters do not depend on frequency, the energy density W of the electromagnetic fields defined by

$$W = \frac{1}{8\pi}\varepsilon E^2 + \frac{1}{8\pi}\mu H^2, \tag{2.3.1}$$

would be negative, when ε and μ are negative. When dispersion exists, the energy density must be written in a different form [70]. That is,

$$W = \frac{1}{8\pi}\Big[\frac{\partial}{\partial\omega}(\omega\varepsilon)\Big]E^2 + \frac{1}{8\pi}\Big[\frac{\partial}{\partial\omega}(\omega\mu)\Big]H^2. \tag{2.3.2}$$

This expression is positive for a very broad class of dispersion equations for $\varepsilon(\omega)$ and $\mu(\omega)$. In order for the energy density W defined by (2.3.2) to be positive, it is required that

$$\frac{\partial}{\partial\omega}(\omega\varepsilon) = \omega + \frac{\partial\varepsilon}{\partial\omega} > 0, \tag{2.3.3}$$

and

$$\frac{\partial}{\partial\omega}(\omega\mu) = \omega + \frac{\partial\mu}{\partial\omega} > 0. \tag{2.3.4}$$

These inequalities in (2.3.3) and (2.3.4) do not, in general, mean that ε and μ cannot be simultaneously negative [3]. However, for these equations to be valid, it is necessary that ε and μ depend on the frequency. Therefore, it can be concluded that left-handed media are frequency **dispersive** media. It is a known fact that, dispersive media, in general, are always dissipative [70]. This means that, the permittivity and permeability should be complex quantities; $\varepsilon = \varepsilon_1 + i\varepsilon_2$ and $\mu = \mu_1 + i\mu_2$. Dispersive media are characterized by $\varepsilon_2 > 0$ and $\mu_2 > 0$. Thus, the refractive index n and the wave vector $\vec{k}$ should also be complex quantities given by $n = n_1 + in_2$ and $k = k_1 + ik_2$.

There is no fundamental objection to the real parts of ε and μ being negative [70]. However, for media at thermodynamic equilibrium, the imaginary parts ε_2 or μ_2 should be positive. Thus, media with negative ε or μ also are causal. Therefore, the real and the imaginary parts of the permittivity ε as well as that of the permeability μ are related by Kramer-Kronig relations [70, 71]. That is,

$$\varepsilon_1 = 1 + \frac{2}{\pi} P \int \frac{\omega' \varepsilon_2(\omega')}{\omega'^2 - \omega^2} d\omega', \tag{2.3.5}$$

$$\varepsilon_2 = -\frac{2}{\pi} P \int \frac{\varepsilon_1(\omega') - 1}{\omega'^2 - \omega^2} d\omega', \tag{2.3.6}$$

where P stands for the principal value of the integral. The same relations hold also for the real and the imaginary parts of the permeability. Since the refractive index in this case is given by

$$n = \sqrt{\varepsilon(\omega)\mu(\omega)}, \tag{2.3.7}$$

the imaginary parts of the permittivity, the permeability and the refractive index always coexist with the real parts in dispersive media, which ascertains that left-handed media must be dissipative.

2.4 Consequences of negative refractive index

Materials with simultaneous negative values of permittivity and permeability with the corresponding negative refractive index are expected to show peculiar characteristics when electromagnetic waves propagates in the media. These media are predicted to show anomalous refraction, reversed Doppler effect, reversed Vavilov-Cherenkov effect, etc.

2.4.1 Anomalous refraction - Snell's law

Suppose a beam of light travels from medium 1 into another medium 2 having permittivities ε_{11} and ε_{21}, and permeabilities μ_{11} and μ_{21}, respectively. If the two media possess positive refractive index with their permittivity and permeability being positive, then we will have an ordinary refraction, i.e., the incident and refracted beams will be in the opposite side of the normal. However, if the second medium is of negative refractive index with $\varepsilon_{21} < 0$ and $\mu_{21} < 0$, then the incident and the refracted beams will be on the same side of the normal, a phenomenon known as anomalous refraction. This can be understood by evaluating the boundary conditions imposed on the tangential components of $\vec{E}$ and $\vec{H}$, and the normal components of $\vec{D}$ and $\vec{B}$. Thus, the tangential components of $\vec{E}$ and $\vec{H}$ at the interfaces are given by

$$\begin{aligned} E_{1t} &= E_{2t}, \\ H_{1t} &= H_{2t}, \end{aligned} \tag{2.4.1}$$

whereas the normal components takes the form

$$\begin{aligned} \varepsilon_{11} E_{1n} &= \varepsilon_{21} E_{2n}, \\ \mu_{11} H_{1n} &= \mu_{21} H_{2n}. \end{aligned} \tag{2.4.2}$$

Assuming that the interfaces are in the xy-plane, it is clear that the x- and y-components of the fields are not changed as the beams propagate from medium 1 to 2, regardless of the signs of the permittivities and permeabilities of the media. As for the normal z-components of the fields, they preserve their directions if $\varepsilon_{11},\ \varepsilon_{21} > 0$ and $\mu_{11},\ \mu_{21} > 0$. However, if $\varepsilon_{21} < 0$ and $\mu_{21} < 0$ while $\varepsilon_{11} > 0$ and $\mu_{11} > 0$, then the directions these components are reversed resulting to a negative refraction, as shown in Fig. 2.3.

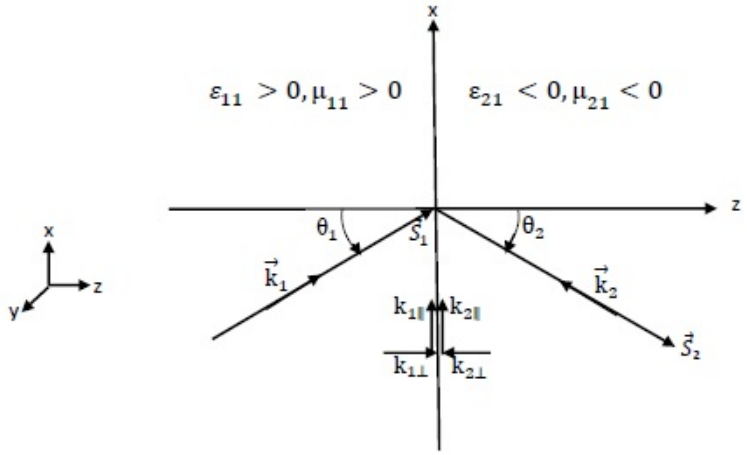

Figure 2.3: Negative refraction from medium with $\varepsilon < 0$, $\mu < 0$.

The relation between the angle of refraction θ_2 and the angle of incidence θ_1, determined from Snell's law, becomes

$$\frac{\sin\theta_1}{\sin\theta_2} = \frac{-\sqrt{\varepsilon_{21}\mu_{21}}}{\sqrt{\varepsilon_{11}\mu_{11}}} = -\frac{n_{21}}{n_{11}}, \tag{2.4.3}$$

where the refractive index, n_2 of media 2 is taken to be negative for $\varepsilon_{21} < 0$ and $\mu_{21} < 0$, simultaneously. Note that (2.4.3) implies that beams of light that enters from an ordinary medium 1 to a left-handed medium 2 undergoes refraction different from that occurring in the conventional media (RHM) - anomalous refraction.

2.4.2 Reversed Doppler effect

The Doppler effect is a phenomenon related to an apparent change in the frequency of a wave when there is a relative motion between the observer and the source of waves. As the object emitting the wave approaches the observer, the interval between the waves diminish - in other words, the radiation is squeezed, resulting to an increase

in frequency. As the object recedes away from the observer, the wave gets stretched, resulting to a decrease in frequency. The apparent frequency ω' measured by an observer when a source of frequency ω moving in a medium (refractive index n) relative to the observer with a velocity $\vec{v}$ is given by [3],

$$\omega' = \gamma(\omega + \vec{k} \cdot \vec{v}), \tag{2.4.4}$$

where $|\vec{k}| = n\omega/c$ and $\gamma = \sqrt{1/(1 - v^2/c^2)}$. Considering emission along the direction of motion of the source, we get the apparent frequency to be

- in RHM with $n = 1$
$$\omega' = \omega\sqrt{\frac{c+v}{c-v}}, \tag{2.4.5}$$
- in LHM with $n = -1$,
$$\omega' = \omega\sqrt{\frac{c-v}{c+v}}. \tag{2.4.6}$$

From (2.4.5), we observe that in RHM the observed frequency ω' is larger than that of the source (ω) when the source is approaching the observer, whereas Eq. (2.4.6) shows that in LHM the frequency measured for the same situation is smaller than ω - a quantity obtained in RHM if the source was receding from the observer. Thus, we conclude that the Doppler effect gets exactly reversed in a LHM compared with that in RHM.

2.4.3 Reversed Vavilov-Cherenkov effect

The phenomenon of Cherenkov radiation is about the emission cone of an electromagnetic radiation which is observed when a charged particle, usually an electron, travels through a medium with a speed greater than the speed of light in that medium.

It results due to the response of the medium to the transit of the charged particle. As the charged particle travels, it disrupts the local electromagnetic field, displacing and polarizing the electrons in the medium. After the transit, the electrons restore themselves to equilibrium with the emission of photons which would constructively interfere to give the observed intensity. Now the angle of the cone of radiation in a normal medium is acute (Fig. 1.4(a)), while that in a LHM is obtuse (Fig. 1.4(b)). To explain this reversal, consider Fig. 2.4, where the charged particle situated at the left corner at time $t = 0$, traverses to right corner with velocity v equal to $z = vt$ in time t. The refractive index of the medium being n, the cone of radiation of the electromagnetic wave emitted travels the distance $z_{em} = v_{em}t = ct/n$. Hence the acute angle of this cone will be

$$\cos\theta = \frac{v_{em}}{v} = \frac{c}{nv}. \tag{2.4.7}$$

Now, for a LHM, the refractive index n has a negative value ($\cos\theta < 0$), and therefore

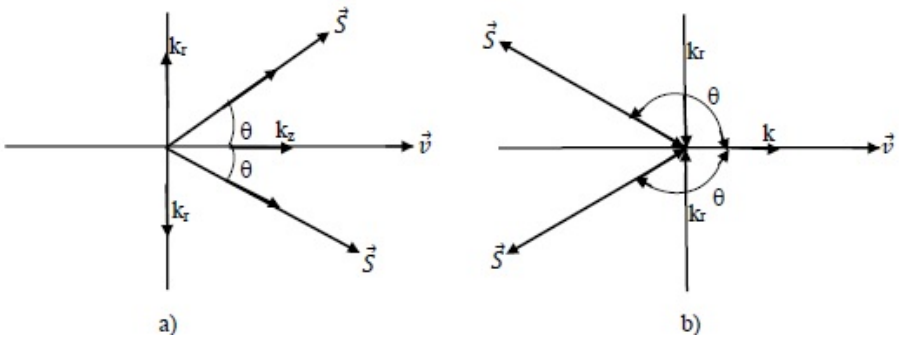

Figure 2.4: (a) The Cherenkov radiations RHM. (b)The Cherenkov radiations LHM.

this angle becomes obtuse, that is, the particle will radiate from a cone behind itself, rather than in front of it.

2.5 Negative refractive index in the microwave frequency region

Following the theoretical analysis of Pendry [7, 68] on the realization of negative permittivity medium (wire structure) [68], and negative permeability medium (split-ring-resonators) [7], the initial transmission experiments were performed by Smith, et al [9] on a one dimensional LHM that consisted of an array of unit cells, each cell consisting of one SRR and one conducting "post". The composite material was found to display anisotropic left-handed transmission band from 4.70 to 5.15 GHz. Scaling the transmission band to x-band frequencies by reducing the overall dimensions of the SRRs, a 2D isotropy was achieved by placing the SRRs along two orthogonal axes in a lattice. Further, the negative permittivity medium has been introduced as wire strips mounted behind the SRRs. Figure 2.5 shows the first LHM made of SRR and thin array of long metallic wires [9]. Since then, considerable interest has been sparked in the field of metamaterials.

Figure 2.5: SRR-thin array of long metallic wires.

Within a few years of the experimental demonstration of LH medium, magnetic metamaterials and consequently negative index materials designs have been advanced

from microwave frequencies to the visible region [72, 73, 74]. Negative permeability is the heart of negative index materials. To achieve magnetic resonance at optical frequencies, however, it is shown that the size of SRRs has to be smaller than 100 nm and the gap between components should be less than 10 nm [75]. Furthermore, the amplitude of the resonant permeability decreases and ceases to reach a negative value in the visible region [76]. Despite the fact that, magnetic permeability goes to unity at optical frequencies [70], researchers [53, 54, 55] reported negative index materials at optical frequencies.

2.6 Effective medium theory

The macroscopic electric and magnetic properties of a material, which are described by, polarization and magnetization, are average behavior of electrons and atoms in the external electric and magnetic fields of electromagnetic waves. This shows that, normal materials are also composites, where individual components are atoms and molecules, whose sizes are much smaller than the wavelength λ of the electromagnetic wave [9]. Thus, the system that consists of array of long metallic wires and nonmagnetic split-ring-resonators can be considered as a homogenous medium provided that the dimension of a unit cell of length a of the system satisfies the following condition:

$$a << \lambda. \tag{2.6.1}$$

If this condition is satisfied, the external electromagnetic wave will not see the fine details of each individual structure inside the unit cell, and the periodic structure can be considered as a homogenous medium. Therefore, the effective permittivity and permeability are valid concepts. [7]

2.7 Permittivity of array of metallic wires

It is known that there are materials, that exist in nature, which possess negative permittivity. For example, metals as plasma media possess negative permittivity up to plasma frequency. However, the application of solid metals in LHM is limited by the fact that the magnitude of ε is too large to match the broad band of frequencies ranging from microwave to optical frequency. The negative permittivity of metals can be shown using the dielectric function in the Drude model, since for metals

$$\varepsilon(\omega) = 1 - \frac{\omega_p^2}{\omega(\omega + i\gamma)}, \tag{2.7.1}$$

where γ is the damping constant and ω_p is the plasma frequency given by

$$\omega_p^2 = \frac{4\pi N e^2}{m_{eff}}, \tag{2.7.2}$$

where N is the number density, e is the electronic charge, and m_{eff} is the effective mass of an electron. For metals the plasma frequency extends up to the ultra violet frequency ($f_p \sim 10^{15}\ Hz$).

Next, consider an array of infinitely long, parallel, and very thin metallic wires of radius r placed periodically at a distance a in a square lattice in the $x - y$ plane with $a >> r$, as shown in Fig. 2.6. Assume that the wavelength λ of the impinging wave satisfies the relation $\lambda >> a >> r$, so that the wave "sees" the structure as a continuum. Suppose the electric field of the incident electromagnetic wave is parallel to the wires (along the z axis), so that the electrons are confined to move along the wires' axis only. This constraint which forces the electrons to move along thin wires has two effects:

1. the effective electron density n_{eff} is apparently reduced because only part of

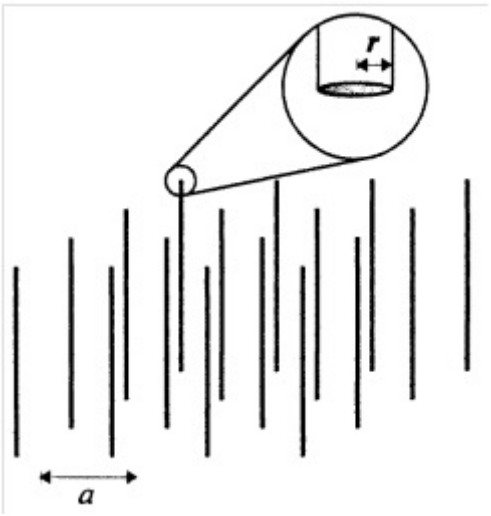

Figure 2.6: An array of metallic wires of radius r and arranged on a square lattice behaving as a low frequency plasma for electric field oriented along the wire.

space is filled by metal

$$n_{eff} = n\frac{\pi r^2}{a^2}, \tag{2.7.3}$$

where n is the density of electrons in the wires themselves, r is the radius of the wire, and a is side length of a cell of the square lattice on which the wires are arranged (Fig. 2.6).

2. there is an increase of the effective electron mass because of the self inductance of the wire structure, which is a magnetic effect. It can be shown that

$$m_{eff} = \frac{2\pi e^2 r^2 n}{c^2} \ln(a/r), \tag{2.7.4}$$

where m_{eff} is the new effective mass of the electrons. For aluminium, $m_{eff} = 2.7233 \times 10^4 m_e$, where m_e is the electron rest mass. This is an enormously enhanced effective mass and shifts the plasma frequency by a correspondingly

large amount. From the classical formula for the plasma frequency

$$\omega_p^2 = \frac{4\pi n_{eff} e^2}{m_{eff}} = \frac{2\pi c^2}{a^2 \ln(a/r)}, \tag{2.7.5}$$

where c is the speed of light in vacuum. Substituting the above values in (2.7.5) results to $\omega_p = 5.15 \times 10^{10}\ rad/s$, which is the microwaves frequency domain.

Equation (2.7.5) shows that the new reduced plasma frequency can be expressed in terms of electron effective mass and charge, which in turn is expressed only in terms of macroscopic parameters of the system, i.e., wire radius and lattice spacing.

Equations (2.7.3 - 2.7.5) are obtained by neglecting the effect of resistance, in reality there is no perfect conductor without resistance, therefore, the effect of resistance should be included. A more careful calculation including resistance gives the following expression for an effective dielectric function of the structure:

$$\varepsilon_{eff} = 1 - \frac{\omega_p^2}{\omega(\omega + i\frac{a^2\omega_p^2}{4\pi^2 r^2 \sigma})}, \tag{2.7.6}$$

where σ is the conductivity of the metal. Rewriting (2.7.6), we have

$$\varepsilon_{eff} = 1 - \frac{\omega_p^2}{\omega(\omega + i\gamma_{eff})}, \tag{2.7.7}$$

where

$$\gamma_{eff} = \frac{a^2\omega_p^2}{4\pi^2 r^2 \sigma} = \frac{c^2}{2\pi\sigma r^2 \ln\frac{a}{r}}. \tag{2.7.8}$$

Typically, for aluminium $\sigma = 3.28 \times 10^{17}\ s^{-1}$ and considering a wire radius $r = 10^{-2}\ cm$, and lattice constant $a = 5 \times 10^{-1}\ cm$, we find that the effective damping factor to be $\gamma_{eff} \approx 0.1\ \omega_p$. Thus by changing these parameters (in effect the plasma frequency), the value of the permittivity can be controlled.

The real part of effective permittivity of the metallic wire arrays defined by (2.7.7) is plotted in Fig. 2.7.

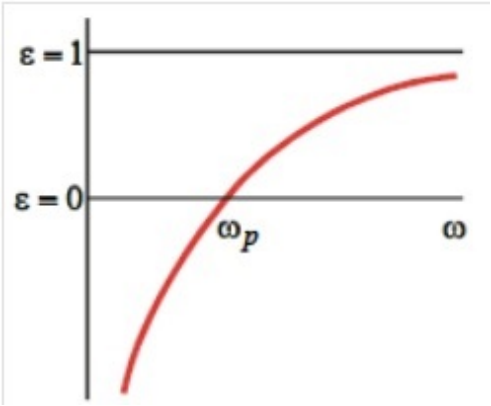

Figure 2.7: The real part of the effective permittivity, ε, of a plasma as a function of ω. Note that below the plasma frequency, ω_p; ε is negative.

2.8 Permeability of split-ring-resonators

Pendry's proposal was not only limited to low plasma frequency structures. He proposed also a structure which could result in negative permeability - a split ring resonator[7]. These resonators act like orbital current in natural magnetic material, since they are current loops. Such a current can be generated, for example, by time-varying magnetic field threading through a conducting coil, simply, as a consequence of Faraday's law. Although the induced current and thus the magnetic moment are normally weak, they can be dramatically enhanced by introducing resonances into the coil. Split-ring-resonators (SRRS) are one of the original designs for strong artificial magnetism. Each SRR is composed of two concentric split rings with the opening at the opposite directions as illustrated in Fig. 2.8. From the point of view of equivalent circuit, an SRR can be considered as an LC circuit with the natural resonant frequency given by $\omega_0 = \sqrt{1/(LC)}$, with L and C denoting the geometric inductance and capacitance of the SRR structure, respectively. In a frequency region centered at

ω_0, the magnetic flux threading through an SRR induces a strong circulating current, resulting in an effective magnetic moment. This induced moment responds in phase or out of phase with respect to the external magnetic field. If the strength of the magnetic response is sufficiently strong, effective magnetic permeability μ_{eff} with a negative value can be achieved.

In a wire structure medium the effective permittivity was derived using the condition that a cell size and the wire dimension are much less than the wavelength, that is, $\lambda \gg a \gg r$, here, also it is assumed the condition that a cell size that which gives effective negative permeability μ_{eff} be constructed so that $\lambda \gg a$, where a is the dimension of a unit cell and averaging of the fields to calculate μ_{eff}. That is,

$$\begin{aligned} \vec{B}_{ave} &= \mu_{eff}\vec{H}_{ave}, \\ \vec{D}_{ave} &= \varepsilon_{eff}\vec{E}_{ave}. \end{aligned} \tag{2.8.1}$$

The important point here is that there is a gap that prevents current from flowing around any one ring. However, there is a considerable capacitance between the two rings, which enables current to flow (see Fig. 2.8). It can be shown that the effective

Figure 2.8: When a magnetic field parallel to the ring axis is switched on it induces currents in the "split rings".

permeability of the SRR structure is given by [7]

$$\mu_{eff} = 1 - \frac{F}{1 + i\frac{\rho c^2}{2\pi\omega r} - \frac{3c^2}{4\pi^3\omega^2 C r^3}}, \tag{2.8.2}$$

where F is the fractional volume of the cell occupied by the interior ring, ρ is the resistivity of the sheets, where r is the radius of the interior ring, and C is the capacitance per unit area between the two rings. The parameter F is given by

$$F = \frac{\pi r^2}{a^2}, \tag{2.8.3}$$

where a is the lattice spacing; whereas the capacitance is

$$C = \frac{1}{4\pi d c^2}, \tag{2.8.4}$$

and where d represents the separation distance between the rings. In view of (2.8.4), (2.8.2) becomes

$$\mu_{eff} = 1 - \frac{\frac{\pi r^2}{a^2}}{1 + i\frac{\rho c^2}{2\pi\omega r} - \frac{3dc^2}{\pi^2\omega^2 r^3}}. \tag{2.8.5}$$

Since there is a capacitance in the system that can balance the inductance, μ_{eff} has a resonant form which is sketched in Fig. 2.9.

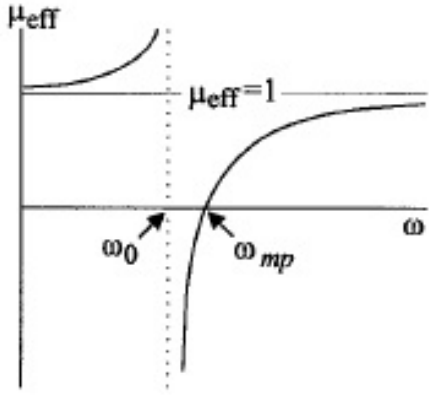

Figure 2.9: The effective magnetic permeability for split-ring shows a resonant structure dictated by the capacitance between the rings and magnetic inductance of the ring $\rho \approx 0$.

Figure 2.9 illustrates the generic form of μ_{eff} for all the structures presented here. The real part of the effective permeability increases from unity at $\omega = 0$ to a large positive values near $\omega = \omega_0$, where it then abruptly passes to a large negative value crossing $\mu = 0$ at $\omega = \omega_{mp}$. The peak value of the permeability is infinite in the case where losses are neglected.

The resonant frequency ω_0 at which μ_{eff} diverges is given by

$$\omega_0 = \sqrt{\frac{3dc^2}{\pi^2 r^3}}, \tag{2.8.6}$$

and ω_{mp} to be the "magnetic plasma frequency" defined by

$$\omega_{mp} = \sqrt{\frac{3dc^2}{\pi^2 r^3 (1-F)}}. \tag{2.8.7}$$

The separation between ω_0 and ω_{mp}, which is a measure of the range of frequencies over which we see a strong effect is determined by F. That is, (2.8.5) indicates that propagating modes occur up to the frequency ω_0, then followed by a gap where no propagating modes exist, followed by propagating modes starting from the frequency $\omega_0/\sqrt{1-F}$. The reason for the gap in propagation is of particular significance, since effective permeability will become negative for this frequency region.

If we take the following parameter values [7]: $r = 2 \times 10^{-1}\ cm$, $a = 5 \times 10^{-1}\ cm$, and $d = 1 \times 10^{-2}\ cm$, we get $f_0 = 2.94 \times 10^9\ Hz$ and $f_{mp} = 4.17 \times 10^9\ Hz$. These values of the frequencies at which the structure is active corresponds to a free-space wavelength of 10 cm which is much greater than the 0.5 cm separation between rings. This is typical of the capacitative structure and implies that the effective medium approximation is excellent [7].

By continuing this analysis, Pendry et al. [7] found a generic function for the

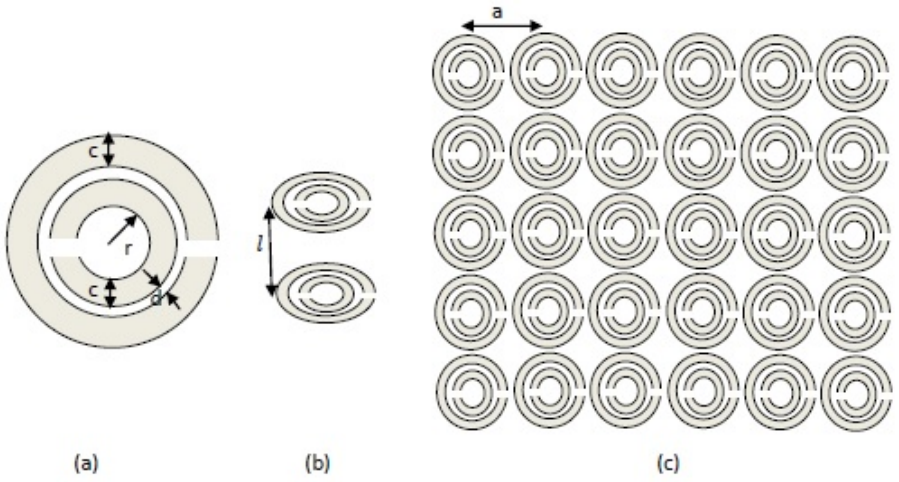

Figure 2.10: (a) Geometry of single SRR, (b) distance between layers, and (c) SRRs grouped into a periodic array.

effective permeability as

$$\mu_{eff} = 1 - \frac{\pi r^2/a^2}{1 - 3ldc_0^2/\pi\omega^2 \ln\frac{2c}{d} r^3 + i(\rho l c_0^2/2\pi\omega r)}, \tag{2.8.8}$$

or,

$$\mu_{eff} = 1 - \frac{F\omega^2}{\omega^2 - \omega_0^2 + i\gamma\omega}, \tag{2.8.9}$$

where ρ is the resistance per unit length of the rings measured around the circumference, ω is the frequency of incident radiation, c_0 is the speed of light in vacuum, c is width of each ring, l is the distance between layers, a is the lattice parameter, r is defined in Fig. 2.10, and F is the fractional area of the unit cell occupied by the interior of the split ring. The capacitance, C per unit length associated with the gaps between the rings in this case is given in cgs unit as

$$C = \frac{1}{4\pi^2} \ln\frac{2c}{d}. \tag{2.8.10}$$

The expressions for ω_0 and γ can be found by comparing the corresponding terms in Eq. (2.8.8) and (2.8.9).

Pendry, et al, pointed out that the system sustains longitudinal magnetic modes at the magnetic plasma frequency, the analog of the plasma modes of a gas of free electrical charges [77, 78]. The geometries consistent with this split-ring-resonators are depicted in Fig. 2.10.

2.9 Summary

In this Chapter, employing Maxwell's curl equations we have characterized left handed media as simultaneously possessing permittivity and permeability. In left handed media when electromagnetic wave is propagating, the wave vector is directed opposite to the Poynting vector, whereas in ordinary media it is directed parallel to the Poynting vector. Some consequence of wave propagation in negative refractive index media are; anomalous refraction (reversal of Snell's law), the Doppler effect, and the Cherenkov effect are explained. The difficulties of realizing left handed media and attempting to realize them is reviewed. The dispersive nature of left handed media is shown using the concept of energy density.

The permittivity from metallic rod structures, and permeability from split ring resonators of artificial materials proposed by Pendry are presented. It is shown that the rods have a negative permittivity just below their plasma frequencies, ω_p, as described by the Drude model, and suggested that a wire medium can be described by a Lorentzian model. The mechanism proposed by Pendry to lower the plasma frequencies is to build thin wires and thereby diluting the average concentration of electrons and enhancing the effective electron mass through self-inductance. The

overall effect lowered the plasma frequency to the microwave region for the given geometries, i.e., radius of the thin rods, the lattice spacing, and the type of the conductor from which the rods are built.

The split-ring-resonator (SRR) can be viewed as an LC circuit. A time-varying magnetic field applied parallel to the axis of the rings induces an emf in the plane of the element, driving currents within the 'split-rings' which result in a dispersive effective permeability. The magnetic activity increases as the capacitance increases and the filling factor decreases. With these structures negative refractive index is achieved in the region where both permittivity and permeability are negative. In both components the lossy nature is related to the resistivity of the conductors that which constitutes them.

Chapter 3

Interaction of a Two-Level Atom with Monochromatic Light

3.1 Introduction

The atom-field interaction is a basic problem in physics. Among the common formalisms used to describe this interaction are the density matrix and the perturbation theory. Almost all properties of the atomic and molecular systems can be described in terms of the atomic wavefunction $\psi(r,t)$. Often, this is accomplished through the application of quantum-mechanical perturbation theory of the atomic wavefunction. This approach can be used to make accurate predictions of the nonresonant response of atomic and molecular systems. However, relaxation processes, which are important for the case of near-resonant excitation, cannot be adequately described by this formalism. A relatively more powerful technique commonly employed to adequately describe the properties of atomic systems that involve relaxation is through the use of the density matrix formulation of quantum mechanics. This formalism is capable of treating effects, such as collisional broadening of the atomic resonances, that cannot be treated by the simple theoretical formalism based on the atomic wave function

[79, 80].

In this Chapter we discuss light-matter interaction between an atomic system and a coherent monochromatic light using the density matrix formalism. In section 3.2, we describe atom-light interaction, taking the atom as quantum system and the light field classically. in section 3.3, the density matrix, its time evolution, and the expectation value of an observable will be discussed. In section 3.4, the steady state solution for the population and coherence using the rotating-wave approximation will be derived, in addition, the density matrix equation of motion for a system of closed two-level atom is solved and the result is applied in section 3.5 to determine the susceptibility of the system. Section 3.6 presents the concept of Rabi oscillations in brief as coupling between the light field and the atomic quantity, namely, the electric dipole moment. The results of the chapter are summarized in section 3.7

3.2 Semiclassical description atomic systems

Consider a quantum-mechanical system, such as an atom, which is known to be in a particular quantum-mechanical state denoted by n. All of the physical properties of the system can be described in terms of the wavefunction $\psi_n(r,t)$ that is appropriate to the state. This wavefunction satisfies the time-dependent Schrodinger equation given by [79]

$$i\hbar\frac{d\psi_n(r,t)}{dt} = \hat{H}\psi_n(r,t), \tag{3.2.1}$$

where $\hat{H}$ is the Hamiltonian. For the description of field-matter interaction the Hamiltonian is written as

$$\hat{H} = \hat{H}_0 + \hat{H}'(t), \tag{3.2.2}$$

where $\hat{H}_0$ is the Hamiltonian for a free atom and $\hat{H}'(t)$ is the interaction Hamiltonian, which describes the interaction of the atom with the electromagnetic field. In the absence of an external field, the general solution of (3.2.1) is

$$\psi_n(r,t) = \phi_n(r)e^{-i(E_n/\hbar)t}. \tag{3.2.3}$$

Here, $\phi_n(r)$ is the spatially varying part of the wavefunction, which satisfies the time-independent Schrodinger equation

$$H_0\phi_n(r) = E_n\phi_n(r). \tag{3.2.4}$$

Assuming that the stationary wavefunctions form a complete, orthonormal set satisfying the condition

$$\int \phi_m^*(r)\phi_n(r)d^3r = \delta_{mn}, \tag{3.2.5}$$

so that the wavefunction of state n can be represented as a linear combination of the stationary wavefunctions. That is,

$$\psi_n(r,t) = \sum_n C_n(t)\phi_n(r), \tag{3.2.6}$$

where $C_n(t)$ is the probability amplitude. The evolution of $\psi_n(r,t)$ in time can be specified in terms of the time evolution of each of the probability amplitude, which is determined by substituting (3.2.6) into (3.2.1). That is,

$$i\hbar\sum_n \frac{dC_n(t)}{dt}\phi_n(r) = \sum_n C_n(t)\hat{H}\phi_n(r). \tag{3.2.7}$$

Then, multiplying both sides of (3.2.7) from the left by $\phi_m^*(r)$ and integrating over all space by making use of (3.2.5), we get

$$i\hbar\frac{dC_m(t)}{dt} = \sum_n H_{mn}C_n(t), \tag{3.2.8}$$

Here, H_{mn} is the matrix elements of the Hamiltonian, $\hat{H}$, defined by

$$H_{mn} = \int \phi_m^*(r)\hat{H}\phi_n^*(r)d^3r. \tag{3.2.9}$$

The expectation value of an observable quantity A of the system is given by

$$\langle A\rangle = \langle\psi_n|\hat{A}|\psi_n\rangle = \langle n|\hat{A}|n\rangle. \tag{3.2.10}$$

In terms of the probability amplitudes, (3.2.10) can be written as

$$\langle A\rangle = \sum_{mn} C_m^* C_n A_{mn}, \tag{3.2.11}$$

where $A_{mn} = \langle\phi_m|\hat{A}|\phi_n\rangle$ is the matrix element of $\hat{A}$.

It is worth noting that Eqs. (3.2.1-3.2.11) provide a complete description of the time evolution of a relaxation "free" system and of all of its observable properties, provided that the initial state and the Hamiltonian operator $\hat{H}$ of the system are known.

3.2.1 Density matrix

Under circumstances, where the precise state of the system is unknown, the density matrix formalism can be used to describe the system in a statistical sense. Let us denote by $p_{n'}$ the (classical) probability function at which the system is in the state n'. Then, the elements of the density matrix, ρ_{nm}, of the system is defined by

$$\rho_{nm} = \sum_{n'} p(n')C_m^* C_n. \tag{3.2.12}$$

The physical interpretations of the elements of the density matrix are: (i) the diagonal elements ρ_{nn} give the probability that the system is in energy eigenstate n, and (ii) the off-diagonal elements ρ_{nm} give the "coherence" between levels n and m, in the

sense that ρ_{nm} will be nonzero only if the system is in a coherent superposition of energy eigenstate n and m [79].

Hence, the expectation value of any observable quantity, in which the exact state of the system is not known, can be calculated using the density matrix. This is accomplished by averaging Eq. (3.2.11) over all possible states of the system. That is,

$$\overline{\langle A \rangle} = \sum_{n'} p(n') \sum_{nm} C_m^* C_n A_{mn} = \sum_{nm} \rho_{nm} A_{mn}. \tag{3.2.13}$$

Further, using the identity

$$\sum_{nm} \rho_{nm} A_{mn} = \sum_{n} \Big(\sum_{m} \rho_{nm} A_{mn} \Big) = \sum_{n} (\hat{\rho}\hat{A})_{nn} = Tr(\hat{\rho}\hat{A}),$$

the expectation value of A defined by equation (3.2.13), becomes

$$\overline{\langle A \rangle} = Tr(\hat{\rho}\hat{A}). \tag{3.2.14}$$

Time evolution of the density matrix

Next, we determine how the density matrix evolves in time. Differentiating (3.2.12), we find that

$$\dot{\rho}_{nm} \equiv \frac{d\rho_{nm}}{dt} = \sum_{n'} \frac{dp(n')}{dt} C_m^* C_n A_{mn} + \sum_{n'} p(n') \Big(C_m^* \frac{dC_n}{dt} + \frac{dC_m^*}{dt} C_n \Big). \tag{3.2.15}$$

Assume that $p(n')$ does not vary in time and using the Schrodinger's equation for the time evolution of the probability amplitudes equation (3.2.8), it can be shown that (3.2.15) simplifies to

$$\dot{\rho}_{nm} = \sum_{n'} p(n') \frac{i}{\hbar} \sum_{\nu} (C_n C_\nu^* H_{\nu m} - C_m^* C_\nu H_{n\nu}), \tag{3.2.16}$$

or,

$$\dot{\rho}_{nm} = \frac{i}{\hbar} \sum_{\nu} (\rho_{n\nu} H_{\nu m} - H_{n\nu} \rho_{\nu m}). \tag{3.2.17}$$

Finally, the summation over ν can be performed formally to rewrite (3.2.17) as

$$\dot{\rho}_{nm} = \frac{i}{\hbar}(\hat{\rho}\hat{H} - \hat{H}\hat{\rho})_{nm} = -\frac{i}{\hbar}[\hat{H}, \hat{\rho}]_{nm}. \tag{3.2.18}$$

Equation (3.2.18) describes how the density matrix evolves in time as the result of interactions that are included in the Hamiltonian $\hat{H}$. However, there are cases where certain interactions (such as those resulting from collisions between atoms) that cannot conveniently be included in a Hamiltonian description, resulting to a nonvanishing value of $dp(n')/dt$ in (3.2.15). Such processes are often modeled by adding phenomenological damping terms to the density matrix equations so that it is made to have the form

$$\dot{\rho}_{nm} = -\frac{i}{\hbar}[\hat{H}, \hat{\rho})]_{nm} - \gamma_{nm}(\rho_{nm} - \rho_{nm}^{(eq)}), \tag{3.2.19}$$

where γ_{nm} is a decay rate. Note that the phenomenological damping term indicates that ρ_{nm} relaxes to its equilibrium value $\rho_{nm}^{(eq)}$ at rate γ_{nm}. Further, we assume $\gamma_{nm} = \gamma_{mn}$ and $\rho_{nm}^{(eq)} = 0$, for $n \neq m$.

3.3 Density matrix description of two-level atom

Consider a nondegenerate two-level atom, with the lower and upper levels denoted by a and b as shown in Fig. 3.1, respectively. Let the energies of levels a and b be $E_a = \hbar\omega_a$ and $E_b = \hbar\omega_b$, with $E_b > E_a$, respectively. In this Section we seek to determine the density matrix equations of motion for a two-level system in the absence of damping effects, when perturbed by a light field. The Hamiltonian for the system is given by

$$\hat{H} = \hat{H}_0 + \hat{V}(t), \tag{3.3.1}$$

where $\hat{H}_0$ is the atomic Hamiltonian and $\hat{V}(t)$ is the interaction Hamiltonian which describes the coupling of the atom with the electromagnetic field.

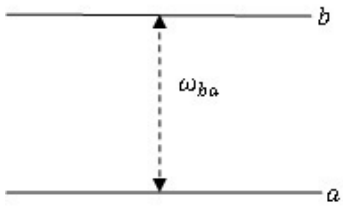

Figure 3.1: A two-level atom.

Employing the electric dipole approximation, the interaction Hamiltonian can be written as

$$\hat{V}(t) = -\hat{\mu}\tilde{E}(t), \tag{3.3.2}$$

where $\tilde{E}(t)$ the time dependent electric optical field and $\hat{\mu}$ is the electric dipole moment which, in general, for a two-atom system takes the form:

$$\hat{\mu} = \begin{pmatrix} \mu_{aa} & \mu_{ab} \\ \mu_{ba} & \mu_{bb} \end{pmatrix}, \tag{3.3.3}$$

whereas $\hat{V}$, in general, has the form

$$\hat{V} = \begin{pmatrix} V_{aa} & V_{ab} \\ V_{ba} & V_{bb} \end{pmatrix}. \tag{3.3.4}$$

Equation (3.3.3) can be simplified by assuming that the atomic wave functions of the states a and b have definite parity so that the diagonal elements of $\hat{\mu}$ vanish, that is, $\mu_{aa} = \mu_{bb} = 0$, and hence

$$V_{aa} = V_{bb} = 0 \tag{3.3.5}$$

On the other hand, the nonzero elements of the interaction Hamiltonian are related by the expression given by

$$V_{ba} = V_{ab}^{*} = -\mu_{ba}\tilde{E}(t). \tag{3.3.6}$$

In addition, for the model of two-level atom, Eq. (3.2.11) which describes the state of the system is a 2×2 matrix, and is given by

$$\hat{\rho} = \begin{pmatrix} \rho_{aa} & \rho_{ab} \\ \rho_{ba} & \rho_{bb} \end{pmatrix}, \tag{3.3.7}$$

where $\rho_{ba} = \rho_{ab}^{*}$. The corresponding equation for the time evolution of the density matrix is given by (3.2.18). That is,

$$\dot{\rho}_{nm} = \frac{-i}{\hbar}\sum_{\nu}(H_{n\nu}\rho_{\nu m} - \rho_{n\nu}H_{\nu m}), \tag{3.3.8}$$

where $m,\ n$ can take on the values a or b. Moreover, the Hamiltonian $\hat{H}_0$ can be decomposed into atomic and interaction parts as follows:

$$\hat{H}_{0,nm} = E_n\delta_{nm}. \tag{3.3.9}$$

Then, substituting (3.3.9) into (3.3.8), we obtain [79]

$$\dot{\rho}_{nm} = -i\omega_{nm}\rho_{nm} - \frac{i}{\hbar}\sum_{\nu}(V_{n\nu}\rho_{\nu m} - \rho_{n\nu}V_{\nu m}), \tag{3.3.10}$$

where $\omega_{nm} = (E_n - E_m)/\hbar$ denotes the transition frequency and here also, similar to m and n, the index ν can only have the values a or b. Explicitly writing the system of equations for the system of two-level atom given by equation (3.3.10) results in the following system of equations:

$$\dot{\rho}_{ba} = -i\omega_{ba}\rho_{ba} + iV_{ba}(\rho_{bb} - \rho_{aa})/\hbar, \tag{3.3.11}$$

$$\dot{\rho}_{bb} = i(V_{ba}\rho_{ab} - \rho_{ba}V_{ab})/\hbar, \tag{3.3.12}$$

$$\dot{\rho}_{aa} = i(V_{ab}\rho_{ba} - \rho_{ab}V_{ba})/\hbar. \tag{3.3.13}$$

Furthermore, adding (3.3.12) and (3.3.13) by making use of (3.3.6), we find that

$$\dot{\rho}_{aa} + \dot{\rho}_{bb} = 0, \tag{3.3.14}$$

which shows that the total population $\rho_{bb} + \rho_{aa}$ is a conserved quantity. Moreover, recall that the diagonal elements of the density matrix, ρ_{aa} and ρ_{bb}, represent probabilities of occupation of states a and b, so that the sum of these probabilities must be equal to unity. That is,

$$\rho_{aa} + \rho_{bb} = 1. \tag{3.3.15}$$

Equations (3.3.11-3.3.13) constitute the density matrix equations of motion for a two-level atom in the absence of relaxation processes. Next we will see the effect of relaxation processes on those density matrix equations.

3.3.1 Closed two-level atom

Let us consider the relaxation process where the upper level b is assumed to decay, via spontaneous emission, to the lower level a at a rate Γ_{ba}, as illustrated schematically in Fig. 3.2. The lifetime of the upper level is given by $T_1 = 1/\Gamma_{ba}$. Such system is known as closed, because any population that leaves the upper level enters the lower level. In addition, it is assumed that the atomic dipole moment, $\hat{\mu}$ is dephased in the characteristic time T_2, leading to a transition line-width given by $\gamma_{ba} = 1/T_2$.

The effect of the relaxation processes on the equations for the time evolution of the density matrix is described mathematically by adding decay terms phenomenologically to Eq. (3.2.19). The result is shown in Eq. (3.2.19), which for the closed

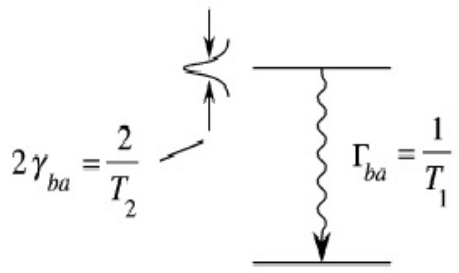

Figure 3.2: Relaxation processes of the closed two-level atom.

two-level system have the following forms:

$$\dot{\rho}_{ba} = -i(\omega_{ba} + \gamma_{ba})\rho_{ba} + iV_{ba}(\rho_{bb} - \rho_{aa})/\hbar, \tag{3.3.16}$$

$$\dot{\rho}_{bb} = -\Gamma_{ba}\rho_{bb} - i(V_{ba}\rho_{ab} - \rho_{ba}V_{ab})/\hbar, \tag{3.3.17}$$

$$\dot{\rho}_{aa} = \Gamma_{ba}\rho_{bb} + i(V_{ba}\rho_{ab} - \rho_{ba}V_{ab})/\hbar. \tag{3.3.18}$$

Note that Eq. (3.3.16) depends on ρ_{aa} and ρ_{bb} only in terms of the difference, $\rho_{bb} - \rho_{aa}$. Hence, it convenient to consider the equation of motion satisfied by this difference. That is, subtracting (3.3.18) from (3.3.17) and using the relation $2\rho_{bb} = (\rho_{bb} - \rho_{aa}) + 1$, we obtain

$$\dot{\rho}_{bb} - \dot{\rho}_{aa} = -\Gamma_{ba}[(\rho_{bb} - \rho_{aa}) + 1] - 2i(V_{ba}\rho_{ab} - \rho_{ba}V_{ab})/\hbar. \tag{3.3.19}$$

Equation (3.3.19) is based on the assumption that only downward spontaneous transitions could occur, so that the population difference under thermal equilibrium is $(\rho_{bb} - \rho_{aa})^{(eq)} = -1$. However, (3.3.19) may be generalized by allowing the possibility that $(\rho_{bb} - \rho_{aa})^{(eq)}$ can have some value other than -1. Thus, its generalized form can be rewritten as:

$$\dot{\rho}_{bb} - \dot{\rho}_{aa} = -\Gamma_{ba}[(\rho_{bb} - \rho_{aa}) - (\rho_{bb} - \rho_{aa})^{(eq)}] - 2i(V_{ba}\rho_{ab} - \rho_{ba}V_{ab})/\hbar. \tag{3.3.20}$$

We therefore observe that the density matrix equations of motion for a closed two-level system reduce to just two coupled equations given by equations (3.3.16) and (3.3.20).

3.4 Steady-state response of a two-level atom to a monochromatic field

Suppose a monochromatic, steady-state field is applied to a closed two-level atom. Below, we seek to examine the nature of the solution to the density matrix equations of motion for such system. In order to accomplish this, let the interaction Hamiltonian for an applied field, in the electric dipole approximation, be given by

$$\hat{V} = -\hat{\mu}\tilde{E}(t) = -\hat{\mu}(Ee^{-i\omega t} + E^* e^{i\omega t}), \tag{3.4.1}$$

where ω is the frequency of the applied monochromatic field. The matrix elements of the interaction Hamiltonian that corresponds to $\hat{V}$ defined by (3.4.1) are then given by

$$V_{ba} = -\mu_{ba}(Ee^{-i\omega t} + E^* e^{i\omega t}). \tag{3.4.2}$$

It is worth noting that Eqs. (3.3.16) and (3.3.20) cannot be solved exactly for V_{ba} given by Eq. (3.4.2). However, they can be solved in an approximation known as the rotating-wave approximation, which asserts that the part of V_{ba} that oscillates as $e^{-i\omega t}$ acts as a more effective driving term for ρ_{ba} than does the part that oscillates as $e^{i\omega t}$. Hence, Eq. (3.4.2) can be approximated to be given by

$$V_{ba} = -\mu_{ba}Ee^{-i\omega t}. \tag{3.4.3}$$

Also, let us define the slowly varying quantity σ_{ba}, in such a way that

$$\rho_{ba}(t) = \sigma(t)_{ba} e^{-i\omega t}. \tag{3.4.4}$$

In view of (3.4.3) and (3.4.4), Eqs. (3.3.16) and (3.3.20) become

$$\dot{\sigma}_{ba} = [i(\omega - \omega_{ba}) - \gamma_{ba}]\sigma_{ba} - i\mu_{ba}E(\rho_{bb} - \rho_{aa})/\hbar, \tag{3.4.5}$$

$$\dot{\rho}_{bb} - \dot{\rho}_{aa} = -\Gamma_{ba}[(\rho_{bb} - \rho_{aa}) - (\rho_{bb} - \rho_{aa})^{(eq)}] + 2i\mu_{ba}(E\sigma_{ab} - E^*\sigma_{ba})/\hbar. \tag{3.4.6}$$

Finally, the steady-state solution, i.e., the solution that is valid long after the transients have died out, of (3.4.5) and (3.4.6) are obtained by setting the left-hand sides equal to zero. Thus, the steady-state solutions are

$$\rho_{ba} = \frac{\mu_{ba}Ee^{-i\omega t}(\rho_{bb} - \rho_{aa})}{\hbar(\omega - \omega_{ab} + i/T_2)}, \tag{3.4.7}$$

and

$$\rho_{bb} - \rho_{aa} = \frac{(\rho_{bb} - \rho_{aa})^{(eq)}[1 + (\omega - \omega_{ab})^2 T_2^2]}{1 + (\omega - \omega_{ab})^2 T_2^2 + (4/\hbar^2)|\mu_{ba}|^2|E|^2 T_1 T_2}. \tag{3.4.8}$$

Here the identities $\Gamma_{ba} = 1/T_1$ and $\gamma_{ba} = 1/T_2$ are used.

3.5 Electric susceptibility of an assembly of two-level atoms

Once the solutions of the components of the density matrix are explicitly known, then the expectation value of any observable physical quantity of the system can be determine using equation (3.2.14). Next, we calculate the polarization of a system of closed two-level atom using the expectation value of the dipole moment, $\hat{\mu}$.

For an assembly of N atoms per unit volume the polarization, in terms of the expectation value of the dipole moment, is defined by

$$\tilde{P}(t) = N\langle\hat{\tilde{\mu}}\rangle, \tag{3.5.1}$$

where $\tilde{P}(t)$ is the polarization. Using (3.2.14), the expectation value of the dipole moment becomes

$$\langle\hat{\tilde{\mu}}\rangle = Tr(\hat{\tilde{\rho}}\hat{\tilde{\mu}}), \tag{3.5.2}$$

where from (3.3.3) and (3.3.7), with $\mu_{aa} = \mu_{bb} = 0$, we find that

$$\hat{\tilde{\rho}}\hat{\tilde{\mu}} = \begin{pmatrix} \rho_{ab}\mu_{ba} & \rho_{aa}\mu_{ab} \\ \rho_{bb}\mu_{ba} & \rho_{ba}\mu_{ab} \end{pmatrix}, \tag{3.5.3}$$

so that (3.5.2) becomes

$$\langle\hat{\tilde{\mu}}\rangle = \rho_{ab}\mu_{ba} + \rho_{ba}\mu_{ab}. \tag{3.5.4}$$

In view of (3.5.4), (3.5.1) becomes

$$\tilde{P}(t) = N\mu_{ba}(\rho_{ab} + \rho_{ba}). \tag{3.5.5}$$

Introducing the complex amplitude P of the polarization through the relation

$$\tilde{P}(t) = Pe^{-i\omega t} + P^*e^{i\omega t}, \tag{3.5.6}$$

the complex susceptibility of the system, $\chi = \chi' + i\chi''$, is defined by

$$P = \chi E. \tag{3.5.7}$$

Using equations (3.5.5-3.5.7 and (3.4.7), the susceptibility becomes

$$\chi = \frac{N|\mu_{ba}|^2(\rho_{bb} - \rho_{aa})}{\hbar(\omega - \omega_0 + i/T_2)}, \tag{3.5.8}$$

where the population difference $(\rho_{bb} - \rho_{aa})$ is given by (3.4.6). Substituting (3.4.6) into (3.5.8) and rationalizing the denominator, we find the susceptibility of the system to be

$$\chi = \frac{N(\rho_{bb} - \rho_{aa})^{eq}|\mu_{ba}|^2(\omega - \omega_{ba} - i/T_2)T_2^2/\hbar}{1 + (\omega - \omega_{ba})^2T_2^2 + 4|\mu_{ba}|^2|E|^2T_1T_2}. \tag{3.5.9}$$

Introducing, the detuning factor, Δ, and the on-resonance Rabi frequency, Ω, which are defined by

$$\Delta = \omega - \omega_{ba}, \tag{3.5.10}$$

and

$$\Omega = \frac{2|\mu_{ab}||E|}{\hbar}, \tag{3.5.11}$$

equation (3.5.9) simplifies to

$$\chi = \frac{N(\rho_{bb} - \rho_{aa})^{eq}|\mu_{ba}|^2T_2(\Delta T_2 - i)}{\hbar(1 + \Delta^2T_2^2 + \Omega^2T_1T_2)}. \tag{3.5.12}$$

Furthermore, separating the real and imaginary parts of χ in (3.5.12), we get

$$\chi' = \frac{N(\rho_{bb} - \rho_{aa})^{eq}|\mu_{ba}|^2(\Delta T_2)T_2}{\hbar(1 + \Delta^2T_2^2 + \Omega^2T_1T_2)}, \tag{3.5.13}$$

and

$$\chi'' = \frac{-N(\rho_{bb} - \rho_{aa})^{eq}|\mu_{ba}|^2T_2}{\hbar(1 + \Delta^2T_2^2 + \Omega^2T_1T_2)}. \tag{3.5.14}$$

Having determined the explicit form of the complex susceptibility, it is straightforward to obtain the corresponding complex permittivity of a closed two-level system using the well-known equation

$$\varepsilon = 1 + 4\pi\chi. \tag{3.5.15}$$

In order to study the behavior of the complex susceptibility, we can write it in terms of the normal (linear) absorption of coefficient of the material system which we

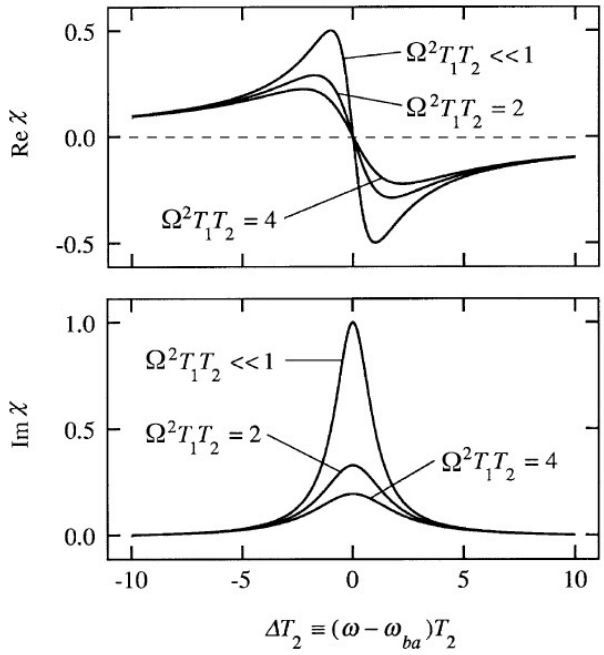

Figure 3.3: Real and imaginary parts of the susceptibility χ (in units of $\alpha_0 c/\omega_{ba}$) plotted as functions of the optical frequency ω for several values of the saturation parameter $\Omega^2 T_1 T_2$ [79].

.

have introduced it in Section 1.8 as:

$$\alpha = 2\frac{\omega}{c}n'' \tag{3.5.16}$$

or

$$\alpha = 2\frac{\omega}{c}Im\sqrt{\varepsilon} = 2\frac{\omega}{c}Im\sqrt{1+4\pi\chi}. \tag{3.5.17}$$

For dilute atomic system $|\chi| << 1$ which is a valid concept [79], and using Eq. (3.5.15), the complex refractive index can be approximated by

$$n = n' + in'' \approx 1 + 2\pi\chi' + i2\pi\chi'', \tag{3.5.18}$$

then identifying n'' from 3.5.17, we get

$$\alpha = 2\frac{\omega}{c}n'' = 4\pi\frac{\omega}{c}\chi''. \tag{3.5.19}$$

Then using 3.5.17 in Eqs. 3.5.13 and 3.5.14, the graphs of χ' and χ'' in units $\alpha_0 c/\omega_{ba}$ of are depicted in Fig. 3.3.

3.6 Rabi Oscillations

Let us consider the interaction of a two level atom with a light field. For the sake of simplicity, let us assume that the system be non degenerate with lower and upper levels a and b, and with energies E_a and E_b ($E_b > E_a$), respectively, and let the transition frequency be $\omega_0 = (E_b - E_a)/\hbar$. The state of the atom may be described by:

$$\begin{aligned} \psi(\vec{r},t) &= C_a(t)\psi_a(\vec{r},t) + C_b(t)\psi_b(\vec{r},t), \\ &= C_a(t)e^{-i(E_a/\hbar)t}\phi_a + C_b(t)e^{-i(E_b/\hbar)t}\phi_b, \end{aligned}$$

where $|C_a(t)|^2 + |C_b(t)|^2 = 1$.

Suppose that the perturbing monochromatic light field to this atom be of the form

$$\vec{E}(\vec{r},t) = \hat{\epsilon}E_0 cos(\vec{k}\cdot\vec{r} - \omega t), \tag{3.6.1}$$

where $\hat{\epsilon}$ is a unit vector in the direction of polarization, that is $\hat{\epsilon} \perp \vec{k}$. The bases vectors in this system evolve according to $\exp(-iE_n/\hbar)$, where, $n = a, b$; so that calculations are easier, if we write the monochromatic field in complex form

$$\vec{E}(\vec{r},t) = \frac{1}{2}\hat{\epsilon}E_0[e^{i(\vec{k}\cdot\vec{r}-\omega t)} + e^{-i(\vec{k}\cdot\vec{r}-\omega t)}]. \tag{3.6.2}$$

Since we take ω_0, ω to be positive, $\omega_0 + \omega >> \omega_0 - \omega$ we can often make the rotating wave approximation of dropping the second exponential.

Under the assumptions that the monochromatic light field interaction is weak compared to atomic effects and that the size of the atom is much less than the wavelength of light, we may make the electric-dipole approximation: the interaction Hamiltonian can be given by $\hat{H}' = -\hat{\mu}\cdot\vec{E}$. Here $\hat{\mu} = -e\hat{r}$ is the dipole operator for the atom and e is magnitude of the charge on the electron. The result of the interaction is that $|\phi_a\rangle$ and $|\phi_b\rangle$ become coupled.

Suppose that the atom is initially in the state $|\psi_a\rangle$. If we neglect spontaneous emission from $|\psi_b\rangle$, then under the rotating-wave approximation and in the Schrodinger representation, the time dependence of the system is given by

$$\begin{aligned} C_a(t) &= e^{-iE_a/\hbar} cos(\Omega t/2t), \\ C_b(t) &= e^{-iE_b/\hbar} sin(\Omega t/2t). \end{aligned} \tag{3.6.3}$$

The quantity defined by

$$\Omega = -\frac{\langle\phi_a|\hat{\mu}\cdot\hat{\epsilon}E_0|\phi_b\rangle}{\hbar}, \tag{3.6.4}$$

or,

$$\Omega = \frac{eE_0\langle\phi_a|\hat{r}\cdot\hat{\epsilon}|\phi_b\rangle}{\hbar}, \tag{3.6.5}$$

is known as the Rabi frequency. The Rabi frequency measures the strength of the coupling between the atomic states and the applied electromagnetic field. Moreover, taking the polarization and the dipole moment to be parallel, and the orthonormality of the state vectors, the Rabi frequency takes a simple form

$$\Omega = \frac{E_0\mu_{ab}}{\hbar}. \tag{3.6.6}$$

3.7 Summary

In two level atomic model, we considered the interaction of a classical light field with the quantum atomic model employing semiclassical approach, in this approach the oscillator strength is measured by the Rabi frequency. The interaction is explained analytically if we apply the rotating wave approximation in which the interaction energy (Hamiltonian) is a slowly varying function of time, this takes place when the light field and the transition frequency are nearly comparable, that is the detuning frequency is small.

The susceptibility of the system for the equilibrium case is derived using the density matrix description of two level atom, showing its dependence on the Rabi frequency, its dependence on this frequency is manifested when the light field is strong which may result non-linearity. As the strength of the field (the intensity of the field) increases, the deep dispersion of the real part of the susceptibility decreases, and the frequency range of the anomalous dispersion increases.

Chapter 4

Electromagnetic Wave Propagation in Structured Metamaterials

4.1 Introduction

Materials that are artificially fabricated to have the desired material properties that do not exist in nature are referred to as metamaterials. Among such type of materials is the structured metamaterial that consists of an array of long metallic wires (ALMWs) and split ring resonators (SRRs) that is assembled to realize negative refractive index (left-handed) media first proposed theoretically by Pendry [7, 68] and demonstrated experimentally by Shelby, et. al [9]. They showed that in a narrow frequency domain in the microwave region, the ALMWs possesses a negative permittivity and the SRRs possesses a negative permeability. Consequently, the composite medium that is assembled from the ALMWs and SRRs behaves as negative refractive index medium in the narrow frequency domain where the effective permittivity and permeability are simultaneously negative.

In this chapter we study the propagation of electromagnetic waves in structured metamaterials (SMMs) that consist of square split-ring resonators and array of long

wire strips made of copper. In Section 4.2, the effective permittivity and permeability are presented and the corresponding refractive index is derived. In section 4.3, permittivity, permeability, and refractive index of SMM in different frequency ranges are analyzed, in particular, the frequency domain where the SMM behaves as negative refractive index medium is identified. Normally, the refractive index possess two resonances. The character of nonanalyticity of the real part of the refractive index of SMM with two resonances is considered in Section 4.4. Section 4.5 is devoted to the analysis of group velocity, group index, superluminal, slow, and backward waves of different types of microwaves propagating in the structured metamaterial. Moreover, it is shown that by appropriately tuning the parameters of the electric (ALMWs) and magnetic subsystems (SRRs), the system can be made to have only one resonance. In Section 4.6 the propagation of EMWs in the SMM with coinciding frequencies of the electron and magnetic subsystems is discussed. Section 4.7, summarizes the results obtained in the Chapter.

4.2 Refractive index of the structured metamaterial

Consider the structured metamaterial that consists of square copper split-ring resonators and array of thin copper wire strips on a dielectric substrate; with the rings and wires placed on opposite sides of the substrate as depicted in Fig. 4.1. Shelby, et. al [9] have analyzed a similar system by introducing a unit cell consisting of six copper SRRs and two metal strips. Choosing the SRR parameter values (refer to Fig. 4.1(a)) to be $w = 0.25\ mm$, $s = 0.30\ mm$, $g = 0.46\ mm$, $\ell = 2.62\ mm$, and wire strips each of length $3a = 1\ cm$, and the resulting SMM was shown to possess LHM

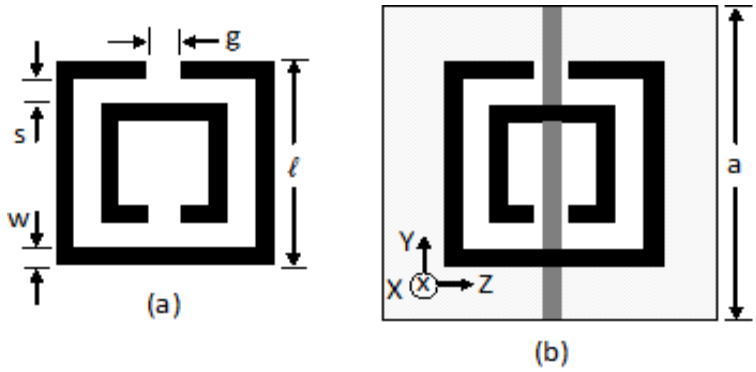

Figure 4.1: (a) Schematic of a single square split-ring resonator (SRR). (b) A schematic showing one possible arrangement of an SRR and a wire strip printed on a square dielectric board of side length a. The wire strip is centered on the SRR and is on the opposite side of the board from the SRR. (Drawings not to scale).

properties between $10.3 - 11.1\ GHz$ frequency domain which lies in the microwave frequency region.

Suppose a plane electromagnetic field is incident on the SMM in such a way that the electric field is polarized parallel to the strips, along the y-axis, the magnetic field directed along the ring axis, x-axis, and its wave vector directed along the z-axis, as depicted in Fig. 4.1(b). For such polarization, the permittivity and permeability of the SMMs can be described by [9]

$$\begin{aligned} \varepsilon(\omega) &= 1 - \frac{\omega_{ep}^2 - \omega_{eo}^2}{\omega^2 - \omega_{eo}^2 + i\gamma\omega}, \\ \mu(\omega) &= 1 - \frac{\omega_{mp}^2 - \omega_{mo}^2}{\omega^2 - \omega_{mo}^2 + i\gamma\omega}, \end{aligned} \tag{4.2.1}$$

where ω_{eo}, ω_{mo} are the resonant frequencies of the electron and magnetic subsystems, respectively; γ is the damping constant of these subsystems (for the sake of simplicity it is chosen to be the same for both subsystems), ω_{ep} and ω_{mp} are parameters related to the electron and magnetic subsystems, respectively. It is worth noting that the

effective permittivity and permeability of SMMs are practically obtained by employing a retrieval procedure from measured data of the complex transmission and reflection amplitudes of a finite length of the metamaterial [81].

Also, note that all known models of LHM in the SHF range have similar frequency dependence of the permittivity and permeability as (4.2.1), but with different values of the parameters [82, 83, 84]. Moreover, when the metallic strips maintain electrical continuity, $\omega_{eo} = 0$ [9], so that the permittivity reduces to the Drude expression. In our case, $\omega_{eo} \neq 0$.

The complex permittivity and permeability in (4.2.1) my be written in standard form as:

$$\varepsilon(\omega) = \varepsilon_1(\omega) + i\varepsilon_2(\omega)$$

$$\mu(\omega) = \mu_1(\omega) + i\mu_2(\omega)$$

Consequently, the real and imaginary parts of the permittivity and permeability in (4.2.1) becomes

$$\begin{aligned}
\varepsilon_1(\omega) &= 1 - \frac{(\omega_{ep}^2 - \omega_{eo}^2)(\omega^2 - \omega_{eo}^2)}{(\omega^2 - \omega_{eo}^2)^2 + (\gamma\omega)^2}, \\
\varepsilon_2(\omega) &= \frac{\gamma\omega(\omega_{ep}^2 - \omega_{eo}^2)}{(\omega^2 - \omega_{eo}^2)^2 + (\gamma\omega)^2}, \\
\mu_1(\omega) &= 1 - \frac{(\omega_{mp}^2 - \omega_{mo}^2)(\omega^2 - \omega_{mo}^2)}{(\omega^2 - \omega_{mo}^2)^2 + (\gamma\omega)^2}, \\
\mu_2(\omega) &= \frac{\gamma\omega(\omega_{mp}^2 - \omega_{mo}^2)}{(\omega^2 - \omega_{mo}^2)^2 + (\gamma\omega)^2}.
\end{aligned} \tag{4.2.2}$$

Further, it will be convenient to measure all frequencies in terms of ω_{eo} and to

introduce the dimensionless frequency $z = \omega/\omega_{eo}$. Then, (4.2.2) takes the form

$$\begin{aligned}
\varepsilon_1(z) &= 1 - \frac{\alpha(z^2-1)}{(z^2-1)^2 + (\nu z)^2}, \\
\varepsilon_2(z) &= \frac{\alpha\nu z}{(z^2-1)^2 + (\nu z)^2}, \\
\mu_1(z) &= 1 - \frac{\beta(z^2 - z_m^2)}{(z^2 - z_m^2)^2 + (\nu z)^2}, \\
\mu_2(z) &= \frac{\beta\nu z}{(z^2 - z_m^2)^2 + (\nu z)^2}.
\end{aligned} \tag{4.2.3}$$

Here, the resonant frequencies of the electron and magnetic subsystems are $z_{re} = 1$ and $z_{rm} \equiv z_m = \omega_{mo}/\omega_{eo}$, respectively, $\nu = \gamma/\omega_{eo}$ is the dimensionless decay constant, and $\alpha = z_e^2 - 1$, $\beta = z_{mp}^2 - z_m^2$ are dimensionless parameters with $z_e = \omega_{ep}/\omega_{eo}$, $z_{mp} = \omega_{mp}/\omega_{eo}$.

The complex refractive index of the metamaterial may be written as

$$n = n_1 + in_2. \tag{4.2.4}$$

Then squaring the the complex refractive index, (4.2.4), we get

$$n^2 = n_1^2 - n_2^2 + 2in_1n_2,$$

which can be written as

$$n^2 = A + iB, \tag{4.2.5}$$

where

$$A = n_1^2 - n_2^2, \qquad \text{and} \qquad B = 2n_1n_2. \tag{4.2.6}$$

Note that for electromagnetic waves to propagate in a medium, $A = n_1^2 - n_2^2 >> 0$; as large n_2 implies decay of the wave in the medium.

Moreover, in terms of the permittivity and permeability the complex refractive index may be written as

$$n(\omega) = \sqrt{\varepsilon(\omega)\mu(\omega)}, \tag{4.2.7}$$

where $\varepsilon(\omega) = \varepsilon_1 + i\varepsilon_2$, and $\mu(\omega) = \mu_1 + i\mu_2$ are the complex permittivity and permeability. Substituting these into (4.2.7) and squaring, we get

$$n^2 = (\varepsilon_1\mu_1 - \varepsilon_2\mu_2) + i(\varepsilon_1\mu_2 + \varepsilon_2\mu_1). \tag{4.2.8}$$

Comparing (4.2.5) and (4.2.8), we get

$$A = \varepsilon_1\mu_1 - \varepsilon_2\mu_2 \qquad \text{and} \qquad B = \varepsilon_1\mu_2 + \varepsilon_2\mu_1. \tag{4.2.9}$$

Next, simultaneously solving (4.2.6) for n_1, we find the real part of the refractive index to be

$$n_1(z) = \pm\sqrt{\frac{\sqrt{A^2 + B^2} + A}{2}}, \tag{4.2.10}$$

and similarly solving (4.2.6) for n_2, we obtain the equation for the imaginary part of the refractive index to be

$$n_2(z) = \sqrt{\frac{\sqrt{A^2 + B^2} - A}{2}}, \tag{4.2.11}$$

where A and B are given by (4.2.9). It is clear that the imaginary part of refractive index n_2 in (4.2.11) of equilibrium systems (no external gain) must be positive which corresponds to decay of EMWs. However, the sign of n_1 in (4.2.10) can be either positive or negative depending on the values of the permittivity and permeability. It's sign is " $-$ " for $\varepsilon_1 < 0$, $\mu_1 < 0$ (LHM) and " $+$ " otherwise.

Table 4.1: Parameters of the structured metamaterial (frequencies in GHz) [9].

f_{eo}	f_{ep}	f_{mp}	f_{mo}	ν	z_m	α	β
10.30	12.80	10.95	10.05	10^{-3}	0.976	0.545	0.178

4.3 Permittivity, permeability, and refractive index of the SMM medium

It is obvious from (4.2.10) and (4.2.11) that the parameters that determine the real and imaginary parts of the complex refractive index are A and B defined by relations (4.2.9). In turn, both A and B are dependent on the values of the permittivity ($\varepsilon_1,\ \varepsilon_2$) and permeability ($\mu_1,\ \mu_2$). Consequently, it is essential to investigate the relative values of these parameters in the various frequency domains of interest. In this section, we calculated and plotted the graphs of (i) the real and imaginary parts of the permittivity, (ii) the parameters A and B, and (iii) the real and imaginary parts of the refractive index, versus the dimensionless frequency z in a wide frequency range according to (4.2.3), (4.2.9), (4.2.10) and (4.2.11) with the parameters of SMMs given in Table 4.1. Because of the large scale of $\omega_{e0} \approx 10^{11} rad/s$ and the necessity to show clearly the frequency domains of RHM and LHM regions, we present the graphs of n_1 and n_2, and the relevant parameters in the following successive frequency bands.

4.3.1 The frequency range $z \leq z_e$

This frequency domain consists of the resonance frequencies of the electric (z_e) and magnetic (z_m) subsystems. The values of these frequencies are $z_e = 1$ and $z_m = 0.976$. The permittivity and permeability as functions of the dimensionless frequency z are shown in Figs. 4.2 and 4.3.

Figure 4.2 depicts the real parts of the permittivity and permeability in the frequency range $0.96 \leq z \leq 1.02$. For the given frequency range the permittivity (ε_1) is negative above $z > 1$, whereas the permeability (μ_1) takes negative values above

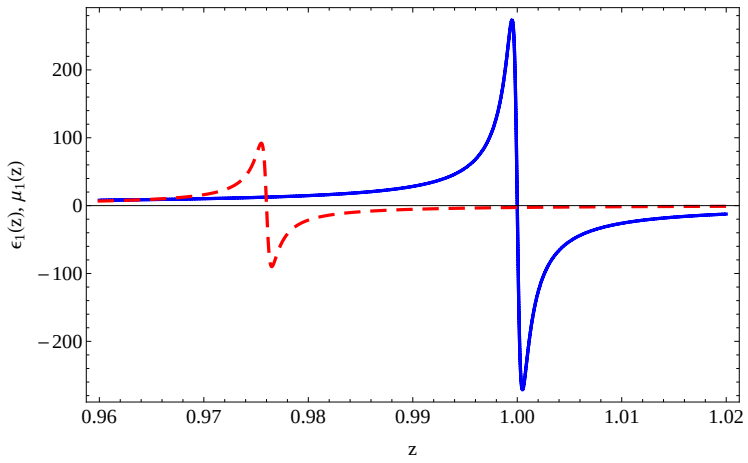

Figure 4.2: The graph of the real parts of the permittivity (solid line) and the permeability (dashed line) versus z in the frequency domain $0.96 \leq z \leq 1.02$. Parameters of SMM are given in Table 4.1.

$z > 0.976$. The peak values at the resonant frequencies are $\varepsilon_1 = \pm 275$ and $\mu_1 = \pm 95$, with values decreasing below 10 on either ends of the frequency domain.

Figure 4.3 shows the imaginary parts of the permittivity and permeability in the same frequency range $0.96 \leq z \leq 1.02$. Again both the permittivity (ε_2) and the permeability (μ_2) attains maximum values at the resonant frequencies with peak values $\varepsilon_2 = 550$ and $\mu_2 = 190$. For frequencies far from the resonances both the permittivity and permeability fast approaches to zero.

The values of the parameters $A = \varepsilon_1\mu_1 - \varepsilon_2\mu_2$ and $B = \varepsilon_1\mu_2 + \varepsilon_2\mu_1$ are plotted as a function of z, as shown in Fig. 4.4. It is evident from the graph that (i) for $z < z_m = 0.976$, $A >> B$ with both A and B taking on positive values, and (ii) for the frequency domain $z_m < z < z_e = 1$, our numerical analysis shows that $|A| >> |B|$ with A taking on negative values whereas B being positive as well as negative. In particular, for the frequency domain $z_m < z < z_e = 1$, with $|A| >> |B|$ with $A < 0$

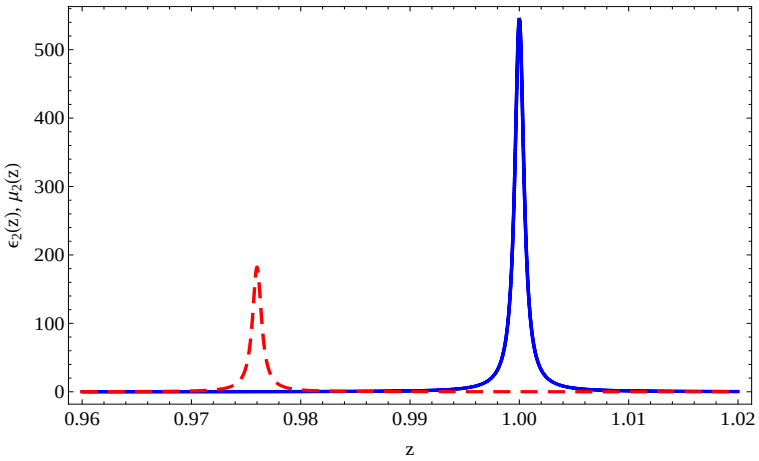

Figure 4.3: The graph of the imaginary parts of the permittivity (solid line) and the permeability (dashed line) versus z in the frequency domain $0.96 \leq z \leq 1.02$. Parameters of SMM are the same as those in Fig. 4.2.

equations (4.2.10) and (4.2.11) may be written as

$$n_1^2 = \frac{\sqrt{A^2 + B^2} - |A|}{2}. \tag{4.3.1}$$

$$n_2^2 = \frac{\sqrt{A^2 + B^2} + |A|}{2}. \tag{4.3.2}$$

Then, expanding (4.3.1) and (4.3.2) with respect to the small ratio $|B|/|A|$ and keeping only the leading terms, we get

$$n_1^2 \approx \frac{B^2}{4|A|} \qquad \Rightarrow \qquad n_1 \approx \frac{|B|}{2\sqrt{|A|}}, \tag{4.3.3}$$

and

$$n_2^2 \approx |A| \qquad \Rightarrow \qquad n_2 \approx \sqrt{|A|}. \tag{4.3.4}$$

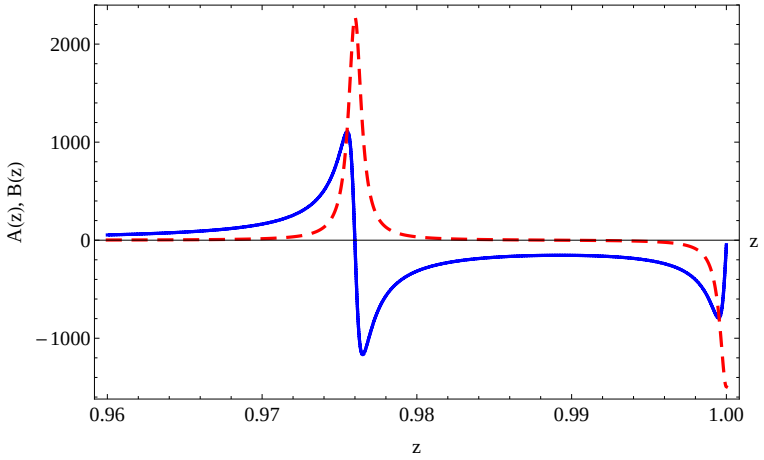

Figure 4.4: The graph of $A(z)$ (solid line) and $B(z)$ (dashed line) versus z in the frequency range $0.96 \leq z \leq 1$. Parameters of SMM are the same as those in Fig. 4.2.

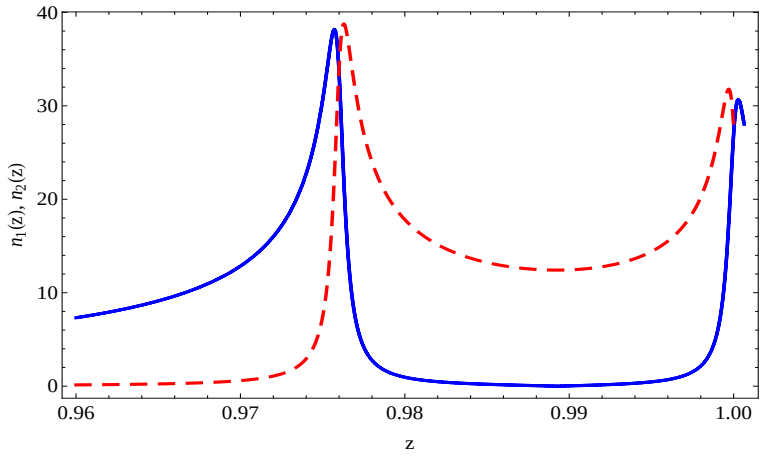

Figure 4.5: The real n_1 (solid line) and imaginary n_2 (dashed line) parts of the refractive index versus z in a frequency range $0.96 \leq z \leq 1$. The peaks correspond to the resonances $z_m = 0.976$ and $z_e = 1$. Parameters of SMM are the same as those in Fig. 4.2.

Writing (4.3.3) and (4.3.4) in terms of the permittivity and permeability and neglecting the products of ε_2 and μ_2 in the expression for A, we get

$$\begin{aligned} n_1(z) &= \frac{|\varepsilon_1\mu_2 + \varepsilon_2\mu_1|}{2\sqrt{|\varepsilon_1\mu_1|}}, \\ n_2(z) &= \sqrt{|\varepsilon_1\mu_1|}. \end{aligned} \tag{4.3.5}$$

Since $|A| >> |B|$, (4.3.5) dictates that

$$n_2 >> n_1. \tag{4.3.6}$$

Equation (4.3.6) implies that in the given frequency domain EMWs propagating in the SMM medium are strongly attenuated resulting in a strong absorption of the EMWs. The profile of $n_1(z)$ and $n_2(z)$ in a frequency range $0.96 \leq z \leq 1$ is depicted in Fig. 4.5. In the frequency band $z < z_m$, the SMM behaves as RHM, with $\varepsilon_1 > 0$, $\mu_1 > 0$ (see Fig. 4.2) and $n_1(z) >> n_2(z)$. On the other hand, for the frequency band between the resonances SMM correspond to RHM with $\varepsilon_1 > 0$, $\mu_1 < 0$ (see Fig. 4.2). Here $n_2 \approx 15 >> n_1$ which results to a very strong absorption of microwaves.

Note that the detailed numerical analysis shows an interesting behavior of $n_1(z)$, in the vicinity of $z = 0.98925$ where $\varepsilon_1 > 0$, $\mu_1 < 0$. Figure 4.6 shows $n_1(z)$ versus z in this frequency band. It is a continuous function of z but its derivative dn_1/dz is discontinuous at $z = 0.98925$ which is a nonanalytic point. It means that $n_1(z)$ is a nonanalytic function of z. Later, we will observe that similar type of nonanalytic behavior of $n_1(z)$ takes place at the frequency $z = 1.1037$ for which, in the vicinity of this frequency, the SMM behaves as RHM with $\varepsilon_1 < 0$, $\mu_1 > 0$.

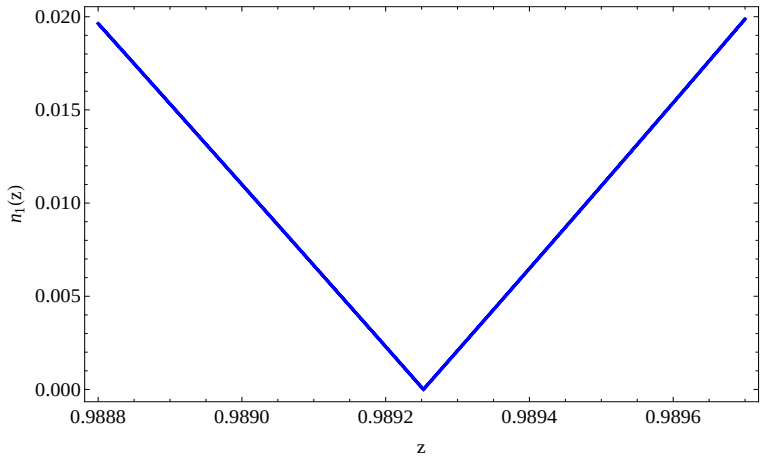

Figure 4.6: The real part n_1 of the refractive index versus z for $0.9888 < z < 0.9897$. Parameters of SMM are the same as those in Fig. 4.5.

4.3.2 The frequency range $z_e \leq z \leq 1.063$

This frequency domain spans from the resonance frequency ($z_e = 1$) of the electron subsystem to the frequency $z = 1.063$ that corresponds to the location where the real part of permeability, μ_1, is equal to zero. Similar to the previous section, the parameters ε_1, ε_2, μ_1, μ_2, A, B, n_1, and n_2 are plotted as functions of the dimensionless frequency z.

Figure 4.7 depicts the real parts of the permittivity and permeability as a function of z in the frequency range $1.005 \leq z \leq 1.063$. For the given frequency range both the permittivity (ε_1) and the permeability (μ_1) are simultaneously negative; with the permittivity varying between $-53 < \varepsilon_1 < -3$ and the permeability between $-2 < \mu_1 < 0$. In this frequency domain, we expect that the SMM system behaves as left-handed medium in the relatively narrow frequency domain $1 < z < 1.063$.

The imaginary parts of the permittivity and permeability as functions of z in

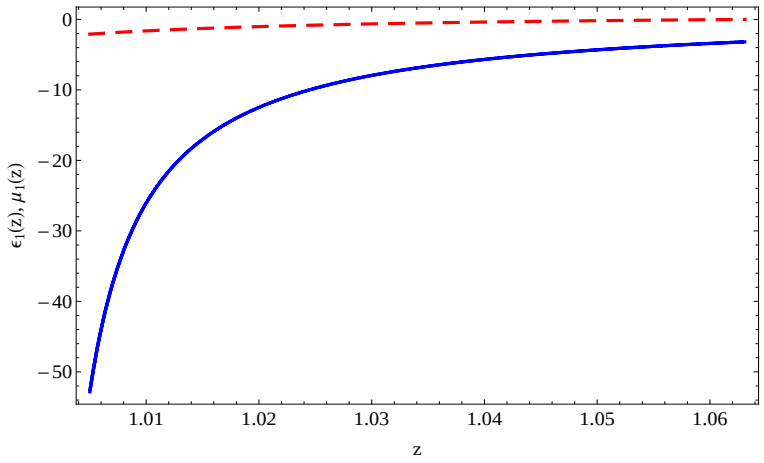

Figure 4.7: The graph of the real parts of the permittivity (solid line) and the permeability (dashed line) versus z in the frequency domain $1.005 \leq z \leq 1.063$. Parameters of SMM are given in Table 4.1

the frequency domain $1.005 \leq z \leq 1.0631$ is shown Fig. 4.8. Note that above the frequency $z = 1.02$ both the permittivity (ε_2) and the permeability (μ_2) are practical zero enabling the propagation of EMWs in the SMM system easy.

The values of the parameters $A = \varepsilon_1\mu_1 - \varepsilon_2\mu_2$ and $B = \varepsilon_1\mu_2 + \varepsilon_2\mu_1$ are plotted as a function of z, as shown in Fig. 4.9. It is observed from the graph that for the frequency range $1.005 < z < 1.063$, $A >> B$ with A taking on positive values and B taking on negative values. In this frequency domain, equations (4.2.10) and (4.2.11) may be simplified as follows:

$$n_1^2 = \frac{\sqrt{A^2 + B^2} + |A|}{2}. \tag{4.3.7}$$

$$n_2^2 = \frac{\sqrt{A^2 + B^2} - |A|}{2}. \tag{4.3.8}$$

Then, expanding (4.3.7) and (4.3.8) with respect to the small ratio $|B|/|A|$ and

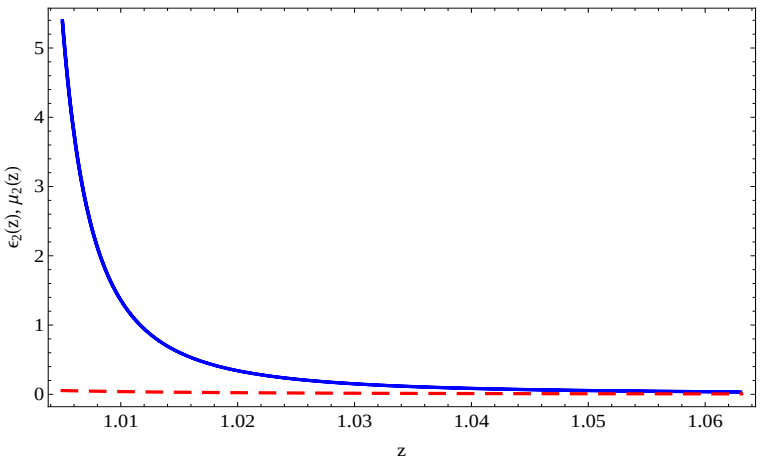

Figure 4.8: The graph of the imaginary parts of the permittivity (solid line) and the permeability (dashed line) versus z in the frequency domain $1.005 \leq z \leq 1.063$. Parameters of SMM are given in Table 4.1

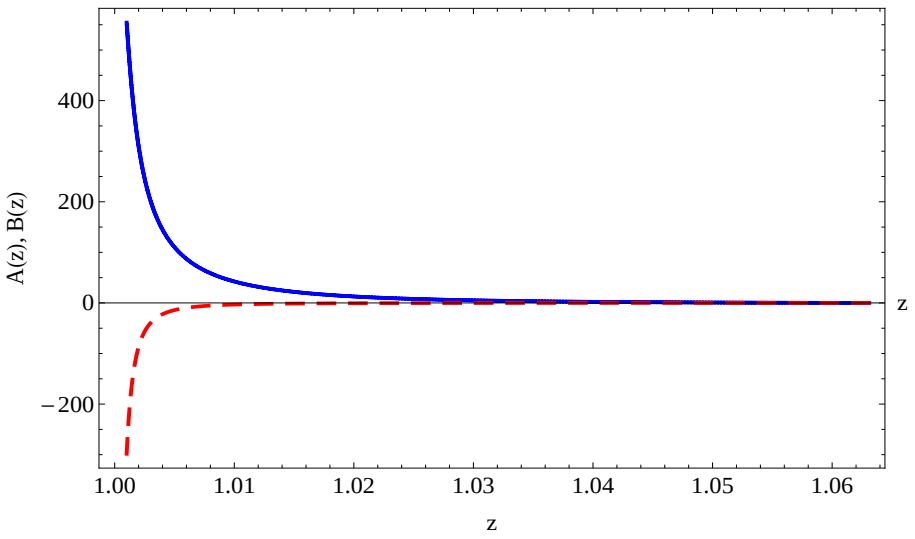

Figure 4.9: The graph of $A(z)$ (solid line) and $B(z)$ (dashed line) versus z in the frequency range $1.005 \leq z \leq 1.063$. Parameters of SMM are the same as those in Fig. 4.5.

keeping only the leading terms, we get

$$n_1 \approx \pm\sqrt{|A|} \qquad \text{and} \qquad n_2 \approx \frac{|B|}{2\sqrt{|A|}}. \tag{4.3.9}$$

Writing (4.3.9) in terms of the permittivity and permeability and neglecting the small quantity $\varepsilon_2\mu_2$ in the expression for A, we obtain

$$\begin{aligned} n_1(z) &= \pm\sqrt{|\varepsilon_1\mu_1|}. \\ n_2(z) &= \frac{|\varepsilon_1\mu_2 + \varepsilon_2\mu_1|}{2\sqrt{|\varepsilon_1\mu_1|}}, \end{aligned} \tag{4.3.10}$$

Consequently, we have

$$n_1 >> n_2. \tag{4.3.11}$$

Note that in the frequency domain where both ε_1 and μ_1 are simultaneously negative, the negative root in (4.3.11) must be taken and the medium behaves as LHM; whereas in the case where both ε_1 and μ_1 are simultaneously positive, the positive root must be taken so that the medium behaves as regular (RHM) medium.

As shown in Fig. 4.7, ε_1 and μ_1 are simultaneously negative in the frequency band $1 < z < 1.063$, and hence the system possesses LHM properties. Figure 4.10 shows the real (n_1) and imaginary (n_2) parts of the refractive index as a function of z that spans the entire LHM domain. Note that when the frequency passes the resonance $z = 1$, $n_1(z)$ rapidly changes from $+30$ to -30 (see Fig. 4.5 and 4.10). The inset in Fig. 4.10 depicts n_1 and n_2 for $1 < z < 1.005$ which corresponds to the beginning of the LHM domain. The real part of refractive index n_1 is negative with $n_1 \approx -30$ at its minimum, i.e., $z = 1.0002$ with $n_2 \approx 15$, and very near to the resonance $z = 1$ the value of n_2 is about 30 (Fig. 4.5). Therefore, at the beginning of the LHM domain, EMWs are strongly absorbed. However, the values of n_2 decrease with increasing z, as shown in Fig. 4.11, attaining its minimum of the order of $n_2 \sim 0.03$ in the vicinity

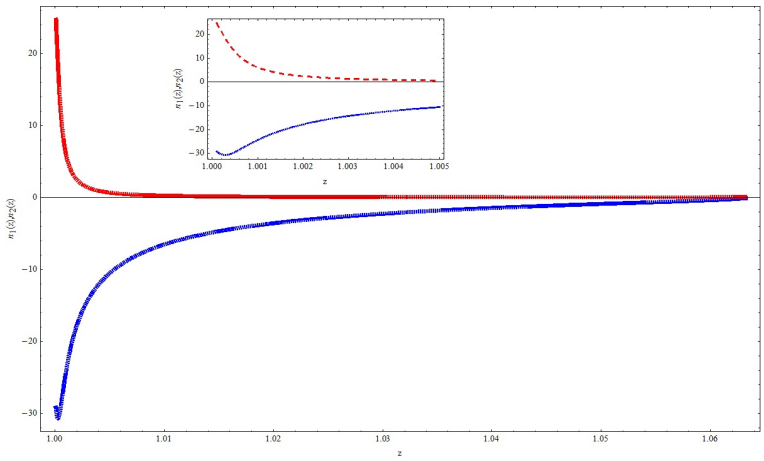

Figure 4.10: The real n_1 (solid line) and imaginary n_2 (dashed line) parts of the refractive index versus z at the LHM domain $1 < z < 1.0631$, where $\varepsilon_1 < 0$, $\mu < 0$. The inset shows the beginning of LHM, $1 < z < 1.005$ where EMWs are strongly absorbed. Parameters of SMM are the same as those in Fig. 4.5.

of the end of the LHM frequency band. Similarly, the values of $|n_1(z)|$ also decrease with increasing z, varying from $n_1 = -30$ just above $z = 1$ to $n_1 \approx -2$ at the end of the LHM frequency band, where $n_2 \approx 0.03$. Consequently, for frequencies far from the resonance the so-called backward waves are expected to propagate, since n_1 is much larger than n_2. We note that the observed LHM frequency domain agrees with that obtained in experiments [9].

4.3.3 The frequency range $z > 1.063$

In this frequency domain the system behaves as RHM as we shall show below. The frequency $z = 1.063$ corresponds to the value where the real part of the permeability of the SMM medium equals zero, i.e., μ_1 changes sign from negative (for $z < 1.063$) to positive (for $z > 1.063$). In Figs. 4.12-4.15 we plotted the permittivity, permeability,

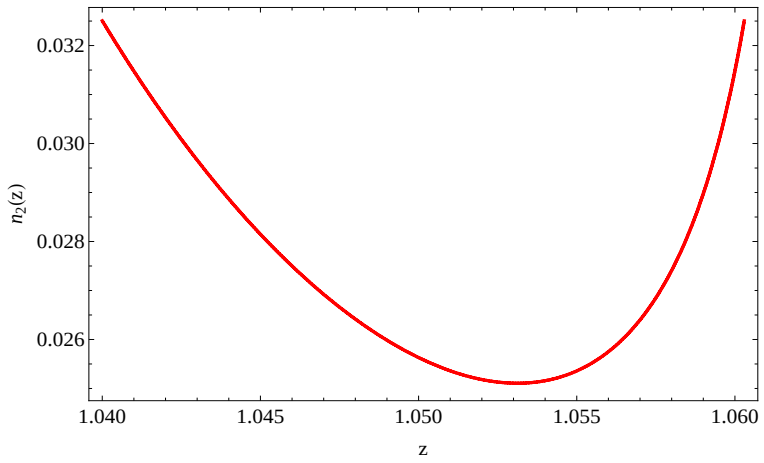

Figure 4.11: The imaginary part n_2 of the refractive index versus z in the frequency band $1.04 < z < 1.06$ of the LHM domain. Parameters of SMM are the same as those in Fig. 4.5.

the refractive index and the parameters A and B as a function of the dimensionless frequency, z.

Figure 4.12 depicts the real parts of the permittivity and permeability for the frequency range $1.063 \leq z \leq 2$. For the given frequency range the permittivity (ε_1) is negative between $1.063 < z < 1.243$ and positive above $z = 1.243$, whereas the permeability (μ_1) is positive in the entire domain. Note that as z increased further from $z = 2$, both ε_1 and μ_1 approaches unity. It is expected that in the frequency range where $\varepsilon_1 < 0$ and $\mu_1 > 0$, EMWs are strongly and hence no propagation.

The graphs of the imaginary parts of the permittivity and permeability as a function of z for $1.0631 \leq z \leq 2$ is depicted in Fig. 4.13. It is observed that apart from for the frequency rage $1.063 < z < 1.4$ where ε_2 and μ_2 varies between $0.034- \sim 0.001$ and $0.006- \sim 0$, respectively, both ε_2 and μ_2 practically approaches zero for all frequencies $z > 1.4$ indicating very little or no absorption of EMWs propagating in the

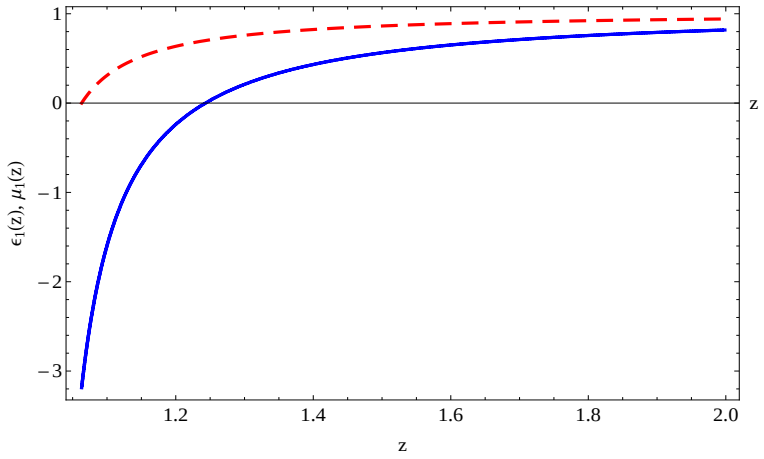

Figure 4.12: The graph of the real parts of the permittivity (solid line) and the permeability (dashed line) versus z in the frequency domain $1.063 \leq z \leq 2$. Parameters of SMM are given in Table 4.1.

SMM. Figure 4.14 shows the graphs of the parameters A and B as a function of z, for the frequency range, $1.0631 < z < 2$, it is observed that the value of $B \sim 0$ whereas A increases with an increase in z for frequencies above $z > 1.243$, approaching unity for large z. This implies that the equations for the refractive index given by (4.2.10) and (4.2.11) for $z > 1.243$ may be approximately written as:

$$n_1(z) \cong \sqrt{A} = \sqrt{|\varepsilon_1 \mu_1|} \qquad \text{and} \qquad n_2(z) \cong 0. \tag{4.3.12}$$

The profile of $n_1(z)$ and $n_2(z)$ in a frequency range $1.063 \leq z \leq 2$ is depicted in Fig. 4.15. In this frequency band, the SMM behaves as RHM. In particular, for $z > 1.243$ both ε_1, μ_1 are simultaneously positive so that EMWs incident on the SMM system propagates. On the other hand, in the frequency band $1.063 < z < 1.243$, where $\varepsilon_1 < 0$, $\mu_1 > 0$, the system possesses the RHM properties and the system is expected to strongly absorb EMWs. Moreover, the detailed numerical analysis shows an interesting behavior of n_1. Figure 4.16 shows $n_1(z)$ versus z in this frequency

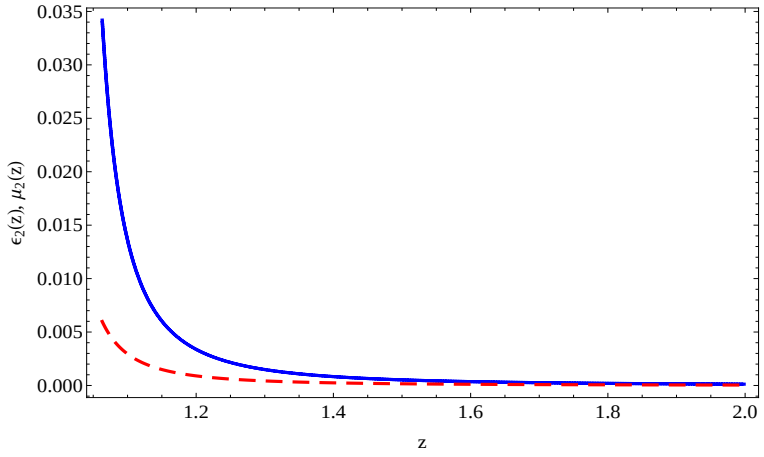

Figure 4.13: The graph of the imaginary parts of the permittivity (solid line) and the permeability (dashed line) versus z in the frequency domain $1.0631 \leq z \leq 2$. Parameters of SMM are given in Table 4.1.

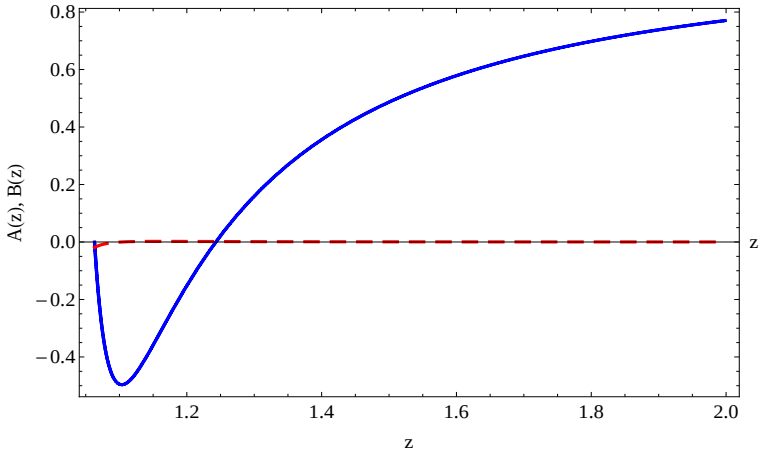

Figure 4.14: The graph of $A(z)$ (solid line) and $B(z)$ (dashed line) versus z in the frequency range $1.063 < z < 2$. Parameters of SMM are the same as those in Fig. 4.5.

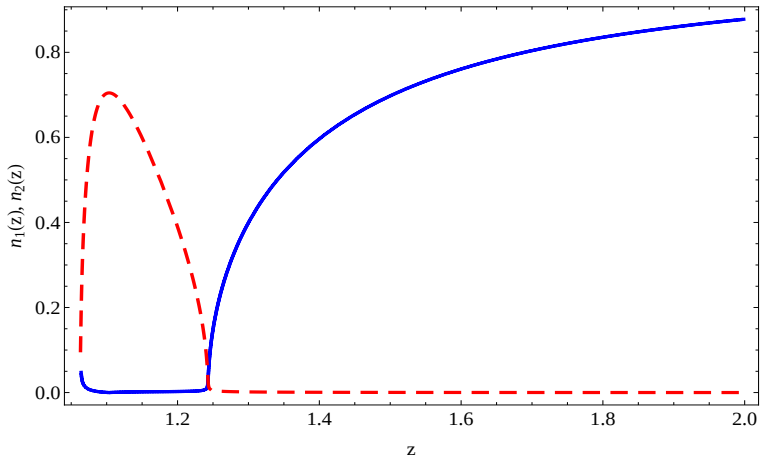

Figure 4.15: The real n_1 (solid line) and imaginary n_2 (dashed line) parts of the refractive index n_1 versus z in the frequency range $1.0631 < z < 2$. Parameters of SMM are the same as those in Fig. 4.5.

band. It is a continuous function of z but its derivative dn_1/dz is discontinuous at $z = 1.1037$. The inset of Fig. 4.16 gives an enlarged fragment of $n_1(z)$ in the vicinity of nonanalytic point. It means that $n_1(z)$ is a nonanalytic function of z. We also note that similar type of nonanalytic behavior of $n_1(z)$ takes place at the frequency $z = 0.98925$ between the resonances with $n_2 \approx 30$, as shown in Fig. 4.6.

The numerical analysis of the refractive index of SMM discussed above shows that it is possible to specify the narrow frequency bands where $n_1(z)$ has a strong frequency dispersion with small enough $n_2(z)$ that allows one to specify a considerably propagating microwaves. In these frequency bands, the group velocity of narrow wave packets demonstrate some interesting peculiarities that we will discuss below. But first we consider analytically the behavior of the real part of refractive index in the vicinity of the frequencies where it is equal to zero.

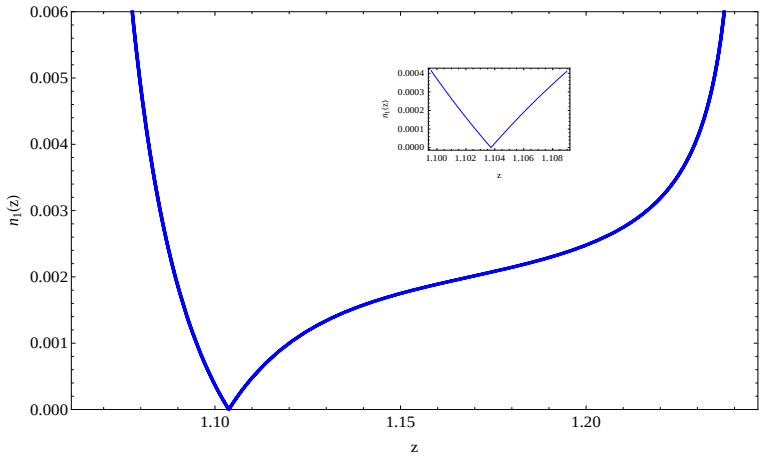

Figure 4.16: The real part n_1 of the refractive index versus z. The inset shows enlarged $n_1(z)$ in the vicinity of the nonanalytic point $z = 1.1037$. Parameters of SMM are the same as those in Fig. 4.5.

4.4 Nonanalyticity of refractive index of SMM with two resonances

The conventional solution of the system of equation (4.2.6) requires the inequality $\varepsilon_2\mu_2 << \varepsilon_1\mu_1$. For $\nu << 1$ it provides $n_2 << n_1$ and results in $n_1 = \pm\sqrt{\varepsilon_1\mu_1}$ with a positive quantity under the square root. But (4.2.6) has one more solution when $\varepsilon_1\mu_1 < 0$, with a large modulus. This is equivalent to stating that $|A| > |B|$ and $A^2 >> B^2$, with $A < 0$. This inequality is shown to be true in the RHM frequency domain between $z_m < z < z_e$, as shown in Fig. 4.4. For instance, from Fig. 4.4 we observe that at the frequency $z = 0.980$, we find that $|A| = 4.7|B|$ and $A^2 = 21.1B^2$. Therefore, for the case the system of equations (4.2.10) and (4.2.11) can be written as

$$n_1^2 = \frac{\sqrt{A^2 + B^2} - |A|}{2}. \tag{4.4.1}$$

$$n_2^2 = \frac{\sqrt{A^2 + B^2} + |A|}{2}. \tag{4.4.2}$$

Then, expanding (4.4.1) and (4.4.2) with respect to the small ratio $|B|/|A|$ and keeping only the leading terms, we get

$$n_1^2 \approx \frac{B^2}{4|A|} \qquad \Rightarrow \qquad n_1 \approx \frac{|B|}{2\sqrt{|A|}}, \tag{4.4.3}$$

and

$$n_2^2 \approx |A| \qquad \Rightarrow \qquad n_2 \approx \sqrt{|A|}. \tag{4.4.4}$$

Neglecting the term $\varepsilon_2\mu_2$ in the expression for A, (4.4.3) and (4.4.4) may be written in terms of the permittivity and permeability as

$$\begin{aligned} n_1(z) &= \frac{|\varepsilon_1\mu_2 + \varepsilon_2\mu_1|}{2\sqrt{|\varepsilon_1\mu_1|}}, \\ n_2(z) &= \sqrt{|\varepsilon_1\mu_1|}. \end{aligned} \tag{4.4.5}$$

From (4.4.5), it is obvious that

$$n_2 >> n_1. \tag{4.4.6}$$

For $|n_1| \approx 1$, the inequality $n_2 >> n_1$ results in a strong absorption of EMWs. In Ref. [85] this case is referred as a nearly perfect absorption. However, for $n_1(z) = 0$, inequality (4.4.6) can be true even for comparatively small n_2 that reduce the absorption of EMWs.

Let us check when the equation $n_1(z) = 0$ has real roots. According to the first relation of (4.4.5) it reduces to

$$\varepsilon_1\mu_2 + \varepsilon_2\mu_1 = 0. \tag{4.4.7}$$

For small damping constant $\nu << 1$ and far from the resonances it is possible to

neglect the term $\nu^2 z^2$ in the denominators of (4.2.3). That is,

$$\begin{aligned} \varepsilon_1(z) &= 1 - \frac{\alpha}{z^2-1}, \\ \varepsilon_2(z) &= \frac{\alpha\nu z}{(z^2-1)^2}, \\ \mu_1(z) &= 1 - \frac{\beta}{z^2-z_m^2}, \\ \mu_2(z) &= \frac{\beta\nu z}{(z^2-z_m^2)^2}. \end{aligned} \tag{4.4.8}$$

Substituting (4.4.8) in (4.4.7) leads to

$$\left(1 - \frac{\alpha}{z^2-1}\right)\frac{\beta\nu z}{(z^2-z_m^2)^2} + \left(1 - \frac{\beta}{z^2-z_m^2}\right)\frac{\alpha\nu z}{(z^2-1)^2} = 0,$$

or,

$$\beta(z^2-1)[(z^2-1)-\alpha] + \alpha(z^2-z_m^2)[(z^2-z_m^2)-\beta]. \tag{4.4.9}$$

Equation (4.4.9) is a biquadratic equation with respect to z. However, further manipulation and substitution of $z^2 = 1 + x$ transforms (4.4.9) to

$$x^2 - 2ax - b = 0, \tag{4.4.10}$$

where $a = \alpha(\beta-\delta)/(\alpha+\beta)$, $b = \delta a$, and $\delta = 1 - z_m^2$. The solutions of (4.4.10) can be written in the form

$$x_{1,2} = a\{1 \mp \sqrt{1+\delta/a}\}. \tag{4.4.11}$$

Formula (4.4.11) shows that $n_1(z) = 0$ at two points. For close resonant frequencies $\delta = 1 - z_m^2 << 1$, it is possible to expand (4.4.11) with respect to the small parameter δ. Therefore, employing the binomial expansion in δ/a, (4.4.11) becomes

$$x_{1,2} = a\{1 \mp \sqrt{1+\delta/a}\} = a\{1 \mp (1 + \delta/2a - \delta^2/8a^2 + ...)\}. \tag{4.4.12}$$

In comparison with δ/a, the second and higher order terms in (4.4.12) are very small and hence can be neglected. Therefore, we obtain

$$x_{1,2} = a\{1 \mp \sqrt{1+\delta/a}\} \approx a\{1 \mp (1 + \delta/2a)\}. \tag{4.4.13}$$

Now taking the upper sign for x_1 and the lower sign for x_2 in (4.4.13), we get

$$\begin{aligned} x_1 &\approx a\{1-(1+\delta/2a)\} = -\delta/2, \\ x_2 &\approx a\{1+(1+\delta/2a)\} = 2a+\delta/2. \end{aligned} \tag{4.4.14}$$

Finally, using the relations $z^2 = 1+x$ and $\delta = 1-z_m^2$, we arrive at

$$\begin{aligned} z_1 &= \sqrt{\frac{1+z_m^2}{2}}, \\ z_2 &= \sqrt{\frac{1+2\alpha\beta}{\alpha+\beta}}. \end{aligned} \tag{4.4.15}$$

Note that the first root z_1 lies between the resonant frequencies z_m and z_e, and the second root z_2 is located above the resonant frequency of the electron subsystem, both in the RHM frequency domains. As it was mentioned in section 4.2, $n_2(z_1) \approx 15$ (see Fig. 4.5) and EMWs strongly decay. In the vicinity of z_2, $n_2 \approx 0.7$ (see Fig. 4.15), which makes the propagation of narrow microwave packets possible.

It is interesting to compare the approximate numerical values of $z_1 = 0.988$ and $z_2 = 1.126$ obtained with the help of (4.4.15) with the parameters of SMM from Table 4.1 and the exact roots of z_1 and z_2 obtained from the equation $n_1(z) = 0$ (Equation (4.2.10) with $A < 0$): $z_1 = 0.989$ and $z_2 = 1.104$. We find a very good agreement for the corresponding z_1 and satisfactory agreement for z_2.

It follows from Fig. 4.16 that in the vicinity of z_2, n_1 can be expressed as

$$n_1(z) = a(z_2)|z - z_2|. \tag{4.4.16}$$

Our numerical evaluation gives $a(z_2) \approx 0.1$. Just for the reference $n_1(z) \approx 60|z - z_1|$. At this point it is worth noting that by increasing the separation between the resonances, the above described nonanalytic behavior of $n_1(z)$ disappears.

In conclusion of this section, we note that the propagation of EMWs in composite media with a zero index of refraction has some peculiarities. Similar cases with

$n_1 = n_2 = 0$ were considered in [86]. The propagation of narrow wave packets centered at the frequency, where $n_1(z) = 0$, in magnetized plasma with ferrite grains and with negligible losses was studied in [87].

4.5 Microwaves in SMM with two resonances

It is known that the group velocity v_g is a physical quantity that properly describes the propagation of narrow wave packets in media and it is given by the following relation [79]

$$v_g = \frac{c}{n_1(z) + z\frac{dn_1(z)}{dz}}, \tag{4.5.1}$$

where c is the speed of light in vacuum and n_1 is the real part of refractive index. It is worth to remind that v_g comes from the Taylor expansion of the frequency $\omega(k)$ in the vicinity of the wave vector k_0 which corresponds to the center of the wave packet. That is,

$$\omega(k) = \omega(k_0) + \omega'(k)|_{k_0}(k - k_0) + \frac{1}{2}\omega''(k)|_{k_0}(k - k_0)^2... \tag{4.5.2}$$

Here $v_g(k_0) = d\omega/dk|_{k_0} \equiv \omega'(k)|_{k_0}$ and describes the velocity of peak of the wave packet provided that we ignore the second and higher derivatives terms in (4.5.2). From this requirement, it follows that v_g has the physical meaning for the narrow wave packets provided that

$$\omega^{(n)}(k_0)(k - k_0)^{n-1} << \omega'(k_0) \equiv v_g(k_0),\ n = 2,\ 3, ..., \tag{4.5.3}$$

where $\omega^{(n)}$ is the n^{th}-derivative of $\omega(k)$. These inequalities allow one to check whether v_g is a "proper" physical quantity or not. Usually, the set of inequalities is limited by $n = 2$.

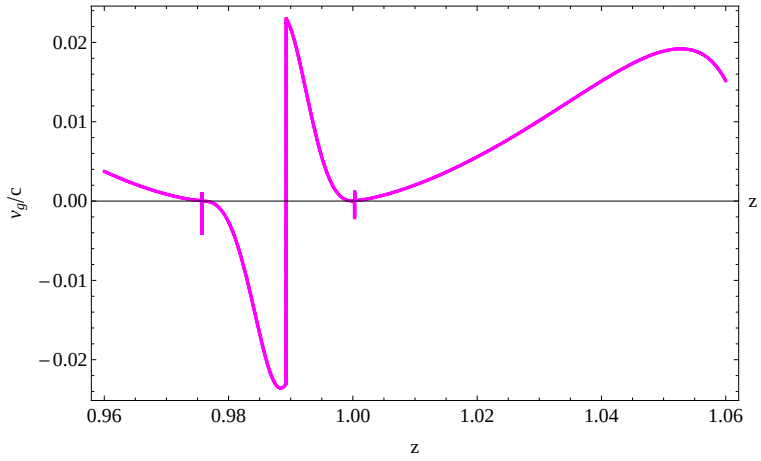

Figure 4.17: The normalized group velocity v_g/c versus z in the frequency band $0.96 < z < 1.06$. Notice the jump of v_g/c which is associated with the nonanalyticity of $n_1(z)$ at the first singular point $z_1 = 0.989$. The small peaks at $z_m = 0.976$ and $z_e = 1$ correspond to v_g/c at the resonances. Parameters of SMM are the same as those in Fig. 4.5.

Below, we calculated the normalized group velocity $v_g(z)/c$ according to (4.5.1) with the help of $n_1(z)$ given by (4.2.10) with the parameters of SMM given in Table 4.1, focusing on the frequency bands where n_2 is small enough to be ignored. The absorption coefficient α' of EMWs is given by [71]

$$\alpha' = \frac{2n_2(z)\omega}{c}, \tag{4.5.4}$$

and the typical length l of decay of EMWs in a medium can be evaluated with $1 \approx 1/\alpha'$. The considerably propagating waves can be specified by imposing the condition $l >> \lambda$, where $\lambda = c/f$ is the wavelength and $f = \omega/2\pi$ is the frequency. For $f = 10\ GHz$, a typical value is $\lambda = 3\ mm$ and we obtain the inequality $n_2 << 1$. Below we assume that $n_2 \leq 0.1$ provides the considerably propagating microwaves.

Figure 4.17 presents the general picture of $v_g(z)/c$ in the frequency range $0.96 \leq$

$z \leq 1.06$. In the frequency band $z \leq z_m$ close to the resonance frequency of the magnetic subsystem, $v_g/c < 1$ is positive and describes slow microwaves. Particularly, in $0.8 < z < 0.92$, the group velocity decreases from $0.18c$ to $0.04c$, as shown in Fig. 4.18. The imaginary part of refractive index in this band is $2.5 \times 10^{-3} < n_2 < 1.75 \times 10^{-2}$ (see the inset in Fig. 4.18) and allows the considerably propagating slow microwaves. It is seen that v_g/c is discontinuous between the resonances of the magnetic and electron subsystems at $z_1 = 0.989$. However, in this band since $n_2 >> 1$ (see Fig. 4.5), there are no propagating waves. Next, for the frequency band $1 < z \leq 1.063$, where the system is LHM, $0 < v_g/c << 1$ which corresponds to the slow microwaves having its maximum $V_g = 0.02c$ at $z = 1.05$ and n_2 is of the order of 0.025 (see Fig. 4.11). The small peak (left side) in Fig. 4.17 corresponds to V_g/c at the resonant point $z = z_m$. The second small peak (right side) in Fig. 4.17 at $z = 1$ is not pronounced clearly on the graph because of the sign change of n_1 (see Figs. 4.5 and 4.10) from positive to negative in the LHM domain.

Figure 4.19 shows $v_g(z)/c$ in the most interesting frequency range $1.065 < z < 1.25$. One can see the jump of the group velocity $\triangle(v_g/c) \approx 20$ results from the nonanalyticity of $n_1(z)$ at the second singular point $z_2 = 1.104$, where $n_1 = 0$. In the frequency band $1.063 < z < z_2$, the group velocity is negative and lies between $-10c$ to $-0.01c$. For $z_2 < z < 1.25$, v_g first increases from $10c$ to $60c$ at $z = 1.17$ and after this decreases to $0.025c$. For this frequency range, Fig. 4.15 shows the maximum value of $n_2 \approx 0.7$ and its minimum ≈ 0.02.

Our numerical analysis of $v_g(z)/c$ and $n_2(z)$ in the frequency range $1.065 < z < 1.25$ allows us to claim that the SMMs can support the considerably propagating slow microwaves (including backward waves). The most favorable situation for the

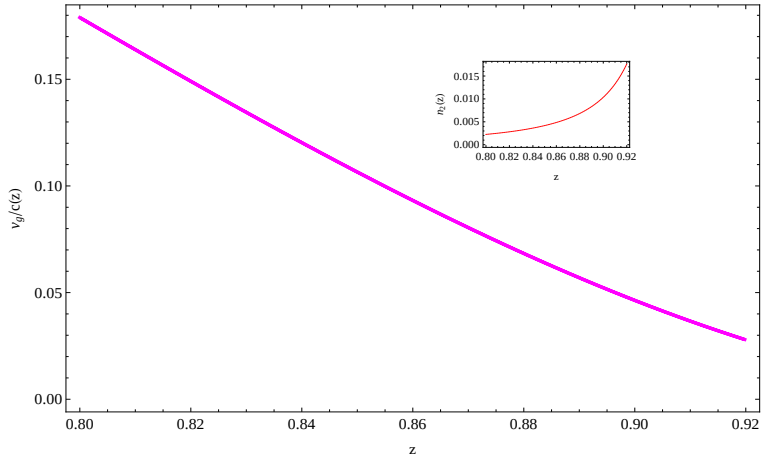

Figure 4.18: The normalized group velocity $v_{g/c}$ versus z in the frequency band $0.8 < z < 0.92$. Parameters of SMM are the same as those in Fig. 4.5. The inset shows the imaginary part of refractive index n_2 versus z.

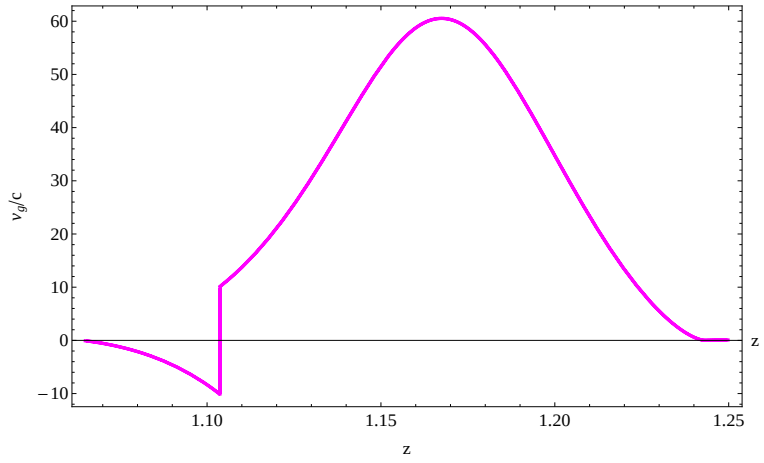

Figure 4.19: The normalized group velocity $v_{g/c}$ versus z in the frequency band $1.065 < z < 1.25$. Notice the jump of $v_{g/c}$ at the second singular point $z_2 = 1.104$ of $n_1(z)$. Parameters of SMM are the same as those in Fig. 4.5.

propagation of superluminal microwaves is $v_g \approx 2c$ with $n_2 \approx 0.15$. By varying the parameters of the SMMs, it is possible to slightly decrease n_2.

Next, we briefly discuss the effect of the nonanalytic behavior of n_1 on the group velocity and propagation of narrow wave packets of microwaves. A rather interesting peculiarity of the group velocity is that it is not a continuous function of z at $z_1 = 0.989$ and at $z_2 = 1.1037$ having a jump, which is associated with the jump of the derivative dn_1/dz. As it was mentioned above, there are no propagating waves in the vicinity of the first singular point. In the vicinity of the second singular point, $z_2 = 1.104$, n_2 is of the order of 0.7 which still supports the propagation of microwaves. With the help of gain components it is possible to decrease n_2 and provide propagating wave in the vicinity of the singular frequencies [88, 89]. In principle gain may be achieved by placing active inclusions designed from diode arrays across the gaps in the SRR units of the structured metamaterials [90, 91]. In this case, for narrow wave packets centered at z_2, one can expect splitting of this wave packet into two packets moving with negative and positive group velocities.

According to [92], the addition of a small negative part to ε_2 practically does not affect n_1 and V_g in the optical frequency range, however it can considerably decrease n_2. However, the problem of microwaves gain in the SMMs requires further study.

4.6 SMM with one resonance

Let us consider a hypothetical SMM with equal (overlapping) resonant frequencies of the magnetic and electron subsystems with $z_m = 1$ and $\beta = \alpha$. In this case we have to set $\mu_1 = \varepsilon_1$ and $\mu_2 = \varepsilon_2$ in (4.2.3). Equations (4.2.10) and (4.2.11) give the

following simple expressions of the real and imaginary parts of refractive index:

$$n_1 = \varepsilon_1 = 1 - \frac{\alpha(z^2-1)}{(z^2-1)^2 + z^2\nu^2}, \\ n_2 = \varepsilon_2 = \frac{\alpha\nu z}{(z^2-1)^2 + z^2\nu^2}. \tag{4.6.1}$$

Now the sign of n_1 automatically specifies the RHM and LHM domains.

Next, we calculated $n_1(z)$ and $n_2(z)$ using (4.6.1) with $\alpha = 0.545$ and $\nu = 0.01$. Figure 4.20 shows $n_1(z)$ and $n_2(z)$ near the resonant frequency $z = 1$ for $\nu = 0.01$. It is seen that at $z = 0.9945$ and $z = 1.0045$, $n_1(z)$ has maximum and minimum ± 25, respectively. The real part of the refractive index is negative in the frequency band $1 < z \leq 1.243$, where the SMM with one resonant frequency corresponds to LHM. Beyond this band, $n_1 > 0$ and it corresponds to RHM. The imaginary part of the refractive index is a Lorentz type with maximum of about 55. For the decay constant $\nu = 0.001$, $n_1(z)$ and $n_2(z)$ have the same pattern as in Fig. 4.20, but with the extremum points $n_1 \approx \pm 230$ and $n_2 \approx 600$ (not plotted, here).

The considerably propagating microwaves are possible only for the frequencies far from the resonance $z = 1$, where $n_2 < 0.1$ according to the criterion assumed in the previous section. The general picture of $v_g(z)/c$ can be understood with the help of Fig. 4.20 and the group index

$$n_g(z) = n_1(z) + z\frac{dn_1(z)}{dz}, \tag{4.6.2}$$

which is the denominator of (4.5.1). Figure 4.21 shows $n_g(z)$ calculated using (4.6.2) with account of (4.6.1) in the frequency range $0.98 < z < 1.02$. The positive and negative superluminal values of v_g/c correspond to the frequency bands, where $n_g(z)$ is close to zero. In the vicinity of $z = 1$, $v_g/c \approx -10^{-4}$, which corresponds to extremely slow microwaves. According to Fig. 4.20, in this frequency band $n_2 >> 1$ which results to a strong absorption of the corresponding microwaves.

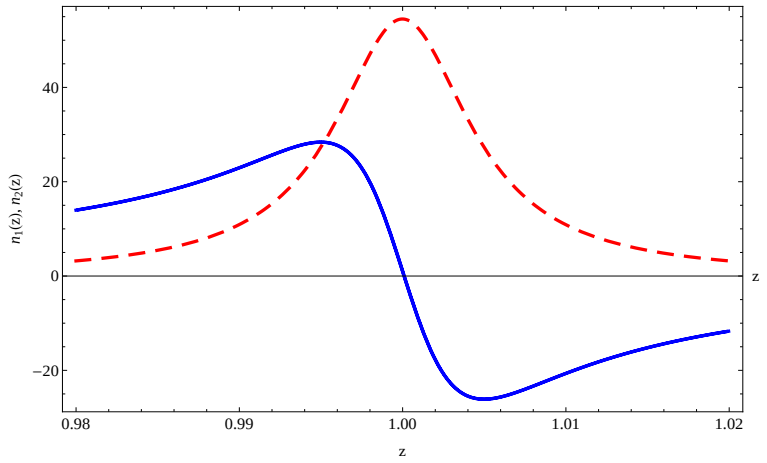

Figure 4.20: The real n_1 (solid line) and imaginary n_2 (dashed line) parts of the refractive index versus z of SMM in the frequency band $0.98 < z < 1.02$. The parameters of SMM $\alpha = 0.545$ and $\nu = 0.01$.

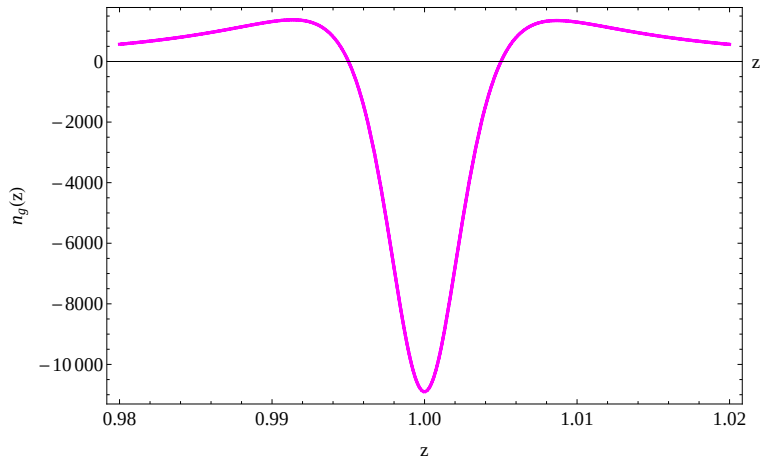

Figure 4.21: The group index n_g of SMM with one resonance versus z in the frequency band $0.98 < z < 1.02$. Parameters of SMM are the same as those in Fig. 4.20.

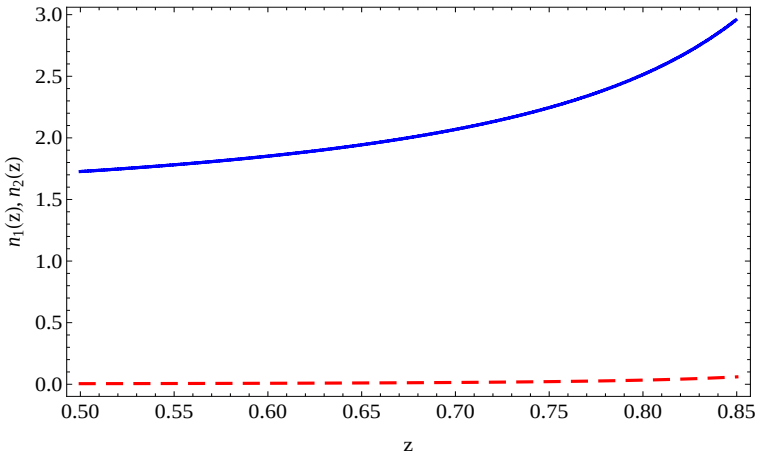

Figure 4.22: The real n_1 (solid line) and imaginary n_2 (dashed line) parts of the refractive index versus z of SMM in the frequency band $0.5 \leq z \leq 0.85$. The Parameters of SMM are the same as those in Fig. 4.20.

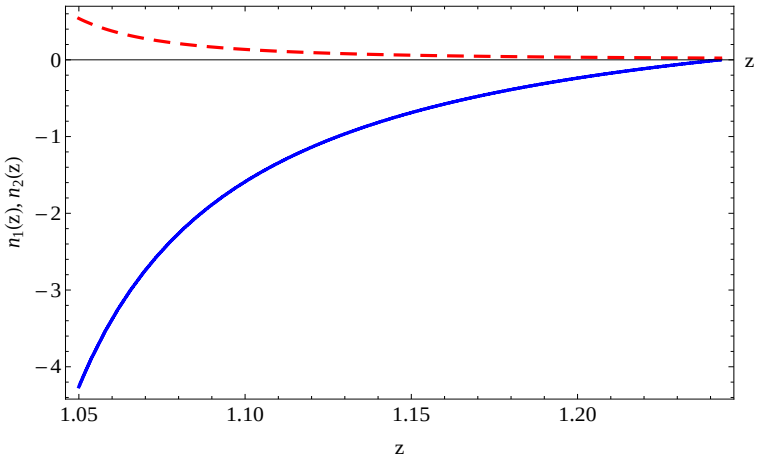

Figure 4.23: The real n_1 (solid line) and imaginary n_2 (dashed line) parts of the refractive index versus z of SMM in the frequency band $1.05 < z < 1.243$. The Parameters of SMM are the same as those in Fig. 4.20.

Our numerical calculations show that slow microwaves with $n_2 < 0.1$ exist in some frequency bands to the left of the resonance for $z < 0.85$ (Fig. 4.22) and to the right of it for $z > 1.175$ (Fig. 4.23). Particularly, in the frequency band $0.5 < z < 0.85$, the group velocity can be interpolated by the linear dependence $v_g = c(0.95 - z)$. In the frequency band $1.2 < z < 2.4$, it is possible to determine the weakly damping microwaves with the group velocity lying in the interval $0.1c < v_g < 0.8c$. We note that a narrow frequency band $1.2 < z < 1.243$ is located at the end of the LHM domain of the SMM with one resonant frequency.

4.7 Summary

We considered the refractive index and group velocity of microwaves in structured metamaterials (SMMs) consisting of strips of copper wire and square copper split-ring-resonators with different and coinciding resonant frequencies. Similar types of SMM have been used for experimental verification of a negative refractive index. We claim that SMMs can be considered as a "laboratory" for studying the slow, superluminal, and backward microwaves. However, only the slow microwaves can be considerably propagating in both types of SMMs. The superluminal microwaves in the SMMs with two resonances are decaying but can be studied experimentally. The experimental study of the superluminal microwaves can be an additional source for clarification of their physical nature and whether the conventional expression of group velocity can be relevant to their description.

We have analyzed, the dispersion of the refractive index both analytically and numerically, and the group velocity numerically in different frequency ranges. Furthermore, we have identified the frequency range where left handed property is observed

that is consistent with the theory of left handed property, namely, $B = \varepsilon_1\mu_2 + \varepsilon_2\mu_1 < 0$. In studying the different frequency range we have taken the resonant frequency of the electron subsystem ($z_e = 1$) as reference. To study the non analytic behavior of the refractive index, we used the parameters A and B allowing the products of the imaginary parts of the permittivity and permeability small in their value, and checked that the non analytic points in frequency agree with numerically obtained ones. In addition, when a wave packet is launched with a frequency that coincides with the none analytic points there may result the splitting of the wave packet into two, propagating to the right and left with respect to that point, as if the point is serving as a source of two packets.

We have also shown that the real part of the refractive index of the SMMs with close resonance frequencies of the magnetic and electron subsystems could be a non-analytic function of the frequency with a discontinuous first derivative. It happens at the frequencies where $n_1 = 0$ and it results in the jump of the group velocity v_g of microwaves. The jump of v_g above the resonant frequency of the electron subsystem supports the weakly decaying superluminal microwaves (negative and positive) and can be checked experimentally.

Moreover, varying the parameters of SMMs has no significant effect in decreasing the imaginary part of the refractive index and the associated absorption. Obtaining the considerably propagating superluminal microwaves requires application of gain components in the SMMs. Formally, it can be done by including a small negative part in the permittivity of the SMM. But it requires to consider how it affects the real part of the refractive index.

Chapter 5

Propagation of Light in an Assembly of Two-Level Atoms

5.1 Introduction

The studies of superluminal, backward, and slow narrow packets of light waves propagating in different media in the frequency range of strong dispersion of the refractive index have had a long history [26]. In 1970 it was reported in Ref. [29] that Gaussian packets of electromagnetic waves can travel in dispersive media with group velocity exceeding the velocity of light in vacuum with no restrictions what so ever. Recently, the topic has been discussed theoretically in many papers again and even some have reported on the experimental realization of such waves in strongly dispersive media [29, 33, 34, 35, 36, 93, 94, 95, 96, 97].

The interesting topic that needs further investigation concerns the superluminal light with group velocity V_g exceeding the speed of light in vacuum. Such a value of V_g is commonly obtained with the help of the conventional formula that does not take into account the dispersion of the imaginary part of the refractive index.

In this Chapter, we consider the evolutions of narrow packets of electromagnetic

waves in a frequency dispersive media. In Section 5.2 we studied the propagation of narrow packets of electromagnetic waves with the consideration of the dispersion of the imaginary part of the refractive index and the conditions in which the physically consistent group velocity can be realized are introduced. In Section 5.3, we consider the group indexes and group velocity of light in an assembly of two-level atoms and determine the frequency bands where the physically acceptable group velocity is attained. Section 5.4, summarizes the results of the chapter.

5.2 Evolution of narrow wave packets in dispersive medium

The profile of a Gaussian wave packet as a function of position and time propagating in a frequency dispersive medium is shown to be given (Eqn. (1.6.14))). Switching from $\omega(k)$ representation to $k(\omega)$ and expanding it using a Taylor's expansion about ω_0, and retaining the first and the linear term in the expansion, along with the dispersion relation between n and k, the Gaussian wave packet for position x and time t, may be rewritten as:

$$E(x,t) = \int_{-\infty}^{\infty} E(\omega) \exp\{i\omega[n(\omega)x/c - t]\} \times \exp[-(\omega-\omega_0)^2/(2\sigma^2)]d\omega. \qquad (5.2.1)$$

where, ω_0 is the central frequency of the wave packet, $E(\omega)$ is its amplitude, σ is the width at frequency ω, c is the speed of light in vacuum, and $n(\omega)$ is the refractive index. In general, the refractive index of the medium $n(\omega)$ is a complex function of ω, given by

$$n(\omega) = n_1(\omega) + in_2(\omega), \qquad (5.2.2)$$

where $n_1(\omega)$ and $n_2(\omega)$ are the real and imaginary parts of the refractive index, respectively.

For the typical expressions of $n(\omega)$ and arbitrary σ, the evaluation of the integral in (5.2.1) is rather complex even in numerical calculations. However, for narrow wave packets the analysis, which can be carried out analytically, becomes relatively simple. Hence, for such narrow Gaussian wave packets of EMWs with central frequency ω_0, the complex refractive index given by (5.2.2) may be expressed in power series expansion around ω_0 as follows:

$$n(\omega) = n(\omega_0) + n'(\omega_0)(\omega - \omega_0) + ..., \tag{5.2.3}$$

where $n'(\omega_0)$ is the first derivative of $n(\omega)$ evaluated at $\omega = \omega_0$. For narrow wave packets the second and higher order terms in the expansion (5.2.3) are small compared with the leading two terms and hence can be neglected. In view of this, substitution of expansion (5.2.3) into (5.2.1) yields

$$E(x,t) = E(\omega_0)\exp\{-\omega_0 n_2(\omega_0)x/c\} \times \exp\{i\omega_0[n_1(\omega_0)x/c - t]\}I. \tag{5.2.4}$$

Here, the notation I represents the following integral:

$$I = \int_{-\infty}^{\infty} \exp^{(-aq^2+ibq)}\, dq, \tag{5.2.5}$$

where the parameters q, a, and b are given by

$$q = \omega - \omega_0,$$

$$a = \frac{1}{2\sigma^2} + \frac{n'_2(\omega_0)x}{c} - \frac{in'_1(\omega_0)x}{c}, \tag{5.2.6}$$

$$b = [n_{g1}(\omega_0) + in_{g2}(\omega_0)]\frac{x}{c} - t, \tag{5.2.7}$$

with n_{g1} and n_{g2} defined by:

$$n_{g1}(\omega) = n_1(\omega) + \omega n_1'(\omega), \tag{5.2.8}$$

$$n_{g2}(\omega) = n_2(\omega) + \omega n_2'(\omega). \tag{5.2.9}$$

The quantity $n_{g1}(\omega)$ is known as the group index [93]. Below, we introduce the imaginary part of the complex group index, $n_{g2}(\omega)$, along with that of the real one, $n_{g1}(\omega)$.

Equation (5.2.5) is the well known Poisson integral. The value of the integral can be shown to be

$$I = \sqrt{\frac{\pi}{a}} \exp[-b^2/4a], \tag{5.2.10}$$

provided that the real part of a is positive. This requirement imposes that the following condition must hold true:

$$\frac{1}{2\sigma^2} + \frac{n_2'(\omega_0)x}{c} > 0. \tag{5.2.11}$$

Consequently, (5.2.4) together with equations (5.2.6)-(5.2.11) describes the evolution of the narrow wave packet propagating in the medium with complex refractive index. To make the analysis of (5.2.4) more clear and simple, we consider narrow wave packet traveling small distance x, so that (5.2.6) reduces to $a = 1/(2\sigma^2)$. In view of this, (5.2.4) is simplified to

$$\begin{aligned} E(x,t) &= E_0 \exp\{-\omega_0 n_2 x/c\} \times \exp\{i\Omega'[n_1 x/c - t]\} \\ &\quad \times \exp\{-\sigma^2[(n_{g1} + n_{g2})x/c - t] \times [(n_{g1} - n_{g2})x/c - t]/2\}, \end{aligned} \tag{5.2.12}$$

where the quantities n_1, n_2, n_{g1}, and n_{g2} are to be evaluated at the central frequency ω_0, and

$$E_0 = \sqrt{2\pi\sigma^2} E(\omega_0),$$

and

$$\Omega' = \omega_0 + \sigma^2 n_{g2}\frac{x}{c}.$$

Let us compare (5.2.12) with the conventional result given in [71, 79], which is obtained by setting $n_{g2} = 0$ in (5.2.12). Therefore, with $n_{g2} = 0$, (5.2.12) reduces to

$$\begin{aligned} E(x,t) &= E_0 \exp\{-\omega_0 n_2(\omega_0)\frac{x}{c} + i\omega_0[n_1(\omega_0)\frac{x}{c} - t]\} \\ &\quad \times \exp\left\{-\frac{\sigma^2}{2v_g(\omega_0)^2}[x - v_g(\omega_0)t]^2\right\}. \end{aligned} \tag{5.2.13}$$

Here, we introduce the group velocity v_g according to the well known relation [79]

$$v_g(\omega) = \frac{c}{n_{g1}(\omega)} \equiv \frac{c}{n_1(\omega) + \omega n'_1(\omega)}. \tag{5.2.14}$$

Equation (5.2.13) shows that in cases where the dispersion of imaginary part of the refractive index is neglected, the narrow wave packet propagating in a frequency dispersive medium can be described by the product of the following two terms:
(i) the "envelope" term given by

$$\exp\left\{\frac{-\sigma^2[x - v_g(\omega_0)t]^2}{2v_g^2(\omega_0)}\right\},$$

(ii) the propagating plane wave given by

$$\exp\{i\omega_0[n_1(\omega_0)\frac{x}{c} - t]\},$$

moving with the group velocity, v_g. The peak of the "envelope" term decreases with increasing x, since $n_2(\omega_0)$ in the first exponent (5.2.13) is positive. Hence, as a result of neglecting the dispersion of the imaginary part of the refractive index, the description of narrow waves propagating in dispersive media assumes a relatively simple and elegant form. However, the account of the dispersion of the imaginary part of the refractive index $n_2(\omega)$ considerably complicates the scenario.

Further, separating the terms involving $n_{g1}(\omega_0)$ and $n_{g2}(\omega_0)$ in the last exponent of (5.2.12), we may rewrite (5.2.12) as

$$\begin{aligned} E(x,t) &= E_0 \exp\{-\omega_0 n_2 \frac{x}{c}\} \times \exp\{i\Omega'[n_1 \frac{x}{c} - t]\} \\ &\quad \exp\left\{\frac{-\sigma^2}{2v_g^2(\omega_0)}[x - v_g(\omega_0)t]^2\right\} \exp\{\sigma^2 (n_{g2}x/c)^2/2\}. \end{aligned} \tag{5.2.15}$$

In view of equations (5.2.13) and (5.2.15), we claim that it is possible to introduce V_g, defined by (5.2.14), having the physical meaning only in the frequency bands where (5.2.11) and the following inequalities hold true:

$$|n_{g2}(\omega_0)| << |n_{g1}(\omega_0)|, \tag{5.2.16}$$

$$[n_{g2}(\omega_0)\sigma x/c]^2 << 1, \tag{5.2.17}$$

$$[n_{g1}(\omega_0)]^2 \sigma x/c << \omega_0 n_2(\omega_0). \tag{5.2.18}$$

Equation (5.2.17) provides a weak damping and can be satisfied for rather narrow wave packet $\sigma << \omega_0$ and small traveling distance $x \sim c/[\omega_0 n_2(\omega_0)]$. Inequality (5.2.16) is new and it imposes important restriction on the conventional definition of v_g. In principle, the superluminal group velocity $v_g > c$ is obtained from (5.2.14) in the frequency band where the following inequality holds true:

$$|n_{g1}(\omega)| \equiv |n_1(\omega) + \omega dn_1(\omega)/d\omega| < 1. \tag{5.2.19}$$

In the next sections we focus on the consistency of equations (5.2.16) and (5.2.19) for the relevant mathematical model of the refractive index of an assembly of two-level atoms.

5.3 Group index and velocity in a system of two-level atoms

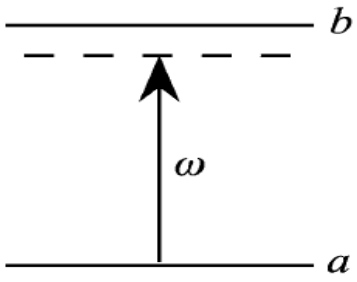

Figure 5.1: Near-resonant excitation of a two-level atom. [79]

Consider a system consisting of an assembly of weakly interacting two-level atoms with the two atomic levels resonantly connected by an optical field. That is, it is assumed that a monochromatic beam of frequency ω interacts with a collection of two-level atoms. Denoting the bottom level by a and the upper level by b, as shown in Fig. 5.1, the refractive index of such a collection of weakly interacting two-level atoms is given by

$$n(\omega) = \sqrt{1 + 4\pi\chi(\omega)}, \tag{5.3.1}$$

where the susceptibility, $\chi(\omega)$. For a system consisting of an assembly of two-level atoms in equilibrium, the susceptibility is shown to be given by (Eqn. (3.5.12)) [79]. That is,

$$\chi(\omega) = \frac{N(\rho_{bb} - \rho_{aa})|\mu_{ba}|^2(T_2\Delta - i)T_2}{\hbar(1 + T_2^2\Delta^2 + T_1T_2\Omega^2)}. \tag{5.3.2}$$

where, N is the density number of atoms, $\omega_{ba} > 0$ is the transition frequency between the energy levels b and a, ρ_{aa} and ρ_{bb} are the diagonal components of the density

matrix describing the difference in population between the levels a and b at thermal equilibrium, μ_{ba} is the atom dipole matrix element, T_1 is the lifetime of the upper level, T_2 is the characteristic time of dephasing dipole moment resulting in the transition line width $1/T_2$, E is the amplitude of monochromatic electric field of the incident electromagnetic wave of frequency ω, Δ is the detuning factor given by

$$\Delta = \omega - \omega_{ba},$$

and Ω is the on-resonance Rabi frequency defined by

$$\Omega = \frac{2|\mu_{ba}|}{\hbar}|E|.$$

Below, we consider an equilibrium case when $\rho_{bb} = 0$ and $\rho_{aa} = 1$, that is, when the upper level is not populated. In the case of $|\chi| << 1$, which is consistent with the model, using (5.3.1) and (5.3.2), we obtain the following expressions for the real and imaginary parts of the refractive index:

$$n_1 = 1 - \frac{\alpha T_2 \Delta}{A^2 + T_2^2 \Delta^2}, \tag{5.3.3}$$

$$n_2 = \frac{\alpha}{A^2 + T_2^2 \Delta^2}, \tag{5.3.4}$$

where the parameters α and A denote

$$\alpha = \frac{2\pi N T_2}{\hbar}|\mu_{ba}|^2,$$

and

$$A = \sqrt{1 + T_1 T_2 \Omega^2}.$$

Note that equations (5.3.3) and (5.3.4) are valid provided that

$$|n_1 - 1| << 1, \qquad \text{and} \qquad |n_2| << 1. \tag{5.3.5}$$

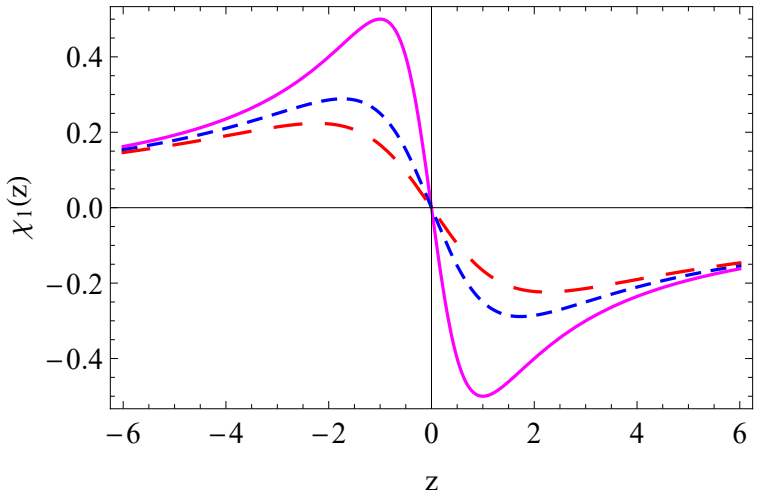

Figure 5.2: Curves of χ_1 versus z for $\alpha = 0.00001$, $\beta = 100$, and (a) $A^2 = 1$ (solid), (b) $A^2 = 3$ (dashed, small), (c) $A^2 = 5$ (dashed, large). (Color online)

For numerical analysis we evaluate α. Taking typical values, $|\mu_{ba}| = 5.5 \times 10^{-18}$ esu (for $3s \rightarrow 3p$ transition of atomic sodium) and $T_2 = 32$ ns [79], we obtain $\alpha = 6 \times 10^{-15} N$, where N is expressed in cm^{-3}. From (5.3.3), (5.3.4) and these numerical values, it is obvious that for $N \leq 10^{13}$ cm^{-3} and $A \geq 1$, the inequalities given by (5.3.5) holds true.

Figures 5.2-5.4 show the graphs of the real part of the susceptibility χ_1, the imaginary part of the susceptibility χ_2 and the real part of the refractive index n_1, near the vicinity of the resonance frequency, in units of α.

Figure 5.2 shows the real part of the susceptibility χ_1 versus the frequency z for different values of A, which contains implicitly the Rabi frequency, Ω. The solid line corresponds the weak field limit, which in turn corresponds to the linear susceptibility where the term that contains the Rabi frequency, $\Omega^2 T_1 T_2$, in A is neglected. The dashed line curves correspond to the strong field actions, in which we can not neglect

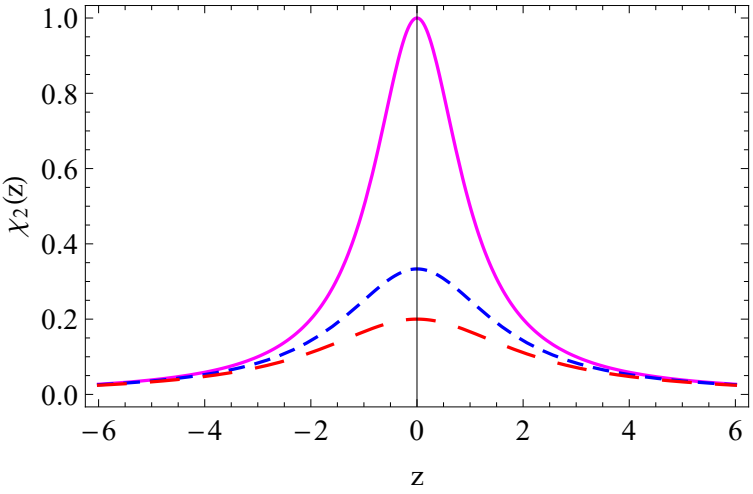

Figure 5.3: Curves of χ_2 versus z for $\alpha = 0.00001$, $\beta = 100$, and (a) $A^2 = 1$ (solid), (b) $A^2 = 3$ (dashed, small), (c) $A^2 = 5$ (dashed, large). (Color online)

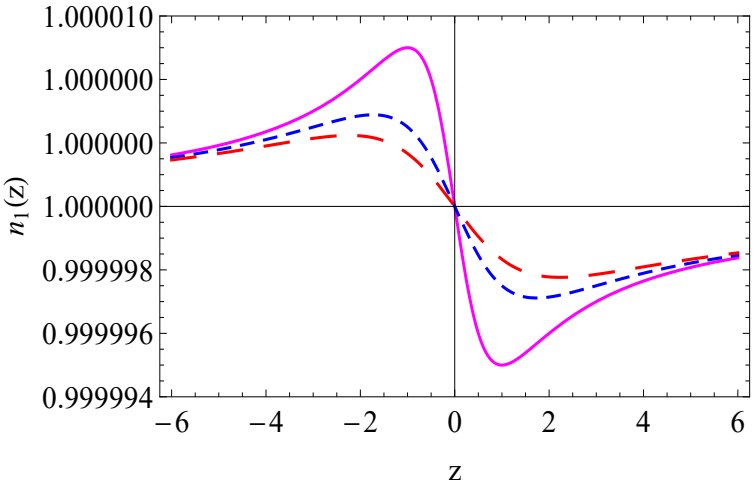

Figure 5.4: Curves of n_1 versus z for $\alpha = 0.00001$, $\beta = 100$, and (a) $A^2 = 1$ (solid), (b) $A^2 = 3$ (dashed, small), (c) $A^2 = 5$ (dashed, large). (Color online)

the term $\Omega^2 T_1 T_2$ that shows the nonlinearity in the susceptibility. The existence of the term $\Omega^2 T_1 T_2$ leads power broadening that which results the decrease of the picks and an increase in the range of the anomalous dispersion region, resulting low dispersion in χ_1. But in all cases the susceptibility maintains its line shape.

Figure 5.3 depicts the imaginary part of the susceptibility χ_2, it has a Lorentzian profile which can be seen from the imaginary parts of the refractive index n_2, (5.3.4). As the field strength increase, like the real part of the susceptibility it broadens and its peaks are decreasing. Such a decrease can be seen from the denominator of equation 5.3.4.

Figure 5.4 shows that the real part of the refractive index n_1, it has similar profile as that of the real part of the susceptibility. It has similar analysis as that of the real part of the susceptibility, since $n_1 \approx 1 + 2\pi\chi_1$.

Further, the real and imaginary parts of the group index n_g can be obtained with the help of (5.2.8), (5.2.9), (5.3.3), and (5.3.4). The results become

$$n_{g1} = 1 - \frac{2\alpha A^2 z}{[A^2 + z^2]^2} - \frac{\alpha T_2 \omega_{ba}[A^2 - z^2]}{[A^2 + z^2]^2}, \tag{5.3.6}$$

$$n_{g2} = \frac{\alpha[A^2 - z(z + 2T_2\omega_{ba})]}{[A^2 + z^2]^2}, \tag{5.3.7}$$

where

$$z = T_2\Delta.$$

It is seen from (5.3.6) and (5.3.7) that far from the resonance frequency $\omega = \omega_{ba}$, where $|z| >> 1$ the approximation $n_{g1} \sim 1$ and inequality $|n_{g2}| << 1$ can be satisfied by choosing the appropriate value of α, such that $\alpha << 1$. Therefore, inequality (5.2.16) for $n_{g1} \sim 1$ and $|n_{g2}| << n_{g1}$ holds true. In these frequency domains the group velocity (5.2.14) has the physical meaning.

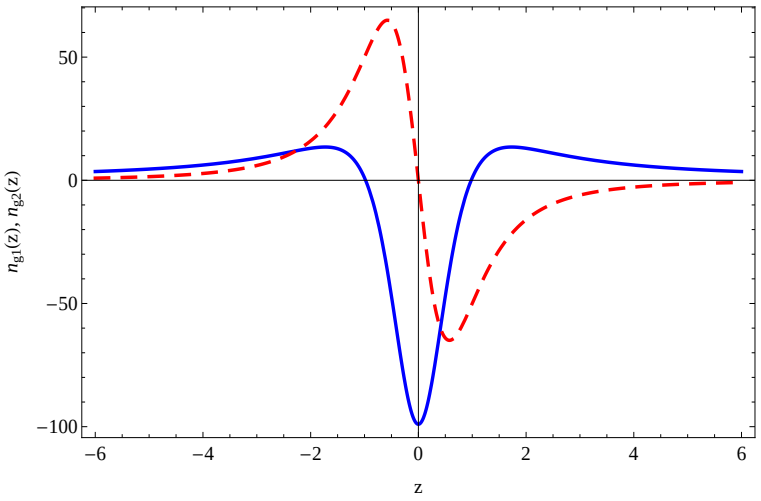

Figure 5.5: Curves of n_{g1} (solid) and n_{g2} (dashed) versus z for $\beta = 100$ and $A = 1$. (Color online)

The frequencies in the vicinity of the resonance $z = 0$ are more interesting. To analyze the group indexes in (5.3.6) and (5.3.7) at these frequencies, one has to take into account that $T_2\omega_{ba} \approx 10^7$, where we choose $T_2 \approx 10^{-8}$ and $\omega_{ba} \approx 10^{15}$. Thus, keeping only the leading terms in (5.3.6) and (5.3.7), we obtain the group indexes to be

$$n_{g1} = 1 - \frac{\beta[A^2 - z^2]}{[A^2 + z^2]^2}, \tag{5.3.8}$$

$$n_{g2} = -\frac{2\beta z}{[A^2 + z^2]^2}, \tag{5.3.9}$$

where

$$\beta = \alpha T_2 \omega_{ba}.$$

It is worth noting that the parameter β can be rather large despite that α is small compared to unity.

Figures 5.5-5.7 show the curves of the real n_{g1} and imaginary n_{g2} parts of the

group index versus z for $\beta = 100$ and different values of A, calculated using (5.3.8). Figure 5.5 shows the curve for $A = 1$. It corresponds to the case where the intensity of the incident wave $|E|^2$ or the on-resonance Rabi frequency is small compared with unit, i.e., $T_1T_2\Omega^2 << 1$. The corresponding $\chi(\omega)$ defined by (5.3.2) coincides with the first order susceptibility [79]. In this case, the real part of the group index n_{g1} is of the known shape [79]. For frequencies $|z| >> 4$, $n_{g1} >> n_{g2}$, and consequently the corresponding group velocity v_g given by (5.2.14) has the physical meaning. But for frequencies $|z| \leq 4$, the situation completely changes. Here, with exception of a narrow frequency band in the vicinity of $z = 0$, $|n_{g2}| > |n_{g1}|$ so that the wave is strongly attenuated and inequality (5.2.16) is not valid. Therefore, the group velocity $|v_g| > c$ has no physical meaning. However, in the frequency range where $|n_{g1}| < 1$, (5.2.14) gives the group velocity corresponding to positive superluminal light. Moreover, in the vicinity of the exact resonance $z = 0$, $n_{g2} \approx 0$ and inequality (5.2.16) holds true, giving $v_g \approx -c/100$ indicating the presence of the slow backward light.

Figure 5.6 shows the curves of n_{g1} and n_{g2} versus z for the same parameters as those in Fig. 5.5, but with $A^2 = 3$, which corresponds to rather intense optical field than the previous case (i.e., $A = 1$). In this case, the peaks of n_{g1} and n_{g2} decrease and become broad compared with Fig. 5.5. Again, one cannot ignore n_{g2} compared with n_{g1} for frequency $|z| \leq 6$. In the vicinity of $|z| \approx 1.6$, the conventional formula (5.2.14) gives superluminal group velocity. However, these velocities have to be discarded as they have no physical meanings since $n_{g2} \sim 10$, near $|z| = 1.6$ resulting in a strongly attenuated wave. On the other hand, in the vicinity of the resonance $z = 0$, for frequency bands where $|n_{g2}| << |n_{g1}|$, equation (5.2.16) is valid,

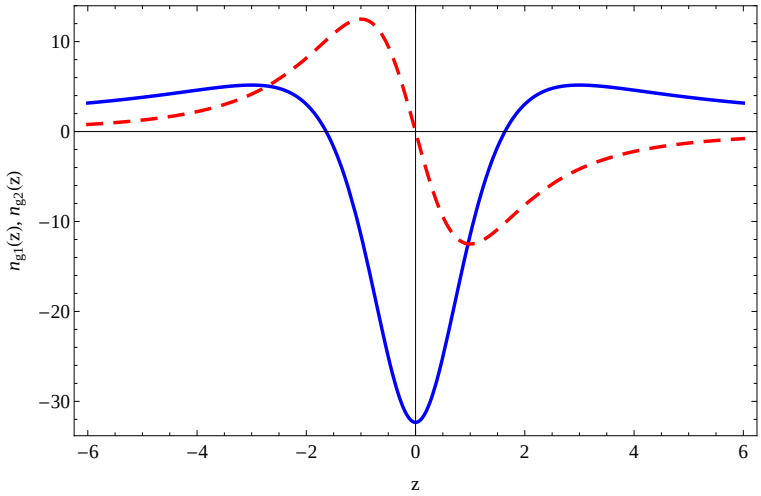

Figure 5.6: Curves of n_{g1} (solid) and n_{g2} (dashed) versus z for $\beta = 100$ and $A^2 = 3$. (Color online)

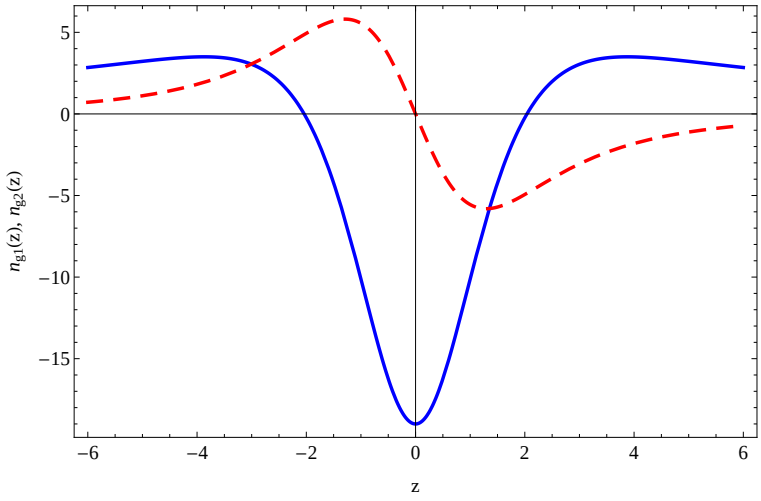

Figure 5.7: Curves of n_{g1} (solid) and n_{g2} (dashed) versus z for $\beta = 100$ and $A^2 = 5$. (Color online)

giving $v_g \approx -c/30$, corresponding to the slow backward light.

Figure 5.7 depicts the curves of n_{g1} and n_{g2} versus z for a much higher intensity of the incident optical wave with $A^2 = 5$. One can observe that the peaks of the group indexes become smaller and wider. This effect can be explained by the theory that the widening of the spectral line results in the presence of intense radiation field [79]. Moreover, the negative peak of n_{g2} becomes broader than those in Figs. 5.5 and 5.6. We can claim that the application of strong optical field of the incident wave results to the broadening of the frequency band where $n_{g1} < n_{g2}$ and consequently the group velocity loses its physical meaning. In the frequency domain that is far from the resonance, i.e., for $z >> 6$, the imaginary group index fast approaches to zero, being negative and (5.2.14) gives physically admissible value of the group velocity, $|v_g| \leq c$.

It is necessary to note that again in the vicinity of the resonance $z = 0$, (5.2.14) results in a physically consistent group velocity corresponding to the slow light. The corresponding group index is obtained from (5.3.8) and the group velocity is given by

$$v_g \approx -c\frac{A^2}{\beta}, \qquad (\beta >> 1). \tag{5.3.10}$$

This result is consistent with the curves of n_{g1} versus z depicted in Figs. 5.5-5.7.

5.4 Summary

The profile of narrow wave packet propagating in a dispersive medium is analyzed with the help of the standard procedure but with the consideration of the dispersion of the imaginary part of the refractive index. In addition to the conventional group index n_{g1}, it contains a new expression n_{g2}, which corresponds to the imaginary part of the complex group index. This quantity significantly changes the profile of the

wave packet compared with the conventional case, with $n_{g2} = 0$.

The behavior of the susceptibility (real and imaginary parts) resulted from the 3s to 3p transition appear the same as those developed theoretically in chapter 3. They show power broadening which is typical of two-level atoms driven by coherent strong fields. As the intensity of the light field increases the peaks of the susceptibility decreases, the anomalous frequency range increases, and the absorption peak decreases.

It is shown that taking into account of the dispersion imaginary part of the group index n_{g2} significantly distorts the shape of Gaussian wave packet, which is demonstrated by introducing the imaginary part of the group index n_{g2} along with the conventional real group index n_{g1}. The latter completely controls the group velocity with the help of the real part of $n(\omega)$ and its derivative with respect to the frequency ω. Our theoretical and numerical analysis show that the physically consistent group velocity v_g for narrow packet of EMW can only be realized in the frequency bands where $n_{g2} << n_{g1}$. By considering the relevant model of the complex refractive index of an assembly of two-level atoms, it is shown that in the frequency bands where the conventional formula of v_g gives the superluminal group velocity, the condition $n_{g2} << n_{g1}$ is violated, confirming the fact that $|v_g| > c$ has no physical meaning.

The main result is that the group velocity calculated using the conventional formula $v_g = c/n_{g1}$ has the physically acceptable value only for frequency ω, where $|n_{g2}(\omega)| << |n_{g1}(\omega)|$. We verify the validity of this inequality with the help of the refractive index of a typical two-level atom model at optical frequency for the equilibrium case and show that it is violated for the frequency range where the conventional formula of v_g gives superluminal group velocity $|v_g| > c$. That is, in the frequency

domain where superluminal light is expected the presence of strong absorption attenuates the wave and makes it impossible to realize the physical superluminal light.

On the other hand, in the vicinity of the resonant frequency where the imaginary part of the refractive index of an equilibrium system is large and results in strong absorption, the imaginary group index $n_{g2} \approx 0$, which allows one to realize the physically consistent group velocity corresponding to the slow light with the real group index $|n_{g1}| >> 1$.

Chapter 6

Conclusions

The propagation of electromagnetic waves in structured metamaterials and a system of two-level atoms is studied theoretically and numerically. Firstly, the dispersion of permittivity, permeability, and refractive index of structured metamaterials made copper array of long metallic wires and a copper SRR in various frequency domains are investigated.

The group velocity in this medium as well as SMM with coinciding resonance with the same parameters is studied, whether they support slow, superluminal, and backward microwaves. Only the slow microwaves can be considerably propagating in both types of SMMs. The superluminal microwaves in the SMMs with two resonances are decaying but can be studied experimentally, and can be an additional source for clarification of their physical nature and whether the conventional expression of group velocity can be relevant to their description.

The real part of the refractive index of the SMMs with close resonance frequencies of the magnetic and electron subsystems is nonanalytic function of the frequency at two frequencies ($z = 0.98925$, and $z = 1.10374$) with a discontinuous first derivative, which results the jump in the group velocity of the microwaves. The jump of v_g

above the resonant frequency of the electron subsystem supports the weakly decaying superluminal microwaves (negative and positive) and can be checked experimentally. Obtaining the considerably propagating superluminal microwaves requires application of gain components in the SMMs. Formally, it can be done by including a small negative part in the permittivity of the SMM. But it requires to consider how it affects the real part of the refractive index.

Secondly, the profile of narrow wave packet propagating in a dispersive medium is analyzed with the help of the standard procedure but with the consideration of the dispersion of the imaginary part of the refractive index. Taking into account of the dispersion imaginary part of the group index n_{g2} significantly distorts the shape of Gaussian wave packet, which is demonstrated by introducing the imaginary part of the group index n_{g2} along with the conventional real group index n_{g1}. The behavior of the susceptibility (real and imaginary parts) show power broadening which is typical of two-level atoms driven by coherent strong fields. As the intensity of the light field increases the peaks of the susceptibility decreases, the anomalous frequency range increases, and the absorption peak decreases.

The theoretical and numerical analysis show that the physically consistent group velocity v_g for narrow packet of EMW can only be realized in the frequency bands where $n_{g2} << n_{g1}$. The group velocity calculated using the conventional formula $v_g = c/n_{g1}$ has the physically acceptable value only for frequency ω, where $|n_{g2}| << |n_{g1}|$. In the vicinity of the resonant frequency the imaginary part of the refractive index of an equilibrium system is large and results in strong absorption, the imaginary group index $n_{g2} \approx 0$, which allows one to realize the physically consistent group velocity corresponding to the slow light with the real group index $|n_{g1}| >> 1$.

List of Publications

1. Abdurahman Ahmed, Vadim N. Mal'nev, and Belayneh Mesfin,"Microwaves in structured metamaterials: slow, superluminal, and backward wave", *Ukrainian Journal of Physics - Solid Matter*, **Vol. 61, No. 2**, 125-133 (2016).

2. Abdurahman Ahmed, Vadim N. Mal'nev, and Belayneh Mesfin, "Superluminal light attenuated by strong dispersion of complex refractive index", *Chinese Physics B*, **Vol. 25, No. 2**, 027801 (2016).

Bibliography

[1] R.M. Walser, *Electromagnetic metamaterials*, Proc. SPIE, **4467**, 1-15 (2001)

[2] Shridhar E. Mendhe, and Yogeshwar Prasad Kosta, *Metamaterials Properties and Applications*, International Journal of Information Technology and Knowledge Management, **4**, 85-89(2011)

[3] V.G. Veselago, *The Electrodynamics of Substances with Simultaneously Negative Values of ϵ and μ*, Sov. Phys. Usp., **10**, 517-526 (1968)

[4] H. Lamb, *On group-velocity*, Proc. London Math. Soc., **1**, 473-479 (1904)

[5] A. Schuster, *An Introduction to the Theory of Optics*, Edward Arnold, London, 313-318 (1904)

[6] Pocklington, *Growth of a wave-group when the group velocity is negative*, Nature, **71**, 607-608 (1905)

[7] J.B. Pendry, A.J. Holden, D.J. Robbins, W.J. Stewart, *Magnetism from conductors and enhanced nonlinear phenomena*, IEEE Trans. Micro. Theory Tech., **47**, 2075-2084 (1999)

[8] D.R. Smith, W.J. Padilla, S.C. Nemat-Nasser, and S. Schultz, *Composite Medium with Simultaneously Negative Permeability and Permittivity*, Phys. Rev. Lett., **84** , 4184-4187 (2000) .

[9] R.A. Shelby, D.R. Smith, and S. Schultz, *Experimental Verification of a Negative Index of Refraction*, Science, **292**, 77-79 (2001)

[10] C.G. Parazzoli, R.B. Greegor, K. Li, B.E.C. Koltenbah, and M. Tanielian, *Experimental Verification and Simulation of Negative Index of Refraction Using Snell's Law*, Phys. Rev. Lett., **90**, 107401 (2003)

[11] M. Bayindir, K. Aydin, E. Ozbay, P. Markos, and C.M. Soukoulis, *Transmission properties of composite metamaterials in free space*, Appl. Phys. Lett., **81**, 120-122 (2002)

[12] Li, S.J. McLean, R.B. Greegor, C.G. Parazzoli, and M.H. Tanielian, *Free-space focused-beam characterization of left-handed materials*, Appl. Phys. Lett., **82**, 2535-2537 (2003)

[13] Marques, J. Martel, F. Mesa, and F. Medina, *A new 2D isotropic left-handed metamaterial design: Theory and experiment*, Microwave Opt. Technology Lett., **35**, 405-408 (2002)

[14] J.T. Huangfu, L.X. Ran, H.S. Chen, X.M. Zhang, K.S. Chen, T.M. Grzegorczyk, and J.A. Kong, *Experimental confirmation of negative refractive index of a metamaterial composed of Omega like metallic patterns*, Appl. Phys. Lett., **84**, 1537-1539 (2004)

[15] A.A. Houck, J.B. Brock, and I.L. Chuang, *Experimental observations of a left-handed material that obeys snell's law*, Phys. Rev. Lett., **90**, 137401 (2003)

[16] L. Ran, J. Huangfu, H. Chen, Y. Li, X. Zhang, K. Chen, and J.A. Kong, *Microwave solid-state left-handed material with a broad bandwidth and an ultralow loss*, Phys. Rev. B, **70**, 073102 (2004)

[17] A.F. Starr, P.M. Rye, D.R. Smith, and S. Nemat-Nasser, *Fabrication and characterization of a negative-refractive-index composite metamaterial*, Phys. Rev. B, **70**, 113102 (2004)

[18] K. Aydin, K. Guven, M. Kafesaki, L. Zhang, C.M. Soukoulis, and E. Ozbay, *Experimental observation of true left-handed transmission peaks in metamaterials*, Optics Letters, **29**, 2623-2625 (2004)

[19] P. Markos and C.M. Soukoulis, *Absorption losses in periodic arrays of thin metallic wires*, Optics Letters, **28**, 10 (2003)

[20] Ghazaleh Kafaie Shirmanesh, Amin Khavasi, and Khashayar Mehrany, *Accurate effective medium theory for arrays of metallic nanowires*, J. Opt., **17**, 025104 (2015)

[21] Wei Song, Zhun Yang, Xin-Qing Sheng, and Yang Hao, *Accurate modeling of high order spatial dispersion of wire medium*, Optics Express, **21**, 29836 (2013)

[22] Philippe Gay-Balmaz and Olivier J.F. Martin, *Electromagnetic resonances in individual and coupled split-ring resonators*, Journal of Applied Physics, **92**, 5, (2002)

[23] P. Markos and C.M. Soukoulis, *Numerical studies of left-handed materials and arrays of split ring resonators*, Phys. Rev. E, **65**, 036622 (2002)

[24] Jiangfeng Zhou, Thomas Koschny, Lei Zhang, Gary Tuttle, and Costas M. Soukoulis, *Experimental demonstration of negative index of refraction*, Appl. Phys. Lett., **22**, 88 (2006)

[25] E. Plum, X.-X. Liu, V. A. Fedotov, Y. Chen, D. P. Tsai, and N. I. Zheludev, *Metamaterials: Optical Activity without Chirality*, Phys. Rev. Lett, **102**, 113902 (2009)

[26] L. Brillouin, *Wave propagation and group velocity*, Academic Press, New York (1960)

[27] M.D. Stenner, D.J. Gauthier, and M.A. Neifeld, *The speed of information in a fast-light optical medium* Nature (London), **425**, 695 (2003)

[28] N. Brunner, V. Scarani, M. Wegmuller, M. Legre, and N. Gisin, *Direct measurement of superluminal group velocity and of signal velocity in an optical fiber*, Phys. Rev. Lett. **93**, 203902 (2004)

[29] Garrett and McCumber, *Propagation of Gaussian light pulse in anomalous dispersive media*, Phys. Rev. A, **1**, 305 (1970)

[30] R.W. Boyd and D.J. Gauthier, *Progress in Optics*, **43**, 497 (2002)

[31] P.W. Milloni, *Fast Light, Slow Light, Left-Handed Light*, Bristol: Institute of Physics Publishing, pp. 3567 (2005)

[32] D.J. Gauthier and R.W. Boyd, **Photonics Spectra**, **41**, 82 (2007)

[33] S.Chu and S. Wong, *Linear Pulse Propagation in an Absorbing Medium*, Phys. Rev. Lett. **48**, 738 (1982)

[34] L.J. Wang, A. Kuzmich, and A. Dogarlu, *Gain-assisted superluminal light propagation*, Nature, **406**, 277 (2000).

[35] A. Schweinsberg, N.N. Lepeshkin, M.S. Bigelow, R.W. Boyd, and S. Jarabo, *Observation of superluminal and slow light propagation in erbium-doped optical fiber*, Europhys. Lett., **73**, 218224 (2006)

[36] M.V. Davidovich, *On the Hartman paradox, electromagnetic wave tunneling and supraluminal velocities*, Physics-Uspekhi, **52**, 4 (2009)

[37] J.D. Jackson, *Classical Electrodynamics*, John Wiley and Sons, New York (1999)

[38] R.Y Chiao, *Superluminal (but causal) proppagation of wave packets in transparent media with inverted atomic population*, Phys. Rev. A, **48**, 1 (1993)

[39] M.S. Bigelow, N.N. Lepeshkin, and R.W. Boyd, *Superluminal and Slow Light Propagation in a Room-Temperature Solid*, Science, **301**, 200 (2003)

[40] M.S. Bigelow, N.N. Lepeshkin, and R.W. Boyd, *Observation of ultraslow light propagation in a ruby crystal at room temperature*, Phys. Rev. Lett., **90**, 113903 (2003)

[41] P.C. Ku, F. Sedgwick, C.J. Chang-Hasnain, P. Palinginis, T. Li, H. Wang, S.W. Chang, and S.L. Chuang, *Slow light in semiconductor quantum wells,* Opt. Lett., **29**, 2291 (2004)

[42] Chen Kai, Wu Ling-An, and Shin Yan-Hua, *Is 'supperluminal' light possible in dispersive media?*, Chinese Phys. Lett., **21**, 770 (2004)

[43] Zhang Qi-Ren, *Relativity and impossibility of superluminal motion*, Chin. Phys. B, **21**, 110301 (2012)

[44] H. Tanka, H. Niurs, K. Hayami, S. Furue, K. Nakayama, T. Kohmoto, M. Kunitomo, and Y. Fukuda, *Propagation of optical pulses in a resonantly absorbing medium: Observation of negative velocity in Rb vapor*, Phys. Rev. A, **68**, 053801 (2003)

[45] D. Ye, G. Zheng, J. Wang, Z. Wang, S. Qiao, J. Huangfu and L. Ran, *Negative Group Velocity in the Absence of Absorption Resonance*, Sci. Rep., **3**, 1628 (2012)

[46] Dexin Ye, Yannick Salamin, Jiangtao Huangfu, Shan Qiao, Guoan Zheng, and Lixin Ran, *Observation of Wave Packet Distortion during a Negative-Group-Velocity Transmission*, Sci. Rep., **08**, 100 (2015)

[47] V.V. Fisano, *Forward and backward plane waves in generalized isotropic medium*, Russian Physics Journal, **57**, 10 (2015)

[48] Hanse C Ohanian, *Classical Electrodynamics*, **Allyn and Bacon, Inc.** (1988)

[49] M.H. Nayfeh, M.K. Brussel, *Electricity and Magnetism*, John Wiley and Sons Inc. (1985)

[50] Amnon Yarive and Pochi Yeh, *Optical Waves In Crystals*, John Wiley and Sons Inc. (1983)

[51] P.Y. Chen, R.C. McPhedran, C.M. de Sterke, C.G. Poulton, A.A. Asatryan, L.C. Botten, and M.J. Steel, *Group Velocity in Lossy Periodic Structured Media*, Phys. Rev. A, **82**, 053825 (2010)

[52] R. Loudon, *The propagation of electromagnetic energy through an absorbing dielectric*, Journal of Physics A General Physics, **4**, 450450 (1970)

[53] G. Dolling, C. Enkrich, M. Wegener, C.M Soukoulis, and J. Linden, *Negative-index metamaterial at 780 nm wavelength*, Optics Lett., **32**, 53-55 (2007)

[54] J.M. Xiao, U.K. Chettior, A.V. Kildishev, V.P. Drachev, and V.M. Shalaev, *Yellow-light negative-index metamaterials*, Opt Lett., **34**, 3478-3480 (2009)

[55] Parry Y. Chen, Ross C. McPhedran, C. Martijn de Sterke, and Michael J. Steel, *Group Velocity in Lossy Periodic Structured Media*, **3**, 1628 (2012)

[56] J.G. Pedersen, S. Xiao, and N.A. Mortensen, *Limits of slow light in photonic crystals*, Phys. Rev. B, **15**, 153101 (2008)

[57] J. Peatross, S.A. Glasgow, and M. Ware, *Average energy flow of optical pulses in dispersive media*, Phys. Rev. Lett., **11**, 2370-2373 (2000)

[58] Donald D. Fitts, *Principles of Quantum Mechanics*, Cambridge University Press (1999)

[59] J.D. Jackson, *Classical Electrodynamics*, John Wiley and Sons, New York (1975)

[60] A. Kasapi, M. Jain, G. Yin, and S. Harris, *Electromagnetically Induced Transparency: Propagation Dynamics*, Phys. Rev. Lett., **74**, 2447-2450 (1995)

[61] M. Kash, V. Sautenkov, A. Zibrov, L. Hollberg, G. Welch, M. Lukin, Y. Rostovtsev, E. Fry, and M. Scully, *Ultraslow Group Velocity and Enhanced Nonlinear Optical Effects in a Coherently Driven Hot Atomic Gas*, Phys. Rev. Lett., **82**, 5229-5232 (1999)

[62] Budker, D. Kimball, S. Rochester, and V. Yashchuk, *Nonlinear Magnetooptics and Reduced Group Velocity of Light in Atomic Vapor with Slow Ground State Relaxation*, Phys. Rev. Lett, **83**, 1767-1770 (1999)

[63] B. Macke and B. Segard, *Propagation of light-pulses at a negative groupvelocity*, The European Physical Journal D, **23**, 125-141 (2003)

[64] B. Segard and B. Macke, *Observation of negative velocity pulse propagation*, Physics Letters A, **109**, 213-216 (1985)

[65] Daniel J. Gauthier, Robert W. Boyd, *Fast light, Slow light, and Optical Precursors: What does it all mean?,* Photonic Spectra, **82**, 82-90(2007).

[66] J. Brown, *Artificial dielectrics*, Progress in dielectrics, **2**, pp. 195-225 (1960)

[67] W. Rotman, *Plasma simulation by artificial and parallel plate media*, IRE Trans. Ant. Propagat., **10**, pp. 82-95 (1962)

[68] J.B. Pendry, A.J. Holden, W.J. Stewart, I. Youngs, *Extremely low frequency plasmons in metallic mesostructures*, Phys. Rev. Lett., **76**, 4773-4776 (1996)

[69] Yangmin Liu and Xiang Zhang, *Metamaterials: a new Frontiers of science and technology*, Chem. Soc. Rev., **40**, 2494-2507 (2011)

[70] L.V. Landau, E.M. Lifshitz, and Pitarsky, *Electrodynamics of Continuous Media*, Pergamon Press, Second Edition (1984)

[71] J.D. Jackson, *Classical Electrodynamics*, John Wiley and Sons, New York (1999)

[72] T.J Yen, W.J. Padilla, N. Fang, D.C. Vier, D.R. Smith, J.B. Pendry, D.N. Basov, and X-Zhong, *Title...*, Science, **303**, 1494-1496 (2004)

[73] S. Linden, C. Enkrich, M. Wegner, J. Zhou, J. Koschny, and C.M. Soukoulis, *Magnetic response of metamaterials at 100 terahertz*, Science, **306**, 1351-1353 (2004)

[74] C.M. Soukoulis, S. Linden, and M. Wegner, *Negative Refractive Index at Optical Wavelengths*, Science, **315**, 47-49 (2007)

[75] J. Zhou, T. Koschny, M. Kafesky, E.N. Economou, J.B. Pendry, and C.M. Soukoulis, *Saturation of the magnetic response of split-ring resonators at optical frequencies*, Phys. Rev. Lett., **95**, 223902 (2005)

[76] J. Zhang, W.J. Fan, N.C. Panoiv, K.J. Melloy, R. Masgood, and S.R.J. Brueek, *Experimental Demonstration of Near-Infrared Negative-Index Metamaterials*, Phys, Rev. Lett., **95**, 137404 (2005)

[77] D. Pines and D. Bohm, *A collective description of electron interactions II: collective versus individual particle aspects of the interactions*, Phys. Rev., **85**, 338353 (1952)

[78] D. Pines and D. Bohm, *A collective description of electron interactions III: Coulomb interactions in a degenerate electron gas*, Phys. Rev., **92**, 609625 (1953)

[79] R.W. Boyd, *Nonlinear Optics*, Academic Press, San Diego (1992)

[80] K. Shimoda, *Introduction to Laser Physics*, Springer-Verlag Berlin Heidelberg GmbH, Second Edition (1987)

[81] M. Kafesaki, T. Koschny, R.S. Penciu, T.F. Gundogdu, E.N. Economou, and C.M. Soukoulis, *Left-handed metamaterials: detailed numerical studies of the transmission properties*, J. Opt. A: Pure Appl. Opt., **7** (2005)

[82] Belayneh Mesfin, V.N. Mal'nev, E.V. Martysh, and Yu.G. Rapoport, *Waves and negative refraction in magnetized plasma with ferrite grains*, Physics of Plasmas, **17**, 112109 (2010)

[83] J.Q. Shen, *Negative refractive index in gyrotropically magnetoelectric media*, Phys. Rev. B, **73**, 045113 (2006)

[84] J. Qui, H.Y. Yao, L.W. Li, S. Zoudi, and T.S. Yeo, *Routes to left-handed materials by magnetoelectric couplings*, Phys. Rev. B, **75**, 155120 (2001)

[85] Subimal Deb and Dutta Gupta, *Absorption and dispersion in metamaterials:Feasibility of device applications*, Pramana - Journal of Physics, **75**, 837 (2010)

[86] Richard W. Ziolkowski, *Propagation in and scattering from a matched metamaterial having a zero index of refraction*, Phys. Rev. E, **70**, 046608 (2004)

[87] Belayneh Mesfin and V.N. Mal'nev, *Slow packets of electromagnetic Waves in magnetized plasma with ferrite grains*, Physics of Plasmas, **19**, 032101 (2012)

[88] A.K. Sarychev and G. Tartakovskii, *plasmonic Metamaterials in actively pumped Host Medium and Plasmonic Nanolaser*, Phys. Rev. B,**75**, 8(2006)

[89] S.A. Ramakrishna, J.B. Pendry, *Optical gain removes absorption and improves resolution in a near-field lens*, Phys. Rev. B, **67**, 201101(R) (2003)

[90] A. Boardman, Y. Rapoport, N. King and V. Malnev, *Creating stable gain in active metamaterials*, J. Opt. Soc. Am. B, **24**, A53A61(2007).

[91] Ilya V. Shadrivov, Steven K. Morrison, and Yuri S.Kivshar *Tunable split-ring resonators for nonlinear negative-indexmetamaterials*, Optics Express **14**, 20, 9344-9349 (2006).

[92] V.N. Mal'nev and Sisay Shewamare, *Slow and fast light in metal/dielectric composites with passive and active host matrices*, Physica B, **426**, 52 (2013)

[93] M.D. Stenner, D.J. Gauthier, and M.A. Neifeld, *The speed of information in a fast-light optical medium* Nature (London), **425**, 695 (2003)

[94] N. Brunner, V. Scarani, M. Wegmuller, M. Legre, and N. Gisin, *Direct Measurement of Superluminal Group Velocity and Signal Velocity in an Optical Fiber*, Phys. Rev. Lett., **93**, 203902 (2004)

[95] D.J. Gauthier and R.W. Boyd, *Fast Light, Slow Light, Optical Precursors: What does it all mean?* , Photonics Spectra, **41**, 82 (2007)

[96] M.E. Tasgn, *Testing the reliability of a velocity definition in dispersive medium*, Archiv-physics.optics, **1**, 1204.5460 (2012)

[97] Abdurahman Ahmed Yonis, Vadim Nickolaevich Malnev, and Belayneh Mesfin Ali, *Superluminal light attenuated by strong dispersion of complex refractive index*, Chin. Phys. B, **25(2)**, 027801 (2016)